Modélisation et simulation numérique de fluides actifs

Astrid Decoene

To cite this version:

Astrid Decoene. Modélisation et simulation numérique de fluides actifs. Mathématiques [math]. Université Paris Sud, 2019. tel-02524898

HAL Id: tel-02524898
https://hal.science/tel-02524898

Submitted on 30 Mar 2020

Université Paris-Sud

École doctorale de mathématiques Hadamard (ED 574)
Laboratoire de mathématique d'Orsay (UMR 8628 CNRS)

Mémoire présenté pour l'obtention du

Diplôme d'habilitation à diriger les recherches

Discipline : Mathématiques

par

Astrid DECOENE

Modélisation et simulation numérique de fluides actifs.

Date de soutenance : 11 décembre 2019

Composition du jury :

Céline GRANDMONT	INRIA Paris (Rapportrice)
Quentin MÉRIGOT	Université Paris Sud(Rapporteur)
Olivier SAUT	Université Bordeaux (Rapporteur)
Marino ARROYO	UPC-BarcelonaTech
Nicole GOUTAL	EDF & Lab. Saint Venant
Emmanuel MAÎTRE	Université Grenoble Alpes
Magali RIBOT	Université d'Orléans
Stéphanie SALMON	Université de Reims

Al Rei dels Patufets.

“Die Revolution ist großartig,
alles andere ist Quark!”
Rosa Luxemburg

Je tiens à remercier en premier lieu toutes et tous les collègues et doctorant.e.s avec qui j'ai eu la chance de travailler ou de discuter.
Les travaux présentés dans ce mémoire sont tous fruits de ces collaborations et échanges.

Je remercie de façon particulière Sébastien Martin et Bertrand Maury, avec qui j'ai toujours autant de plaisir à travailler.

Merci à Céline Grandmont, Quentin Mérigot et Olivier Saut d'avoir accepté et pris le temps d'évaluer ce mémoire.

Merci enfin à Marino Arroyo, Nicole Goutal, Emmanuel Maître, Stéphanie Salmon et Magali Ribot d'avoir accepté de faire partie de ce jury.

Table des matières

Liste des publications

Articles en préparation

A. Decoene, L. Gouarin, L. Lacouture, S. Martin. *3D simulation of active thin structures in a viscous fluid and application to mucociliary transport.*

S. Chibbaro, A. Decoene, S. Martin, F. Vergnet. *Irreversibility and chaos in biological active matter.*

Prépublications

A. Decoene, S. Martin, F. Vergnet. *A smooth extension method for elliptic transmission problems.* https ://hal.archives-ouvertes.fr/hal-02146271v1

Articles publiés

A. Decoene, S. Martin, B. Maury. *Direct simulation of rigid particles in a viscoelastic fluid.* Journal of Non-Newtonian Fluid Mechanics, 260, 1–25 (2018).
https ://hal.archives-ouvertes.fr/hal-01456089/file/DMM17.pdf

S. Bertoluzza, A. Decoene, L. Lacouture, S. Martin. *Local error analysis for the Stokes equations with a punctual source term.* Numerische Mathematik, 140(3), 677–701 (2018).

S. Bertoluzza, A. Decoene, L. Lacouture, S. Martin. *Local error estimates of the finite element method for an elliptic problem with a Dirac right-hand side.* Numer Methods Partial Differential Eq., 2017 ; 00 :1-24. https ://hal.archives-ouvertes.fr/hal-01150745v2/document.

M. Khalife, A. Decoene, F. Caetano, L. de Rochefort, E. Durand, D. Rodriguez. *Estimating absolute aortic pressure using MRI and a one-dimensional model.* Journal of Biomechanics, Elsevier, 2014, 47 (13), pp.3390-3399.

A. Decoene, B. Maury. *Moving meshes with freefem++.* Journal of Numerical Mathematics, 20(3-4), 195-214 (2012).

N. Aguillon, A. Decoene, B. Fabreges, B. Maury and B. Semin, *Modelling and simulation of 2D stokesian Squirmers.* ESAIM : Proceedings Vol. 38 , page 36 (2012).

B. Semin, A. Decoene, J.-P. Hulin, M. François et H. Auradou. *Flow-induced oscillation of a confined tethered cylinder below the vortex shedding threshold.* J. Fluid Mech. 690, 345-365 (2012).

A. Decoene, S. Martin, B. Maury. *Microscopic modelling of active bacterial suspensions*, Mathematical Modelling of Natural Phenomena, Vol. 6, No. 5, pp. 98-129 (2011).

A. Decoene, A. Lorz, S. Martin, B. Maury, M. Tang. *Simulation of self-propelled chemotactic bacteria in a Stokes flow.* ESAIM : Proceedings, 30 (Mathematical Modelling in Medicine), 105-124 (2010).

L. Mari, C. Biotto, A. Decoene, L. Bonaventura. *A coupled ecological-hydrodynamic model for the spatial distribution of sessile aquatic species in thermally forced basins.* Ecological Modelling, 220(18) :2310-2324, September 2009.

A. Decoene, L. Bonaventura, E. Miglio, F. Saleri. *Asymptotic derivation of the section averaged shallow water equations for river hydraulics.* M3AS, Vol. 19, No. 3, March 2009.

A. Decoene, J.-F. Gerbeau. *Sigma transformation and ALE formulation for three-dimensional free surface flows.* International Journal for Numerical Methods in Fluids, vol. 59, issue 4, pp. 357-386, February 2009.

E. Audusse, M.-O. Bristeau, A. Decoene. *Numerical simuations of 3D free surface flows by a multilayer Saint-Venant model.* International Journal for Numerical Methods in Fluids, Vol. 56, I. 3, 331-350, 2007.

A. Decoene, J.-F. Gerbeau. *A conservative MURD scheme on moving domains. Application to the three-dimensional free surface flows.* Proceedings of Eccomas CFD 2006, P. Wesseling, E. Onate, J. Periaux (editors), 2006, p. 1-12.

V. Martin, F. Clément, A. Decoene, J.-F. Gerbeau. *Parameter identification for a one-dimensional blood flow model.* ESAIM : Proceedings, Septembre 2005 vol. 14, 174-200. Eric Cancès and Jean-Frédéric Gerbeau, Editors.

Paris, 6 décembre 2019

Introduction

Ce mémoire regroupe et décrit mes travaux de recherche depuis la fin de mon doctorat en 2006. Ces travaux ont été consacrés à la modélisation et à la résolution numérique de problèmes issus de la mécanique des fluides, avec un intérêt particulier porté sur l'interaction entre les fluides visqueux et des entités microscopiques actives.

En effet, depuis mon arrivée au laboratoire de mathématiques d'Orsay en 2008, mon activité de recherche s'est surtout concentrée sur la modélisation mathématique et numérique de fluides actifs, ainsi que l'analyse des comportements collectifs qui y émergent. Ces fluides se composent typiquement d'un fluide visqueux (l'écoulement est non inertiel), dans lequel se meuvent des organismes vivants dotés d'une activité interne. Je me suis lancée sur ce sujet avec Sébastien Martin *(MAP5, Université Paris Descartes)* et Bertrand Maury *(LMO)*, dans l'idée initialement d'étendre les méthodes numériques conçues pour des suspensions passives aux entités actives. Nous avons par la suite collaboré avec différentes personnes sur ce sujet, dont Loic Lacouture et Fabien Vergnet, tous deux ayant effectué leur thèse au *LMO* sous notre direction ; Silvia Bertoluzza *(IMATI CNR, Italie)*, Sergio Chibbaro et Corrado Maurini *(Laboratoire Jean Le Rond d'Alembert, Paris 6)*. Nous avons également interagi avec un bon nombre de physiciens s'intéressant à ce même sujet, notamment Salima Rafai et Philippe Peyla du LiPhy *(Laboratoire Interdisciplinaire de Physique)* à Grenoble, qui mènent à la fois un travail expérimental et numérique sur les suspensions d'algues auto-propulsées, les *Chlamydomonas Rheinartdii* [129].

Ce sujet très riche m'a permis d'aborder à la fois des questions de modélisation, d'analyse et de calcul [45, 1, 44]. Nous avons d'une part proposé des modèles mathématiques à l'échelle microscopique, c'est-à-dire à l'échelle des entités actives, pour des suspensions de micro-nageurs et des fluides entraînés par des cils. D'autre part, nous avons proposé des méthodes numériques adaptées, soit à leur résolution pour un grand nombre d'entités, soit à leur description fine, en 2d et/ou en 3d. Ces méthodes ont toutes en commun d'être robustes, relativement simples à implémenter, et ne pas comporter de paramètres numériques et non physiques à régler, mis à part les pas de discrétisation. Les simulations réalisées ont montré une bonne conformité qualitative avec les expériences et les résultats théoriques connus, notamment en ce qui concerne les caractéristiques rhéologiques des suspensions de micro-nageurs et le phénomène de bioconvection. Elles nous ont permis d'étudier de façon assez précise les phénomènes collectifs qui y émergent. Les méthodes numériques développées nous ont également amenés à nous intéresser à des questions plus fondamentales : l'analyse numérique de la méthode des éléments finis appliquée à la résolution de problèmes elliptiques avec terme source non régulier (typiquement une mesure de Dirac) [12, 11]. Ou encore le développement d'une nouvelle méthode de domaine fictif pour des problèmes de transmission elliptiques [47].

Dans les systèmes étudiés, de par la taille des entités actives qui est de l'ordre du micron, le nombre de Reynolds est bas et le régime est essentiellement non inertiel, c'est-à-dire que les effets visqueux sont dominants et les effets inertiels négligeables. Je me suis néanmoins aussi intéressée à des écoulements inertiels, cette fois-ci non actifs. Il s'agit là pour la plupart de travaux réalisés en collaboration avec des chercheurs d'autres disciplines, notamment des physiciens et mécaniciens. En effet, j'ai continué à travailler sur la thématique de ma thèse, qui concernait les écoulements à surface libre hydrostatiques, et en particulier leur résolution dans le code industriel *Telemac-3D*, développé au *Laboratoire National d'Hydraulique et Environnement (LNHE)*, un département de la division recherche et développement d'*EDF*. La collaboration avec le *LNHE* a été poursuivie, notamment avec la thèse de P. Quemar que j'ai co-encadrée avec Emmanuel Audusse et Olivier Lafitte (*Laboratoire LAGA, Université Paris 13*), et qui portait sur l'analyse et l'amélioration du code *Telemac-3d* (cette fois-ci pour les écoulements non hydrostatiques). Pendant mon post-doctorat au *MOX (Politecnico di Milano)* de 2006 à 2008, j'ai travaillé avec Luca Bonaventura et Fausto Saleri sur un autre solveur pour les écoulements à surface libre, appelé *STRATOS*, et en particulier sur la dérivation asymptotique d'un modèle réduit pour le cas des eaux peu profondes [42]. Deux autres travaux sont issus d'une collaboration avec des expérimentateurs, dans le but d'associer les deux outils complémentaires que sont l'expérience physique et la simulation numérique. Le premier concerne l'étude d'une nouvelle instabilité oscillatoire observée expérimentalement par B. Semin et ses collaborateurs (*Laboratoire FAST, Université Paris Sud*) sur un cylindre confiné dans un écoulement inertiel [140]. Le deuxième concerne une collaboration avec des chercheurs en imagerie médicale (*Laboratoire IR4M, Université Paris Sud*) sur la caractérisation des écoulements sanguins dans l'aorte [89].

Les écoulements inertiels ont des propriétés complètement différentes, puisque les équations les gouvernant sont non linéaires et les termes de convection doivent être pris en compte. Cependant, ces travaux ont en commun avec mes travaux sur les fluides actifs à bas Reynolds le fait qu'ils concernent des écoulements posés sur des domaines dont les frontières bougent ou se déforment, et les outils numériques pour traiter les interfaces et frontières mobiles sont similaires. En effet, les méthodes pour résoudre des écoulements dans des domaines mobiles peuvent être classées en deux grandes catégories :

1. Les méthodes à maillage fixe. Celles-ci sont basées sur un maillage couvrant le domaine d'intérêt qui contient strictement le domaine occupé par le fluide. Comme les équations sont écrites sur l'ensemble du domaine, y compris dans certaines zones où il n'y a pas de fluide, le terme *méthode de domaine fictif* est parfois utilisé pour qualifier cette approche. De telles méthodes sont bien adaptées à une implémentation simple et à l'utilisation de maillages cartésiens et de solveurs rapides, en particulier pour la résolution d'interactions fluide-particules ou fluide-structure. Les différentes phases peuvent être prises en compte très simplement en utilisant une fonction caractéristique de la phase solide (voir par exemple [87]), ou au moyen d'une fonction niveau (*Level Set*) [23].
2. Les méthodes à maillage mobile. Le maillage suit le domaine occupé par le fluide de façon à rester conforme aux frontières et interfaces du domaine à chaque instant. On peut donc s'attendre à une meilleure précision en espace, mais cet avantage est au prix de la manipulation d'un maillage qui bouge, ce qui peut poser problème en termes de qualité du maillage et de robustesse du processus itératif en temps. L'approche repose sur le suivi des frontières et interfaces du domaine, sans identifier les sommets du maillage aux particules de fluide. Il y a donc une certaine liberté dans le choix du mouvement du maillage, et l'approche est généralement appelée *Arbitrary Lagrangian Eulerian* (ALE) (voir [81, 86]).

J'ai été amenée à utiliser et développer ces deux types de méthodes dans mes travaux, en fonction du niveau de précision et d'efficacité de calcul désiré. Dans ce mémoire, je décris en particulier la nouvelle méthode de domaine fictif que nous avons développée dans le cadre de la thèse de Fabien Vergnet (Chapitre 3), ainsi qu'une approche ALE pour la résolution d'écoulements à surface libre (Chapitre 4).

Les travaux synthétisés dans ce mémoire ont été regroupés en quatre chapitres, dont les trois premiers s'articulent autour de la modélisation des fluides actifs, et le dernier autour des écoulements inertiels dans lesquels une ou plusieurs frontières bougent ou se déforment. Après cette longue introduction, un premier chapitre est consacré à la simulation directe de suspensions actives. Le deuxième chapitre concerne la modélisation de fluides visqueux entraînés par des cils actifs, le troisième chapitre se focalisant sur un modèle d'interaction complète entre un fluide visqueux et une structure élastique active. Le quatrième chapitre est consacré à la modélisation et la simulation numérique de quelques écoulements inertiels à frontières mobiles. Une dernière partie enfin concerne quelques travaux en cours et mes perspectives de recherche pour le futur.

Chapitre 1 : Simulation directe de suspensions actives

Certains micro-organismes, comme les bactéries *Escherichia coli* ou les micro-algues *Chlamydomonas Reinhartdii*, ont la capacité de nager dans un fluide visqueux et leur vitesse peut atteindre plusieurs fois leur taille par seconde, malgré le régime de bas nombre de Reynolds dans lequel ils vivent. Cette nage engendre des dynamiques collectives étonnantes, qui ont éveillé un grand intérêt dans la communauté scientifique ces dernières décennies. On observe en effet dans les suspensions actives, au-delà d'une certaine concentration, une transition vers un mouvement collectif qui ne correspond pas à la simple addition des mouvements individuels. Les formes les plus évidentes de cette dynamique sont l'apparition de tourbillons dont la taille dépasse largement celle des micro-organismes qui les engendrent, le phénomène de bioconvection lorsque l'hydrodynamique est couplée à un mécanisme de chimiotactisme, et le comportement rhéologique anormal de la suspension : la viscosité effective d'une suspension active peut augmenter ou diminuer par rapport à la même suspension passive, selon le type de nage, la forme des nageurs et leur concentration.

L'étude de la dynamique collective dans les suspensions actives peut se faire à différents niveaux : expérimental, analytique/théorique et numérique. Du point de vue mathématique, la plupart des modèles proposés et analysés, notamment pour étudier le comportement chimiotactique des suspensions actives, sont des modèles macro- ou mésoscopiques (cinétiques), qui tiennent compte de la nage des micro-organismes de façon moyennée (sous la forme d'une densité ou d'une densité de probabilité). Mais ces modèles font intervenir certains paramètres qui ne sont pas accessibles de façon directe, comme par exemple la viscosité effective de la suspension. Dans nos travaux nous nous sommes intéressés avec S. Martin et B. Maury à la modélisation et à la simulation de ces suspensions au niveau microscopique [45, 1, 44]. Une telle approche nous paraît essentielle car elle permet de mieux comprendre certains phénomènes d'un point de vue plus élémentaire, et ainsi de valider ou améliorer les modèles macroscopiques. Notre but était d'utiliser des modèles suffisamment simples et des méthodes numériques suffisamment performantes et robustes pour simuler des suspensions actives avec le plus grand nombre possible d'entités actives, tout en garantissant une précision suffisante à la fois du modèle et des méthodes pour que les ingrédients essentiels jouant un rôle dans la dynamique collective soient pris en compte de façon précise.

En particulier, nous avons travaillé sur un modèle représentant chaque nageur par une particule rigide de forme ellipsoïdale à laquelle on associe un dipôle de forces représentant l'autopropulsion. Le signe de ce dipôle détermine si le nageur se pousse ou se tracte dans le fluide. Les équations gouvernant le fluide et celles gouvernant les particules rigides sont traitées de façon fortement couplées, ce qui permet une bonne description de leur interaction, ingrédient essentiel pour reproduire des effets collectifs comme celui sur la rhéologie. On considère un domaine ouvert et borné $\Omega \subset \mathbb{R}^d$, d étant la dimension, et on note B le domaine rigide constitué de l'ensemble des corps rigides B_i pour $i = 1, \ldots, N$, $\Omega \setminus \bar{B}$ désignant alors le domaine fluide. Le régime étant non-inertiel, le problème fluide considéré est le suivant :

$$\begin{cases} -\nabla \cdot \underline{\underline{\sigma}}(\mathbf{u}, p) = \sum\limits_{i=1,\ldots,N} \mathbf{f}_{P_i} \chi_{P_i} & \text{dans} \quad \Omega \setminus \bar{B}, \\ \nabla \cdot \mathbf{u} = 0 & \text{dans} \quad \Omega \setminus \bar{B}, \end{cases}$$

où $\mathbf{u}$ et p sont respectivement les champs de vitesse et de pression dans le fluide, $\underline{\underline{\sigma}}$ est le tenseur des contraintes qui s'écrit $\underline{\underline{\sigma}} = \mu(\nabla \mathbf{u} + (\nabla \mathbf{u})^T) - p\mathbb{I}$ pour un fluide Newtonien, et $\mathbf{f}_{P_i}$ est la force volumique de propulsion appliquée par le nageur i sur le fluide, χ_{P_i} désignant la fonction caractéristique associée à la région dans le fluide sur laquelle elle s'applique. La dynamique des particules est gouvernée par l'équilibre des forces et des moments sur chaque corps rigide B_i, de centre de gravité $\boldsymbol{x}_i$:

$$\begin{cases} \displaystyle\int_{B_i} \rho \mathbf{g} + \int_{B_i} \mathbf{f}_{B_i} - \int_{\partial B_i} \underline{\underline{\sigma}}(\mathbf{u}, p) \cdot \mathbf{n} = 0 & \forall i \in \{1, ..., N\}, \\ \displaystyle\int_{\partial B_i} (\boldsymbol{x} - \boldsymbol{x}_i) \times \underline{\underline{\sigma}}(\mathbf{u}, p) \cdot \mathbf{n} = 0 & \forall i \in \{1, ..., N\}, \end{cases}$$

où ρ est le terme de flottabilité, positif car les nageurs sont légèrement plus denses que le fluide, et $\mathbf{f}_{B_i}$ désigne la rétroaction sur le nageur de la force de propulsion qu'il applique sur le fluide ; celle-ci vérifie :

$$\int_{B_i} \mathbf{f}_{B_i} \, \mathrm{d}\boldsymbol{x} = \int_{P_i} \mathbf{f}_{P_i} \, \mathrm{d}\boldsymbol{x}.$$

Le système est complété par des conditions limites particulières au bord du domaine Ω, et par une équation qui traduit la continuité des vitesses aux interfaces fluide-particule :

$$\mathbf{u} = \mathbf{v}_i + \omega_i \times (\boldsymbol{x} - \boldsymbol{x}_i) \quad \text{sur } \partial B_i, \ \forall i \in \{1, ..., N\},$$

$\mathbf{v}_i$ et ω_i désignant respectivement les vitesses de translation et angulaire du nageur i.

Le problème d'interaction fluide-particule est résolu en dimension 2 par une méthode éléments finis associée à une approche de type domaine fictif : nous résolvons un problème de Stokes classique posé sur le domaine entier (incluant le fluide et les corps rigides), la contrainte de rigidité dans la partie occupée par les particules étant relaxée en introduisant un terme de pénalisation associé à cette contrainte réécrite sous la forme $\mathbb{D}(\mathbf{u}) = 0$, où $\mathbb{D}(\mathbf{u})$ est le tenseur des déformations du fluide. Cette approche numérique a été appliquée dans [87] et [99] à la simulation de suspensions de particules passives, et nous l'avons réutilisée dans le contexte des particules actives. Les éventuels chevauchements entre particules rigides dus aux erreurs numériques doivent être gérés afin de garantir la robustesse des simulations. Nous utilisons pour cela une méthode numérique proposée dans [114], basée sur des collisions inélastiques entre particules rigides, que nous avons étendue aux particules ellipsoïdales. A chaque pas de temps nous résolvons ainsi le problème fluide-particules, ce qui permet de calculer une approximation des vitesses de translation et de rotation des nageurs $\mathbf{v}_i$ et ω_i, et de mettre à jour leur position et orientation de nage.

La méthode de pénalisation n'est néanmoins pas applicable en dimension 3, car le terme de pénalisation dégrade fortement le conditionnement de la matrice associée au problème de Stokes, qu'il faut inverser à chaque pas de temps. Une méthode itérative n'est donc pas envisageable en l'état pour résoudre le système linéaire associé, or les méthodes directes impliquent le stockage des matrices ce qui n'est pas raisonnable en dimension 3. D'autres méthodes de domaine fictif doivent être utilisées si l'on souhaite faire des simulations directes de suspensions actives en 3d, comme par exemple la méthode développée dans [60]. Une autre possibilité est d'utiliser un préconditionneur adapté comme dans [31].

Les simulations réalisées avec notre modèle ont montré une bonne conformité qualitative avec les expériences et les résultats théoriques connus, notamment en ce qui concerne les caractéristiques rhéologiques des suspensions et le phénomène de bioconvection [45, 1, 44]. Elles ont également révélé un phénomène très intéressant, qui indique qu'au delà d'une certaine concentration en micro-nageurs, la dynamique macroscopique des suspensions n'est plus réversible, ce qui est en contradiction avec le caractère parfaitement symétrique des équations microscopiques par rapport à une inversion du temps. Afin de mieux comprendre ce phénomène, nous avons procédé à une étude détaillée des configurations et de la dynamique du système. En particulier, nous avons mis en évidence et quantifié son comportement chaotique dès un nombre très petit de particules, et calculé la densité de probabilité pour différentes grandeurs, comme par exemple la corrélation par paires des particules dans l'écoulement. Ceci afin de caractériser les configurations les plus probables. Ce travail est en cours de finalisation et a été fait en collaboration avec S. Chibbaro, du laboratoire *Jean Le Rond d'Alembert*. Il est présenté dans ce manuscrit dans la dernière partie qui concerne les travaux en cours et les perspectives de recherche.

Enfin, les aspects chimiotactiques ont été intégrés, prenant en compte la consommation individuelle d'oxygène et le mode de déplacement caractéristique des bactéries, appelé *run-and-tumble*, qui leur permet de se déplacer vers les gradients favorables de nutriments. L'intégration de ces phénomènes nous permet de reproduire les instabilités hydrodynamiques complexes favorisant des mouvements bioconvectifs.

Chapitre 2 : Modélisation de fluides visqueux entraînés par des cils

Dans le cadre de la thèse de Loic Lacouture, que j'ai co-encadrée avec S. Martin et B. Maury, nous nous sommes intéressés à des fluides complexes actifs dans lesquels l'activité provient de structures fines appelées cils. C'est le cas par exemple du mucus bronchique, mis en mouvement par le battement coordonné de cils nappant les parois des bronches. Ce mécanisme, appelé transport mucocilaire, est nécessaire à l'évacuation des impuretés inhalées et de nombreuses pathologies - asthme, bronchite chronique - résultent de son dysfonctionnement. L'étude de ce mécanisme comporte des aspects de modélisation, d'analyse et de calcul intéressants, en lien avec des applications potentielles en médecine. Mais des cils actifs sont présents dans bien d'autres fluides biologiques, par exemple dans l'oreille interne ou dans le cerveau [155]. Notre objectif est de proposer un outil d'analyse et de simulation numérique permettant d'étudier l'impact sur ces fluides biologiques du battement des cils et la dépendance de certains paramètres comme leur densité.

Etant donné que nous souhaitons pouvoir faire des simulations à grand nombre de cils, afin d'étudier les mouvements collectifs émergeant dans ces fluides, il nous faut considérer un modèle d'interaction fluide-structure impliquant un coût de résolution réduit. Nous avons ainsi choisi d'éviter les contraintes de taille en considérant une approche asymptotique de ce problème : les structures fines sont modélisées comme des variétés de dimension 1 immergées dans l'espace à 3 dimensions. Cet objet mathématique est obtenu formellement en faisant tendre le diamètre du cil vers 0, tout en maintenant constante la résultante de la force appliquée par le cil sur le fluide, afin que l'objet ne disparaisse pas complètement du fluide dans ce régime asymptotique. Cette approche permet de remplacer l'effet de chaque structure sur le fluide par une force linéique (distribution de Dirac le long d'une courbe 1d). On travaille alors à mouvement des structures fines imposé, et on déduit de ce mouvement la force linéique qu'elles appliquent sur le fluide à chaque instant. Nous utilisons pour cela la "slender-body theory" [37], basée sur une dérivation asymptotique en un petit paramètre ϵ qui est le rapport entre l'épaisseur a et la longueur L du cil :

$$\mathbf{f}(s,t) = \frac{2\pi\mu}{\ln(L/a)}\left(2\mathbb{I}_3 - \frac{\partial_s\boldsymbol{\xi}(s,t)\otimes\partial_s\boldsymbol{\xi}(s,t)}{\|\partial_s\boldsymbol{\xi}(s,t)\|^2}\right)\partial_t\boldsymbol{\xi}(s,t) + O(\frac{1}{(\ln(L/a))^2}),$$

où $\mathbf{f}(\cdot,t)$ désigne la force exercée par le cil sur le fluide à l'instant t, et $\boldsymbol{\xi}(\cdot,t)$ la position du cil, en coordonnées curvilignes.

Numériquement, chaque force linéique est approchée par N forces ponctuelles afin de simplifier les calculs. Ce modèle aboutit à la résolution des équations de Stokes avec des masses de Dirac ponctuelles en terme source, qui s'écrit si l'on considère M cils dans un fluide de viscosité μ :

$$\left\{\begin{array}{rcll} -\mathrm{div}(\mu\nabla\mathbf{u}) + \nabla p & = & \sum\limits_{i=1}^{M}\big(\sum\limits_{n=1}^{N}\delta_{\boldsymbol{\xi}_i(s_n,t)}\,\mathbf{f}_i(s_n,t)\big) & \text{dans } \Omega, \\ \mathrm{div}(\mathbf{u}) & = & 0 & \text{on } \Omega, \\ \mathbf{u} & = & 0 & \text{dans } \partial\Omega, \end{array}\right.$$

où $\boldsymbol{\xi}_i(s_n,t)$ désigne la position du $i$ème cil à l'instant t au point de coordonnée curviligne s_n, et $\mathbf{f}_i(s_n,t)$ est la force ponctuelle exercée sur le fluide à l'instant t au point $\xi_i(s_n,t)$.

La présence de termes sources ponctuels entraîne une dégradation de la régularité de la solution, qui n'appartient pas à l'espace des fonctions H^1 comme dans le cas classique. Ainsi, les résultats standards sur les ordres de convergence de la méthode des éléments finis ne s'appliquent pas, et l'on observe en pratique un ordre de convergence très dégradé. Afin d'améliorer la vitesse de convergence, plusieurs auteurs ont proposé d'utiliser des mailles localement raffinées près de la singularité [5, 38]. Mais cette procédure augmente la complexité du maillage et le coût de calcul, même si le maillage n'est raffiné que localement, et ce d'autant plus que le nombre de termes sources ponctuels est grand. Dans [58], Eriksson a mis au point une méthode numérique pour résoudre le problème de Laplace avec terme source singulier et récupérer l'ordre de convergence optimal : la solution numérique est recherchée sous la forme $u_0 + v_h$, où u_0 est une fonction connue contenant la singularité de la solution, et v_h est la solution numérique d'un problème régulier. Cette méthode a été étendue au problème de Stokes par L. Lacouture dans [93], et est appliquée dans ce travail pour résoudre le problème décrit précédemment. Cette approche s'inscrit dans la classe des méthodes de soustraction, utilisées dans plusieurs contextes tels que l'électroencéphalographie [92] et plus récemment pour la simulation du flux sanguin dans des réseaux microvasculaires [152].

Le modèle numérique obtenu a été implémenté par L. Lacouture dans le code CAFES (Cartesian Finite Element Solver) [60] développé au *LMO*, et nous l'avons appliqué à la modélisation du transport mucociliare. Les cils bronchiques baignent dans une couche de fluide (appelée la PCL) dont la viscosité est environ 50 fois moindre que le mucus, et ils peuvent pénétrer ce-dernier pendant leur battement. Nos simulations prennent bien en compte cette différence de viscosité, les équations de Stokes étant résolues pour une viscosité constante par morceaux. Notre approche permettant de simuler l'effet d'un nombre très important de cils sur le mucus, nous avons réalisé une série de simulations pour étudier et quantifier l'efficacité du transport mucociliaire en fonction de la densité de cils. Ces résultats ont mis en évidence les effets collectifs émergeant à partir d'une certaine valeur de cette densité et leur impact sur l'efficacité du transport mucocilaire.

En parallèle de ces travaux, nous nous sommes intéressés à l'analyse numérique de la méthode des éléments finis appliquée à la résolution de problèmes elliptiques avec terme source non régulier (typiquement une mesure de Dirac). Les solutions de ces problèmes n'ayant pas la régularité H^1, la convergence de la méthode éléments finis est sous-optimale. Cependant, on peut montrer que l'ordre optimal est optimal si l'on considère des normes locales, c'est-à-dire sur tout sous-domaine qui exclue la singularité. Nous avons démontré un résultat de convergence quasi-optimale (à un facteur logarithmique près) en norme locale H^s, pour $s \geq 1$, et une convergence optimale en norme locale H^1 pour le cas des éléments finis P^1-Lagrange, sur une famille de maillages quasi-uniformes en dimension 2 d'espace pour un Dirac ponctuel, et en dimension 3 pour un Dirac le long d'une courbe 1D. Nos résultats ont été obtenus en utilisant les estimations d'erreur locales de type Nitsche et Schatz, une version faible du lemme de dualité d'Aubin-Nitsche et une condition inf-sup discrète. Les résultats ont été initialement obtenus pour le cas du Laplacien [12], puis dans le cas du problème de Stokes [11].

Chapitre 3 : Un modèle d'interaction fluide-structure active

Dans le travail présenté au chapitre 3, nous nous intéressons à la *simulation directe* des fluides actifs entraînés par des cils, basée sur la résolution directe des équations fondamentales de la physique gouvernant l'interaction entre le fluide visqueux et les structures actives, afin d'inclure de façon exhaustive les interactions hydrodynamiques.

Le modèle que nous présentons au chapitre 2 décrit l'effet des cils sur le fluide visqueux dans lequel ils baignent, mais la rétroaction du fluide n'est pas prise en compte, et nous travaillons à mouvement des cils imposé. Or, dans les bronches, leur mouvement peut être perturbé par le fluide si celui-ci n'est pas au repos. En réalité, chaque cil est piloté par des moteurs internes qui aboutissent *de facto* à une dynamique dépendant de l'interaction avec le fluide [155] ; la dynamique sera donc différente selon la viscosité du fluide, mais aussi selon que celui-ci est au repos ou non. ll est notamment connu que les cils bronchiques interagissent lorsqu'ils se trouvent à une distance suffisamment faible, et synchronisent leurs battements de façon à rendre le transport mucociliaire plus efficace. Des expériences faites *in vitro* sur des cellules épithéliales de bronches de lapin montrent l'apparition d'une onde métachronale en sens inverse à l'écoulement, au-delà d'une certaine densité de cils [16, 68]. La façon dont les cils interagissent est sujette à discussion ; l'émergence de cette synchronisation résulterait principalement des forces hydrodynamiques. Plusieurs paramètres peuvent avoir une influence sur le mouvement des cils, notamment leur densité, ainsi que la viscosité et l'épaisseur de la couche de fluide dans laquelle ils battent. Dès lors, travailler à mouvement imposé devient incompatible avec l'étude fine de l'impact de ces paramètres sur la dynamique individuelle mais aussi collective.

De nombreux travaux se sont intéressés à la simulation numérique des fluides actifs ciliés, basée sur une représentation individuelle des entités actives qui évoluent dans le fluide porteur, mais ils reposent le plus souvent sur un mouvement imposé des structures et une résolution tronquée des équations de Stokes [144, 18]. Des travaux plus récents se sont concentrés sur la simulation directe des équations de Stokes couplées à des structures fines actives 3d, mais dont le mouvement est prescrit [30].

Quelques travaux se sont intéressés à la modélisation du mouvement des cils en soi [52], mais ils ne s'attèlent pas à la simulation de l'interaction avec le fluide d'un grand nombre de cils. A notre connaissance, seul un papier récent réalise des simulations directes sur des forêts de cils conséquentes [29], à partir d'un modèle phénoménologique pour la prise en compte de l'effet du fluide sur les cils. Dans tous les cas, ces modèles négligent la rétroaction du fluide sur les cils ou induisent une approximation des forces hydrodynamiques à courte ou à longue portée.

C'est à cette problématique que nous nous sommes attaqués dans le cadre de la thèse de Fabien Vergnet, que j'ai co-encadrée avec S. Martin et B. Maury. En collaboration avec Corrado Maurini de *l'Institut Jean Le Rond d'Alembert*, nous avons proposé un modèle d'hyper-élasticité 3d non linéaire de type Saint Venant-Kirchoff pour les structures, dans lequel l'activité interne du cil est prise en compte à travers l'ajout d'un tenseur de contraintes actives. Considérons un domaine ouvert et borné $\Omega_s \subset \mathbb{R}^d$, avec $d = 2, 3$, qui représente le milieu élastique non déformé. Notons $\mathbf{d}_s \in \mathbb{R}^d$ le déplacement de la structure dans le temps, définie dans Ω_s, E le tenseur des déformations non-linéaires, et F le gradient des déformations :

$$E(\mathbf{d}_s) = \frac{1}{2}\left(\nabla \mathbf{d}_s + \nabla \mathbf{d}_s^t + \nabla \mathbf{d}_s \nabla \mathbf{d}_s^t\right),$$

$$F(\mathbf{d}_s) = Id + \nabla \mathbf{d}_s.$$

On suppose que le solide élastique suit une loi de comportement donnée par la loi de Saint Venant-Kirchhoff, ainsi le tenseur des contraintes passives s'écrit :

$$\Sigma(\mathbf{d}_s) = 2\mu_s E(\mathbf{d}_s) + \lambda_s \mathrm{Tr}(E(\mathbf{d}_s))\mathrm{Id},$$

où μ_s et λ_s sont les coefficients de Lamé. Le cil étant actif, il est nécessaire de modéliser les contraintes internes ; on définit pour cela un tenseur des contraintes actives Σ^* dépendant du temps et de l'espace. Enfin, les cils vivant dans un régime à bas nombre de Reynolds, on peut négliger les effets inertiels. En l'absence de forces extérieures le modèle pour la structure active s'écrit alors, en formulation Lagrangienne :

$$\begin{cases} -\nabla \cdot \left(F(\mathbf{d}_s(t))\left(\Sigma\left(\mathbf{d}_s(t)\right) - \Sigma^*(t)\right)\right) & = 0, \quad \text{dans } \Omega_s, \\ \left(F(\mathbf{d}_s(t))\left(\Sigma(\mathbf{d}_s(t)) - \Sigma^*(t)\right)\right) \cdot \mathbf{n} & = 0, \quad \text{sur } \partial\Omega_s \setminus \Gamma_s, \\ \mathbf{d}_s(t) & = 0, \quad \text{sur } \Gamma_s, \end{cases}$$

où Γ_s est le bord auquel la structure est ancrée, et où le déplacement est nul. L'effet du tenseur des contraintes actives Σ^* peut être interprété comme une force supplémentaire agissant sur la structure qui s'écrit $\nabla \cdot (F(\mathbf{d}_s)\Sigma^*)$.

Pour modéliser le tenseur Σ^* nous suivons une approche utilisée pour les tissus biologiques tels que les artères et les muscles [119]. Celle-ci consiste à traduire le comportement actif du tissu par des déformations élastiques locales dans la direction de ses fibres. Dans notre cas, cela revient à traduire la dynamique de cisaillement à l'intérieur d'un cil par des déformations élastiques dans la direction des microtubules, qui induisent une flexion du cil. Le tenseur dépend alors d'une fonction scalaire appelée le "scénario d'activité" qu'il faut déterminer. Si le scénario est bien choisi, ce modèle permet de reproduire les déformations effectivement observées sur les cils.

Le problème fluide est gouverné par les équations de Stokes, et il est couplé au problème solide à travers les conditions aux limites à l'interface fluide structure traduisant la continuité des vitesses et des contraintes normales.

Une fois le modèle développé, nous nous sommes attelés à la résolution numérique de l'interaction fluide-structure active. Deux méthodes éléments finis ont été proposées, basées sur des algorithmes itératifs qui permettent de résoudre le couplage fort des deux problèmes, afin d'éviter d'éventuelles instabilités numériques [28]. La première méthode est assez classique et repose sur une formulation ALE du problème à interface mobile, permettant de travailler sur des maillages qui suivent l'interface à chaque pas de temps. Une formulation variationnelle du problème est écrite sur des espaces fonctionnels contraints pour la vitesse du fluide et le déplacement de la structure, la contrainte exprimant la continuité des vitesses à l'interface. Le problème de minimisation sous contraintes en découlant est traité en formulation point-selle et résolu avec un algorithme itératif d'Uzawa, ce qui permet à chaque itération de l'algorithme de résoudre les problèmes (fluide et structure) séparément et d'utiliser ainsi des solveurs classiques pour l'un et l'autre. Cette méthode permet une résolution très précise du problème, puisque le maillage est conforme à l'interface fluide-structure à chaque pas de temps et que la méthode des éléments finis appliquée à chaque problème stationnaire converge à l'ordre optimal. Cependant, son coût est très élevé : la méthode d'Uzawa nécessite de nombreuses itérations et à chaque itération, il faut résoudre un problème de Stokes sur un domaine grand et complexe (le problème d'élasticité est résolu rapidement car le domaine structure est petit). De plus, lorsque les déplacements de la structure deviennent grands, il est nécessaire de remailler régulièrement, sans quoi les éléments du maillage dégénèrent.

Cette résolution du problème fluide-structure a été implémentée par F. Vergnet dans le solveur éléments finis FEniCS [105], et nous avons obtenu des résultats préliminaires pour des simulations en 2d. Elles montrent notamment la forte dépendance des déformations des cils par rapport à la viscosité du fluide, pour un scénario d'activité donné. Des simulations à 2 cils montrent également que le déphasage entre les cils influence fortement leur mouvement lorsqu'ils sont placés à une distance suffisamment petite pour qu'ils interagissent.

Afin de réduire le coût de calcul, nous avons développé une méthode de domaine fictif de type contrôle, basée sur une approche initialement développée dans [6] pour résoudre des problèmes aux limites dans des géométries complexes, par exemple dans une boîte contenant un obstacle. Celle-ci a ensuite été utilisée pour résoudre l'interaction entre un fluide et des particules rigides [59], et nous l'avons étendue à un cadre plus général qui est celui des problèmes de transmission elliptiques, et en particulier aux problèmes d'interaction fluide-structure. Cette méthode permet d'utiliser un maillage fixe et structuré pour la résolution du problème fluide, tout en préservant l'ordre optimal de la méthode éléments finis. L'idée de la méthode est d'étendre le problème fluide au domaine entier (fluide+structure), et chercher un second membre L^2, à support dans le domaine structure, tel que la restriction de la solution au domaine fluide soit égale à la solution recherchée. Ainsi, le problème fluide est non contraint, et peut être discrétisé avec un maillage fixe et non-conforme à l'interface, ce qui permet l'utilisation d'un maillage structuré et d'une méthode éléments finis classique qui converge à l'ordre optimal. Cette méthode est par ailleurs assez simple à mettre en oeuvre ; elle aboutit à une formulation aux moindres carrés de la condition de continuité des vitesses à l'interface fluide-structure, pour laquelle des méthodes de minimisation classiques peuvent être utilisées. Un avantage de la méthode est aussi qu'elle permet naturellement de découpler les problèmes fluide et structure, et de les résoudre indépendamment sur des maillages différents. Le problème fluide est ainsi résolu sur un maillage fixe et structuré, non conforme à l'interface, alors que le problème structure peut être résolu de façon très précise sur un maillage indépendant qui ne couvre que la partie solide. La méthode est de ce fait particulièrement adaptée aux problèmes impliquant plusieurs structures de volume petit devant celui du fluide, comme c'est le cas dans le problème qui nous intéresse. Nous décrivons cette méthode en détail dans [47] pour des problèmes de transmission elliptiques plus généraux, et en particulier pour un problème fluide-structure linéaire. La méthode est essentiellement analysée au niveau continu et l'analyse numérique reste à faire. Il nous faut également optimiser les solveurs de résolution afin de tirer entièrement profit de la méthode, en utilisant notamment des solveurs rapides adaptés aux maillages structurés, avant de l'appliquer à notre problème d'interaction fluide-structure active.

Chapitre 4 : Quelques écoulements inertiels à frontières libres ou mobiles

Le dernier chapitre de ce mémoire regroupe plusieurs travaux que j'ai effectués en parallèle de mes recherches sur les fluides actifs, en collaboration avec plusieurs chercheurs, notamment d'autres disciplines. Ils concernent cette fois-ci des écoulements où les effets inertiels sont importants et ne peuvent être négligés ; mais ils ont en commun avec les travaux présentés dans les chapitres précédents de traiter d'écoulements à frontières libres ou mobiles, et les outils numériques permettant de gérer les interfaces mobiles sont similaires.

Je présente tout d'abord quelques travaux sur les écoulements hydrodynamiques à surface libre. Ceux-ci sont modélisés par les équations de Navier-Stokes écrites dans un domaine qui se déplace dans la direction verticale, la surface libre étant considérée comme une fonction "univoque" du plan horizontal, ce qui exclut les déferlements. Le domaine mobile peut alors être défini à chaque instant $t \geq 0$ comme suit :

$$\Omega(t) = \{(x,z) \in \mathbb{R}^d \ / \ x \in \omega \quad \text{et} \quad b(x) < z < \eta(x,t)\},$$

où ω est un sous-domaine borné et fixe de $\mathbb{R}^{d-1}$ ($d = 2$ ou 3 étant la dimension du problème), et où $\eta(\cdot,t)$ et b sont deux fonctions définies sur ω qui décrivent respectivement la surface libre et le fond de l'écoulement. Les champs de vitesse $\mathbf{u}$ et de pression p dans l'écoulement sont gouvernés par les équations de Navier-Stokes posées à chaque instant $t \geq 0$ dans le domaine $\Omega(t)$ et qui s'écrivent, si l'on considère un fluide Newtonien à densité constante ρ :

$$\left\{ \begin{array}{rcl} \dfrac{\partial \mathbf{u}}{\partial t} \ + \ (\mathbf{u}\cdot\nabla)\mathbf{u} \ - \ \dfrac{1}{\rho}\nabla\cdot\left(\underline{\underline{\sigma}}(\mathbf{u},p)\right) & = & \mathbf{g}, \\ \nabla\cdot\mathbf{u} & = & 0, \end{array} \right.$$

où $\underline{\underline{\sigma}} = \ \nu(\nabla\mathbf{u} +^t \nabla\mathbf{u}) - p\mathbf{I}$ est le tenseur des contraintes.

La dynamique du domaine est gouvernée par la condition cinématique à la surface libre qui traduit le fait que les particules de fluide se trouvant à la surface y restent : soit $(x(t), z(t))$ la trajectoire d'une particule à la surface de l'écoulement au temps t, elle satisfait $z(t) = \eta(x(t),t)$ et $\dfrac{d}{dt}(\eta(x(t),t) - z(t)) = 0$, et l'on a donc

$$\frac{\partial \eta}{\partial t}(x,t) \ + \ u(x,z,t)\cdot\nabla\eta(x,t) \ = \ w(x,z,t), \qquad x \in \omega, \quad z = \eta(x,t).$$

Cette équation exprime le mouvement de la surface libre comme la convection de la fonction scalaire η, définie sur le domaine à une ou deux dimensions ω, à la vitesse horizontale u évaluée à la surface libre, avec un terme source égal à la vitesse verticale correspondante w. Ce qui peut aussi s'écrire sous la forme simple :

$$\frac{\partial \eta}{\partial t} \ = \ \mathbf{u}\cdot\frac{\mathbf{n}}{n_z},$$

où $\mathbf{n}$ est la normale unitaire sortante à la surface libre, et n_z sa composante verticale. Le système est fermé par des conditions limites appropriées aux autres frontières, typiquement des conditions d'imperméabilité et de frottement s'il s'agit de parois :

$$\mathbf{u} = 0, \qquad (\sigma \cdot \mathbf{n})^T \cdot \mathbf{t} \;=\; -c_f(\mathbf{u})\,\mathbf{u} \cdot \mathbf{t},$$

où $c_f(\mathbf{u})$ est un coefficient de frottement dépendant de la vitesse du fluide près de la paroi et $\mathbf{t}$ désigne une matrice composée de deux vecteurs tangents au bord (si l'on est en 3d).

Lorsque le rapport entre les échelles verticale et longitudinale est suffisamment petit, l'approximation des eaux peu profondes (dite *Shallow Water*) est généralement introduite et les équations tridimensionnelles sont réduites à un système bidimensionnel ou unidimensionnel, de façon à réduire le coût de calcul (voir par exemple [154]). On considère alors les équations de Saint-Venant, dont les variables sont la hauteur d'eau ou l'aire de la section orthogonale à l'écoulement (notée A) et le débit Q, ces deux variables dépendant du temps et de la coordonnée longitudinale. En dimension 1 ces équations s'écrivent :

$$\left\{\begin{array}{l} \dfrac{\partial Q}{\partial t} \;+\; \dfrac{\partial}{\partial x}\left(\beta \dfrac{Q^2}{A}\right) + \; gA\dfrac{\partial \eta}{\partial x} \;=\; -\,\alpha Q \\ \dfrac{\partial A}{\partial t} \;+\; \dfrac{\partial Q}{\partial x} \;=\; 0, \\ \end{array}\right.$$

où β est le coefficient de correction du moment et α le coefficient de frottement. Afin que ce système soit fermé il faut ajouter une relation entre l'aire de la section A et la surface libre η en chaque point. Une version avec termes visqueux de ce système a été dérivée formellement par analyse asymptotique dans [67], à partir des équations de Navier-Stokes à surface libre bidimensionnelles. Les effets visqueux sont pris en compte dans un terme de frottement et un terme de diffusion 1*d*. Cependant, afin de pouvoir faire des simulations réalistes, il est nécessaire de considérer un écoulement tridimensionnel et turbulent. Ainsi, nous avons présenté dans [42] une dérivation asymptotique du modèle pour eaux peu profondes habituellement utilisé en hydraulique fluviale, à partir des équations de Navier-Stokes moyennées (en anglais Reynolds-Averaged Navier-Stokes equations, ou RANS) tridimensionnelles, qui intègrent des modèles de turbulence. Il s'agit d'un travail réalisé en collaboration avec Luca Bonaventura et Fausto Saleri (*MOX, Politecnico di Milano*) ; la dérivation est effectuée à l'ordre 2 en ϵ, le rapport entre la hauteur d'eau et la taille du domaine 2d, et prend en compte les effets de frottement non-linéaires et les différentes viscosités turbulentes. Si l'on applique le modèle que nous avons obtenu à un cas simple où la section de l'écoulement est rectangulaire, on retrouve le système de Saint Venant classique décrit plus haut, à l'exception du terme de frottement. Notre dérivation montre en effet qu'afin de prendre en compte les effets d'ordre deux, il faut corriger le terme de frottement classique par un terme qui dépend de la viscosité turbulente verticale. Ce résultat est consistant avec les formules empiriques classiquement utilisées pour ce modèle (voir par exemple [32]), et en constitue ainsi une justification *a posteriori*. De plus, il permet de déterminer le terme de frottement à utiliser dans les cas où ces formules asymptotiques ne sont pas valables.

Dans la suite du chapitre je détaille deux approches différentes pour résoudre numériquement les équations de Navier-Stokes à surface libre. Cela me permet en passant de détailler dans un cas particulier l'utilisation du formalisme ALE pour le suivi de frontières ou interfaces mobiles. En effet les deux approches présentées reposent sur une approximation par éléments finis sur des maillages conformes au domaine fluide à chaque instant. Le maillage tridimensionnel initial est obtenu en empilant le maillage horizontal sur une certaine quantité de couches du fond à la surface. Puisqu'il ne bouge que dans la direction verticale, ceci permet de conserver un maillage structuré dans la direction verticale à chaque pas de temps et ainsi réduire les coûts de calcul.

La première approche, que nous décrivons dans [48], me semble être la plus simple et la plus naturelle : à chaque pas de temps, la surface libre est tout d'abord convectée, ce qui permet de mettre à jour le domaine, puis les équations de Navier-Stokes sont résolues dans le nouveau domaine avec un schéma que l'on peut choisir selon les propriétés que l'on désire conserver au niveau discret (conservation de la masse, positivité de la hauteur d'eau, possibilité d'utiliser de grands pas de temps...). Nous utilisons par exemple une méthode des caractéristiques pour la convection de η dans le domaine ω ; et un schéma semi-implicite et semi-Lagrangien pour résoudre les équations de Navier-Stokes à chaque pas de temps. La convection des vitesses est traitée par une méthode des caractéristiques en formalisme ALE décrite en détail dans le chapitre. Le problème de Stokes généralisé obtenu après discrétisation en temps est résolu en formulation mixte avec des fonctions éléments finis stables pour la condition inf-sup (voir [125],[19]). L'avantage de ce schéma est qu'il est inconditionnellement stable, c'est-à-dire qu'il n'y a pas de restriction de type CFL (Courant Friedrichs Lax) sur le pas de temps [113]. L'utilisation de grands pas de temps est ainsi tolérée et les états stationnaires, s'ils existent, sont atteints rapidement. Cependant, il ne conserve pas la masse d'eau exactement, ce qui est un défaut important pour les applications en hydraulique. Dans le cadre de la thèse de Pierrick Quemar [126], nous avons proposé un algorithme alternatif qui rectifie ce défaut, et pour lequel nous pouvons démontrer un résultat de stabilité de la solution du problème discrétisé en temps et en espace, sous des hypothèses assez fortes sur la régularité du domaine et du maillage. Cependant, nous perdons le caractère inconditionnel de la stabilité du schéma, qui est soumis à une CFL associée aux pas de discrétisation horizontaux (Δx et Δy).

La deuxième approche est celle utilisée dans plusieurs codes résolvant ces équations pour l'hydraulique fluviale ou maritime [25, 26], et notamment le logiciel Telemac3d [79], qui a été analysé par P. Quemar pendant sa thèse. Cette approche est basée sur une décomposition de la pression en pression hydrostatique et correction de pression dynamique, qui tire profit du fait que le maillage est structuré sur la verticale. Avec cette décomposition, la variable surface libre η apparaît explicitement dans les équations de quantité de mouvement. Les équations sont résolues en utilisant une méthode de projection dans l'esprit de la méthode de Chorin-Temam (voir par exemple [72]), ce qui revient à résoudre d'abord une étape de prédiction hydrostatique, dans laquelle la vitesse et la surface libre satisfont l'hypothèse de pression hydrostatique, puis corriger la vitesse en utilisant la pression dynamique comme multiplicateur de Lagrange associé à la contrainte de divergence nulle. De nombreux auteurs ont procédé à cette décomposition car elle permet de traiter les écoulements hydrostatiques en ne résolvant que l'étape de prédiction d'une part, et d'autre part elle permet de réduire le coût de calcul pour les écoulements non-hydrostatiques. En effet, la procédure souvent utilisée est basée sur un traitement explicite du terme de diffusion horizontale, ce qui permet de remplacer l'étape hydrostatique par une équation portant seulement sur la variable 2d η, et l'étape de correction, qui correspond à la résolution d'un problème de Darcy, peut être résolue en résolvant simplement un problème de Poisson sur la pression. De plus, les deux systèmes ainsi obtenus ne nécessitent pas d'utiliser des éléments finis satisfaisant la condition discrète inf-sup pour admettre une solution unique. Cependant, cette stratégie, qui vise essentiellement à réduire le coût de calcul de l'algorithme, présente plusieurs inconvénients importants que je détaille dans le chapitre. Des tests numériques mettent notamment en évidence la forte diffusion numérique introduite par cette approche.

Le travail présenté ensuite concerne l'étude numérique d'une nouvelle instabilité oscillatoire observée expérimentalement par B. Semin et ses collaborateurs (*Laboratoire FAST, Université*

Paris Sud) sur un cylindre confiné dans un écoulement inertiel [140]. Afin d'aider à mieux comprendre le mécanisme sous-jacent, nous avons effectué des simulations numériques à l'aide d'une méthode éléments finis sur maillage mobile et conforme à la géométrie du cylindre à chaque pas de temps. Cette méthode permet d'obtenir une bonne précision et l'instabilité est correctement reproduite. Nos simulations ont notamment permis de calculer les forces hydrodynamiques sur le cylindre pour différentes valeurs de la densité du cylindre et du nombre de Reynolds, et ainsi mieux caractériser l'instabilité. La dernière partie de ce chapitre concerne une collaboration avec des chercheurs du laboratoire *IR4M (Imagerie par résonance magnétique et multi-modalités)* de l'*Université Paris Sud*, sur la caractérisation du flux sanguin dans l'aorte en combinant des simulations numériques et des données d'imagerie par résonance magnétique [89]. L'un des buts de ce travail est de trouver un moyen d'estimer la pression dans l'artère de façon non invasive, question récurrente et difficile dans ce domaine. Nous avons travaillé sur un modèle 1D pour les écoulements sanguins dans les artères déjà bien connu dans la littérature. Il s'agit d'un système de lois de conservations hyperboliques, et nous avons utilisé un schéma au volumes finis classique d'ordre 2 pour le résoudre. L'une des difficultés que nous avons rencontré est le traitement des conditions limites. En effet, quand il s'agit de faire des comparaisons avec l'expérience, les conditions limites standard ne conviennent plus, et il faut chercher à modéliser le plus finement possible ce qui se passe aux interfaces. L'autre difficulté importante est l'estimation des caractéristiques physiques de la parois artérielle, qui interviennent en paramètre du modèle 1d. Les chercheurs de l'IR4M ont développé une technique expérimentale pour mesurer de façon non invasive la compliance des artères. Ce sont ces mesures que nous utilisons dans le modèle numérique, et elles ont permis d'obtenir des résultats en bon accord avec les résultats expérimentaux

Travaux en cours et perspectives

La dernière partie de ce manuscrit est dédiée à la description de quelques travaux en cours et de mes perspectives de recherche pour le futur. J'y décris tout d'abord l'étude en cours sur la brisure au niveau macroscopique de la symétrie temporelle des équations microscopiques dans nos simulations de suspensions actives. Puis je présente un projet en cours depuis quelques années en collaboration avec Jean-Baptiste Lagaert (*LMO, Université Paris Sud*) et des médecins du *Centre Hépato-Biliaire de l'Hôpital Paul Brousse*, ainsi qu'un biologiste de l'*Université Paris Sud*, sur la modélisation mathématique de la régénération du foie. Nous travaillons en ce moment sur un modèle d'Edo permettant d'étudier l'interaction entre le processus de régénération du foie et la circulation entérohépatique des acides biliaires. Mes projets de recherche pour les années à venir concernent en premier lieu la modélisation des fluides actifs entraînés par des cils, et en particulier celle du transport mucociliaire. Je souhaite notamment développer, à partir de nos travaux préalables sur le sujet, un véritable outil numérique pour la simulation directe efficace et robuste de fluides faisant intervenir un grand nombre de cils actifs. Enfin, un nouveau projet est en train de débuter dans lequel je souhaite m'investir activement. Il s'agit d'une collaboration avec des chercheurs du laboratoire *BioMaps (Laboratoire d'imagerie biomédicale multimodale Paris-Saclay)*, spécialistes d'imagerie médicale, qui s'intéressent à la modélisation de la perfusion tumorale. Notre objectif est de développer un modèle numérique capable de représenter, à partir d'images IRM, le réseau de vascularisation d'une tumeur et de résoudre l'écoulement fluide et le transport de l'oxygène dans les micro-vaisseaux et dans les tissus.

Chapitre 1

Direct numerical simulation of active suspensions

In this chapter I present a joint work with Sébastien Martin (MAP5, Université Paris Descartes) and Bertrand Maury (LMO, Université Paris Sud) on the direct numerical simulation of suspensions of micro swimmers [1, 44, 45]. The study of collective dynamics in active suspensions can be done at different levels : experimental, analytical/theoretical and numerical. From a mathematical point of view, most of the models proposed and analyzed, in particular to study the chemotactic behavior of active suspensions, are macro- or mesoscopic (kinetic) models, which take into account the swimming of microorganisms in an averaged way. These models involve some parameters that are not directly accessible, such as the effective viscosity of the suspension. We are interested in the modeling and the simulation of these suspensions at the microscopic level. Such an approach seems essential to us because it allows to better understand certain phenomena from a more elementary point of view, and thus to validate or improve the macroscopic models. Our goal is to use sufficiently simple models and sufficiently efficient and robust numerical methods to simulate active suspensions with the largest possible number of active entities, while ensuring sufficient accuracy of both the model and the approximation so that the essential ingredients that play a role in the collective dynamics are taken into account.

1.1 Introduction

This work deals with the direct numerical simulation of suspensions of micro swimmers, that can be artificial or alive like self-propelled bacteria and algae. The important point these swimmers have in common is that they are so small that, at their scale, the fluid is essentially viscous and inertial effects can be neglected when describing their locomotion. They live in the low Reynolds regime ($\mathrm{Re} \sim 10^{-2}$), and thus they can only swim by moving their body or flagella in a way that is not symmetric under time reversal (see [35, 104] and references therein). Indeed, due to the absence of inertia, whatever forward motion is produced, it will be exactly canceled by the same backward motion. Mathematically, this can be explained by the symmetry under time reversal of the Stokes equations governing viscous flows.

Different types of micro swimmers can be considered, presenting different cell shapes, sizes and types of motility. The most studied micro-organisms that are able to swim in a viscous fluid are the self-propelled bacteria *Escherichia coli* and *Bacillus subtilis*. These are very common bacteria that can be found in digestive tracts of animals, or in soil and water. Individual cells of these bacteria are rod-shaped (length of order $2-4\mu$m, diameter of order 1μm) and they have long helical flagella, randomly distributed over their body and attached to motors within the cell membrane [104, 148], that are responsible for propulsion. They push themselves forward, and therefore they are usually classified as "pushers". Another type of intensively studied swimming micro-organism is *Chlamydomona reinhardtii*, an algae that pulls itself forward thanks to two short cilia attached to the front of their body, and that perform a breath stroke which is asymmetric in time and thus allows for a net displacement in the forward direction. These swimmers are qualified as "pullers".

It has been observed that above a certain concentration, the global motion of active suspensions highly differs from the sum of individual motion. Actually, intriguing collective dynamics can emerge, depending on the concentration but also on the type of activity and the shape of the swimmers. These dynamics appear in different forms : the most struggling, easily observable, is the emergence of collective patterns in bacterial suspensions, such as jets and whirls, whose size is much larger than the size of the individual swimmers ; the ratio can attain one order of magnitude (see for instance [53]). In nearly close-packed suspensions, one can observe large swimming structures that move chaotically, giving the appearance of turbulence. Furthermore the velocity of the flow is significantly enhanced by these dynamics, with collective flow speeds that can exceed the speed of the individual bacterium by an order of magnitude [147]. Other observable patterns can emerge in such suspensions, based on the bioconvection phenomenon [120]. In shallow suspensions for instance, chemotactic active cells like self-propelled bacteria swim upward toward the oxygen-rich air/fluid interface. Since they are denser than water, accumulation at the interface results in an unstable gradient of mean fluid density, creating convective dynamics and instabilities of the Rayleigh Taylor type (see for instance [121]). But the most spectacular effects pertain to abnormal rheological behaviors in sheared flows : the apparent viscosity of an active suspension may be higher or smaller than the corresponding passive suspension, depending on the type of motility, the cell's shape and the concentration. Experimental studies have evidenced a decrease of the effective viscosity in suspensions which include swimmers that push themselves forward as for instance *Bacillus subtilis* and *Escherichia coli*, see [146]. Conversely one may observe an increase of the effective viscosity in suspensions which include swimmers that pull themselves forward like *Chlamydomonas reinhardtii*, see [129].

Many essential questions arise when observing these collective dynamics. The most controversed is whether hydrodynamic interactions alone are sufficient to generate these turbulence-like structures. Another interesting question is how these dynamics depend on the different parameters of a suspension, like concentration, cell's geometry, and type of motility. In particular, do spherical swimmers also generate coherent structures at high concentration ? Do pullers act like pushers on the fluid when the volume fraction is high ?

Interestingly, asymptotic analysis in the dilute and semi-dilute regimes [77] have shown that an active suspension results in a change in viscosity if there is an anisotropy in the orientation distribution of the microswimmers. Such an anisotropy appears in suspensions of elongated pushers or pullers, when the concentration is high enough and hydrodynamic interactions between the swimmers lead to particular alignments [121]. Numerical studies performed in dilute to moderate concentration regimes have confirmed these observations [133, 77, 84]. In previous works, different strategies were used : for instance in [133, 134] elongated cells were considered but near-field interactions were strongly limited ; in [85, 83, 82, 120] a database of pairwise interactions in simulations of a suspension of many spherical swimming cells was used as in the Stokesian Dynamics method, hence using a better approximation of the close-range interactions. A more recent work by Delmotte and coauthors [50] uses a finite force-multipole expansion to perform large-scale simulations of active suspensions in moderate concentration regimes. However these approaches introduce severe limitations in the description of the multi-body interactions which play a crucial role in the behaviour of near close-packed microstructures. Our work in-tends to demonstrate how direct simulation using efficient and robust numerical methods can help understanding and predicting the collective dynamics arising in suspensions of swimming micro-organisms. In particular direct simulation aims at solving numerically the fundamental equations coupling the motion of many individual swimmers and a viscous fluid : the only modeling assumption relies on the self propulsion mechanism of a micro-swimmer but hydrodynamic interactions are solved directly preserving the strongly coupled fluid-structure interaction, without neglecting the far-field nor the near-field interactions. In particular lubrication forces are not neglected, they can be resolved at an arbitrary precision that depends on the local mesh size.

We perform 2D simulations and discuss both the generation of coherent structures and the rheology properties of the suspensions from dilute to concentrated regimes. The differences between pushers and pullers are evidenced, as well as the impact of the geometric form of the swimmer, highlighting the intrinsic importance of the type of motility and elongation in the collective behaviour of the resulting active fluid.

1.2 Microscopic model

“Pushers” are swimmers whose flagellar apparatus is located at the back of the cell body. The flagella generate a thrust force at the back which is cancelled by the drag force on the cell body in the front. In contrast, “pullers” typically propel themselves through flagella attached at the front of their cell body that execute a breaststroke-like motion. We model each micro-organism as a rigid ellipsoidal particle moving in the fluid. The flagella are not materialized ; we only take into account the resultant force they exert on the particles and on the fluid. In fact, the complex movement of the locomotion structures results in an effective force acting on the fluid in a zone with non-zero volume, downstream (in the case of pushers), or upstream (in the case of pullers) of the organism. Therefore we associate to each swimmer a dipole of forces, homogeneously distributed on the rigid body and on an elongated ellipsoidal region in the fluid representing the location of the flagella appendage.

More precisely, the swimmer’s body is represented by an ellipsoid B and the force exerted by the flagellar bundle on the fluid is supported in a very elongated ellipse P, placed at a constant distance from the bacterial body. The propulsion force $\mathbf{F}_B$ is directed outward from the center of B, parallel to the majorsemiaxes of B and P, and has some orientation angle θ, as shown in Figures 1.1 and 1.2.

A suspension is modeled by N swimmers in a two-dimensional domain $\Omega \subset \mathbb{R}^2$ filled with a Newtonian fluid governed by the Stokes equations. Denoting by $(B_i)_{i=1,\dots,N}$ the rigid particles representing the body of the swimmers, strongly included in Ω (see right in Figure 1.1), and by $B = \cup_i B_i$ the whole rigid domain, the suspension has a volume concentration of $\phi = |B|/|\Omega|$, where $|\omega|$ denotes the measure of a domain ω . At the initial time the particles are distributed randomly over the fluid (without overlapping). The position of the center of the ith particle is denoted by $\boldsymbol{x}_i$, and by $\mathbf{v}_i$ and ω_i its translational and angular velocities.

The total force exerted on the fluid by the ith organism has a constant magnitude f_P and is denoted by $\mathbf{F}_{P_i}$:

$$\mathbf{F}_{P_i} = -f_P \boldsymbol{\tau}_i = \int_{P_i} \mathbf{f}_{P_i} \,\mathrm{d}\boldsymbol{x}, \quad \text{with} \quad \mathbf{f}_{P_i} = -\frac{f_P}{|P_i|}\boldsymbol{\tau}_i,$$

where $\boldsymbol{\tau}_i$ is given by the orientation angle θ_i. Since each swimmer is force and torque-free, the

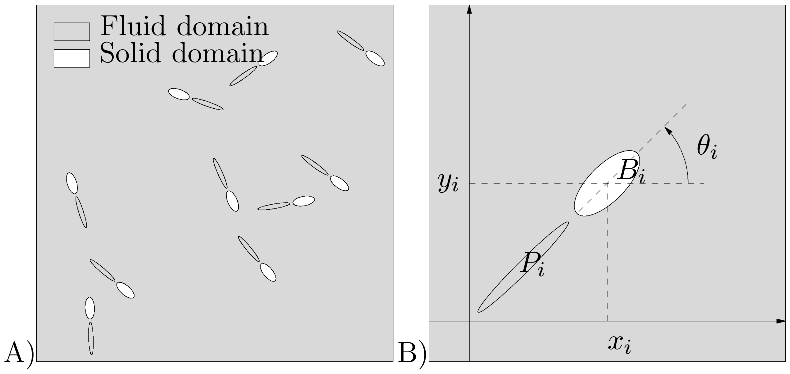

Figure 1.1 – A) Domain Ω is made of a solid domain B (collection of rigid bodies of the bacteria) and a fluid domain $\Omega \setminus B$. B) Each bacterium is modeled by a rigid body B_i. Its position is characterized by the coordinates $\mathbf{x}_i = (x_i, y_i)$ of its center of mass and its orientation θ_i. The action of the flagellar bundle over the fluid is located at a fluid region P_i which can be deduced from the position of the rigid body.

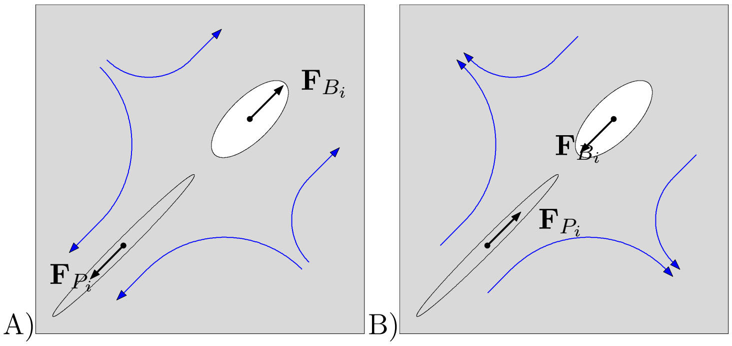

Figure 1.2 – Individual models of microswimmers. A) a pusher is represented by a rigid body and a flagellar area. B) A puller can be modeled by inverting the propulsion force.

total force exerted by the flagella on B_i, denoted by $\mathbf{F}_{B_i}$, is equal to $-\mathbf{F}_{P_i}$, and we can write :

$$\mathbf{F}_{B_i} = f_P \boldsymbol{\tau}_i = \int_{B_i} \mathbf{f}_{B_i} \, \mathrm{d}\boldsymbol{x}, \quad \text{with} \quad \mathbf{f}_{B_i} = \frac{f_P}{|B_i|} \boldsymbol{\tau}_i.$$

The Reynolds number is typically less than 10^{-2} (see for instance [10, 148]), therefore inertial effects can be neglected and the fluid flow is described by the Stokes equations :

$$\left\{ \begin{array}{rcll} -\nabla \cdot \underline{\underline{\sigma}}(\mathbf{u}, p) & = & \mathbf{f}_f & \text{in} \quad \Omega \setminus \bar{B}, \\ \nabla \cdot \mathbf{u} & = & 0 & \text{in} \quad \Omega \setminus \bar{B}, \end{array} \right. \tag{1.1}$$

where $\mathbf{u}$ and p are the velocity and pressure field in the fluid, and where the stress tensor $\underline{\underline{\sigma}}$ writes

$$\underline{\underline{\sigma}} = 2\mu \mathbb{D}(\mathbf{u}) - p\,\mathbb{I}, \quad \text{where} \quad \mathbb{D}(\mathbf{u}) = \frac{\nabla \mathbf{u} + (\nabla \mathbf{u})^T}{2}$$

since we consider a Newtonian fluid. This system is completed by specific boundary conditions : no-slip boundary conditions on the boundary ∂B_i of each rigid particle :

$$\mathbf{u} = \mathbf{v}_i + \omega_i \times (\boldsymbol{x} - \boldsymbol{x}_i) \text{ on } \partial B_i, \, \forall i \in \{1, ..., N\}, \tag{1.2}$$

and some Dirichlet or periodic conditions on $\partial\Omega$. The forces considered on the fluid are the forces exerted by the flagella :

$$\mathbf{f}_f = \sum_{i=1,\dots,N} \mathbf{f}_{P_i} \chi_{P_i},$$

where χ_{P_i} is the characteristic function associated to the region P_i and χ_{B_i} is the characteristic function associated to the particle B_i. Finally, force and torque balance for each body writes :

$$\left\{ \begin{array}{rcll} \displaystyle\int_{B_i} \rho \mathbf{g} + \int_{B_i} \mathbf{f}_{B_i} - \int_{\partial B_i} \underline{\underline{\sigma}} \cdot \mathbf{n} & = & 0 & \forall i \in \{1, ..., N\}, \\ \displaystyle\int_{\partial B_i} (\boldsymbol{x} - \boldsymbol{x}_i) \times \underline{\underline{\sigma}} \cdot \mathbf{n} & = & 0 & \forall i \in \{1, ..., N\}, \end{array} \right. \tag{1.3}$$

where ρ denotes the buoyant density of swimmers, which is positive since these are slightly denser than the fluid, and $\mathbf{g} = (0, -g)$ is gravity.

The motion of each bacterium B_i is then set by its instantaneous velocity :

$$\mathbf{u}(\boldsymbol{x}, t) = \mathbf{v}_i(t) + \omega_i(t) \times (\boldsymbol{x} - \boldsymbol{x}_i(t))$$

defined on ∂B_i. More precisely, the individual translational velocity is equal to the average velocity :

$$\mathbf{v}_i(t) = \frac{1}{|\partial B_i(t)|} \int_{\partial B_i} \mathbf{u}(t, \boldsymbol{x}) \, \mathrm{d}\boldsymbol{x}, \tag{1.4}$$

and the individual angular velocity is equal to

$$\omega_i(t) = \frac{1}{|\partial B_i(t)|} \frac{\displaystyle\int_{\partial B_i} \mathbf{u}(t, \boldsymbol{x}) \times (\boldsymbol{x} - \boldsymbol{x}_i(t)) \, \mathrm{d}\boldsymbol{x}}{\displaystyle\int_{\partial B_i} |\boldsymbol{x} - \boldsymbol{x}_i(t)|^2 \, \mathrm{d}\boldsymbol{x}}. \tag{1.5}$$

The swimmers dynamics are then set by the differential equations :

$$\dot{\boldsymbol{x}}_i(t) = \mathbf{v}_i(t)\,, \qquad \dot{\theta}_i(t) = \omega_i(t). \tag{1.6}$$

These introduce a dependency in time into the problem : Stokes equations are steady, but their solution depends on time because the configuration of the swimmers inside the fluid varies in time.

1.3 Numerical scheme

The coupled fluid-particle problem is solved using a specific numerical method, based on the finite element method applied to solve a classical Stokes problem in the whole domain Ω, and a penalty method to enforce the rigid motion constraint inside the rigid domain B. Eventual numerical overlap between rigid particles due to errors in the solution of the Stokes equations must be prevented in order to guarantee robustness of the simulations. We use a numerical method proposed in [114], where inelastic collisions between rigid particles are computed. Denoting by $\Delta t > 0$ the time step, the fluid-particle problem (1.1)-(1.3) is solved at each time step $t = t^n = n\Delta t$, allowing to compute an approximation of the translational and angular velocities $\mathbf{v}_i^n$ and ω_i^n for each swimmer. The position and orientation of each swimmer at time t^{n+1} can then be updated by solving the ODEs (1.6) using for instance a first order explicit Euler method :

$$\boldsymbol{x}_i^{n+1} = \boldsymbol{x}_i^n + \Delta t\, \mathbf{v}_i^n\,, \qquad \theta_i^{n+1} = \theta_i^n + \Delta t\, \omega_i^n. \tag{1.7}$$

The time algorithm reads as follows : in a first step, the fluid-particle problem is solved without taking into account the possible overlapping of the particles (thus defining an *a priori* velocity of the swimmers), then the projection of this *a priori* velocity onto the set of admissible velocities is computed. Finally, the position and orientation of each swimmer is updated.

A fictitious domain approach

Our purpose is to avoid mesh generation of the moving and complex fluid domain, therefore we choose a fictitious domain approach. One possibility is to use an iterative algorithm on an auxiliary field, composed by Lagrange multipliers, which warrants the rigid motion constraint of the particles (see for instance [71, 70]). An alternative to this are penalty methods : the rigid motion constraint is obtained by relaxing a term in the variational formulation, what amounts to replace rigid zones by highly viscous ones (see [87, 99, 153]). In this work we choose a penalty method already used in [99] for the simulation of passive particles in a fluid.

Let us first introduce the following constrained functional spaces :

$$K_\nabla \;=\; \left\{\mathbf{u} \in H_0^1(\Omega),\ \nabla\cdot\mathbf{u} = 0\right\}, \quad K_B \;=\; \left\{\mathbf{u} \in H_0^1(\Omega),\ \mathbb{D}(\mathbf{u}) = 0 \text{ a.e. in } B\right\}.$$

K_∇ is the space of divergence free functions defined on Ω and K_B is the space of functions which do not deform B. The solution to the initial problem, defined on $\Omega \setminus \bar{B}$, can be extended on the whole domain Ω by a function in K_B : $\mathbf{u}(\boldsymbol{x},\cdot) = \mathbf{v}_i + \omega_i \times (\boldsymbol{x} - \boldsymbol{x}_i)$ in B_i for every i, and we still denote this extension by $\mathbf{u}$. The problem in variational form can then be written as the minimization of the functional

$$J(\mathbf{u}) \;=\; \mu \int_\Omega |\mathbb{D}(\mathbf{u})|^2 \;-\; \int_\Omega \mathbf{f}\cdot\mathbf{u}$$

on $K_B \cap K_\nabla$, where

$$\mathbf{f} = \sum_{i=1}^{N} \left(\mathbf{f}_b^i\,\chi_b^i + \mathbf{f}_p^i\,\chi_p^i\right).$$

The rigid motion constraint is relaxed by introducing the following penalty term in the functional to minimize :

$$\int_B \frac{1}{\varepsilon}\,\mathbb{D}(\mathbf{u}) \,:\, \mathbb{D}(\mathbf{u}),$$

so that $\mathbb{D}(\mathbf{u})$ goes to zero in B when ε goes to zero and $\mathbf{u}$ tends to a rigid motion in B.

The variational formulation obtained is : find $\mathbf{u}_\epsilon \in H_0^1(\Omega)$ and $p \in L_0^2(\Omega)$ such that

$$\left\{ \begin{array}{rcll} 2\mu \displaystyle\int_\Omega \mathbb{D}(\mathbf{u}_\epsilon) : \mathbb{D}(\widetilde{\mathbf{u}}) + \frac{2}{\varepsilon}\int_B \mathbb{D}(\mathbf{u}_\epsilon) : \mathbb{D}(\widetilde{\mathbf{u}}) - \int_\Omega p_\epsilon \nabla\cdot\widetilde{\mathbf{u}} & = & \displaystyle\int_\Omega \mathbf{f}\cdot\widetilde{\mathbf{u}}, & \forall \widetilde{\mathbf{u}} \in H_0^1(\Omega), \\ \displaystyle\int_\Omega q\,\nabla\cdot\mathbf{u}_\epsilon & = & 0, & \forall q \in L_0^2(\Omega), \end{array} \right. \tag{1.8}$$

It has been proven in [87] that, in this framework, the penalty method converges linearly in ε : the solution $\mathbf{u}_\epsilon$ of problem (1.8) converges to the solution $\mathbf{u}$ of the initial problem as ε vanishes, and the convergence is of order 1 in ε. We refer to [115] for a detailed analysis of a scalar version of this problem, which provides an error estimate for the space-discretized problem at the order $\varepsilon + h^{1/2}$.

However, this method is not applicable in 3 dimensions, because the penalty term strongly degrades the condition number of the matrix that has to be inverted at each time step (and which comes from the penalized Stokes problem). An iterative method would therefore converge too slowly for solving the associated linear system, and since direct methods involve the storage of matrices their use is not reasonable in 3 dimensions. Other fictitious domain methods must be used if one wishes to make direct simulations of active suspensions in 3d, like for example the method proposed in [60] for passive suspensions. Another possibility is to use a suitable preconditioner as in [31].

Contact algorithm

Assuming, as we did in our model, that particle surfaces are smooth and that Stokes model is valid at any scale, it is known that contacts are not supposed to happen (see [66, 80]). Yet in actual simulations, collisions between particles are likely to occur. From a numerical point of view, it means that the particles may overlap when their positions are updated after the velocity field computation. The treatment of possible overlaps is even more important in the case of dense suspensions, if we want to avoid small time steps. For that purpose we use a numerical method introduced in [114] in the context of dry granular flows, with inelastic collisions between grains. We propose to integrate this approach in the wet situation. The interest in the procedure relies on the possibility to use any suitable solver for the computation of the dynamics. Contacts are handled at a second stage, without any consideration of the proper dynamics. The method consists of projecting the velocity field onto some convex admissible set depending on the current configuration, so that particles do not overlap. In this work, the contact algorithm has been extended to the case of ellipsoidal particles. Since no analytical expression of the minimal distance between two ellipses is available, an approximation of this distance must be computed at each time, by solving the problem of searching for the proximal points on a each pair of ellipsoidal particles.

1.4 Results and analysis of the collective dynamics

In this section we show how our model reproduces collective dynamics in moderate to dense 2D suspensions, and we assess the question of the dependency of these dynamics on the concentration, the geometry of the swimmers and the type of motility. After validating the numerical model on a certain amount of test cases for a passive particle (*i.e.* for $F_p = 0$), for which an analytical solution is available, we have tested the model for active particles.

Figure 1.3 represents the fluid flow and the streamlines near an isolated pusher-like swimmer. When inverting the propulsion force, a pusher becomes a puller with the same flow field in absolute value. It is qualitatively in agreement with the direct measurement of the flow field around microorganisms performed by Drescher and coauthors in [54]. The far-field flow produced by a swimmer very much resembles to the flow created by a force-dipole (see for instance [104]) : pushers repel fluid along the swimming axis and draw fluid in to the sides, whereas pullers draw fluid in along the elongated direction, and push fluid out from the sides. However, our computational model also takes into account hydrodynamics interactions at short range, which are important in the close interaction of swimmers, especially in dense suspensions.

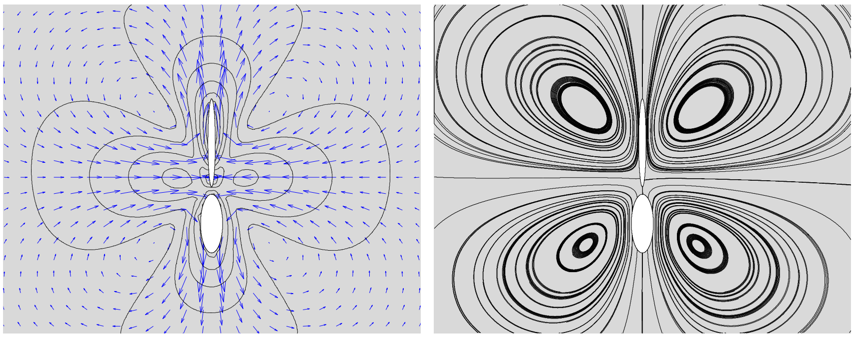

Figure 1.3 – Fluid flow velocity and streamlines near an elongated pusher-like swimmer in a fluid at rest. This model is used to mimic the behaviour of *Bacillus subtilis*.

Weak turbulence

The collective dynamics observed experimentally on monolayer films of bacterial suspensions [147] are qualitatively reproduced in our simulations. These have been performed in a square domain with a mesh of 250 nodes on each side has been used, so that, in average, there are around mesh cells per swimmer body. Figure 1.4 shows the results obtained running a simulation in a biperiodic domain with 1024 elongated pusher-like particles. The solid fraction attained in

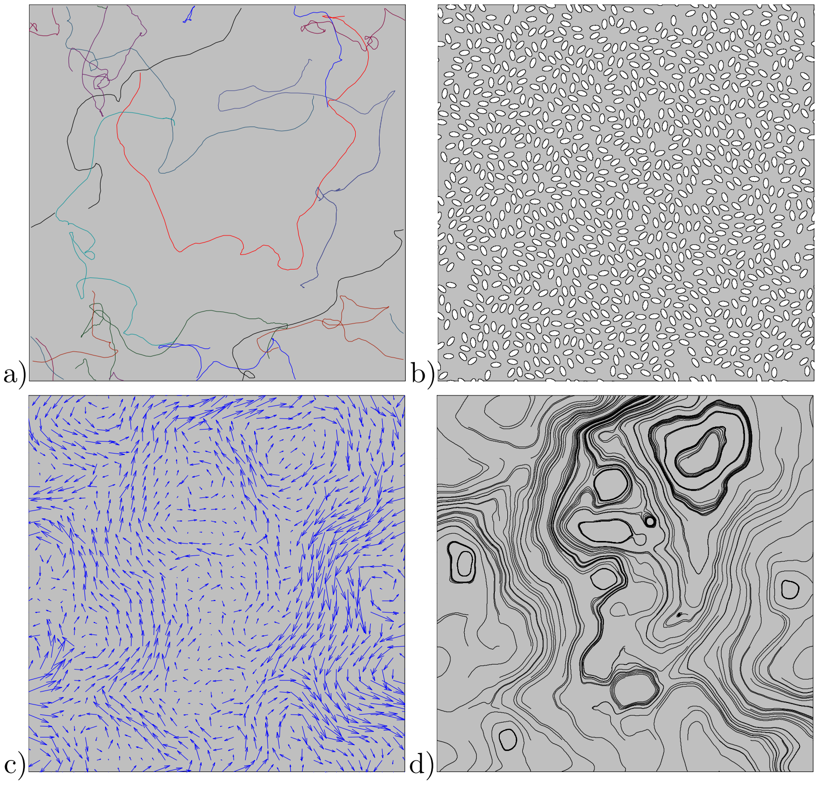

Figure 1.4 – Dense suspension of 1024 microswimmers (solid fraction : 28.9%) : a) trajectories of ten bacteria over 200 time steps. b) distribution of the bacteria at a given time step. c) velocity field at a given time step. d) streamlines at a given time step

the box is of 28.9%. Figure 1.4a) shows the trajectories of ten randomly chosen swimmers over 200 computational time steps. The chaotic trajectories are relevant of the strong hydrodynamic interactions occurring at this concentration, and the mixing effect they have. Figure 1.4b) shows the distribution of the active particles in the simulation box at a particular time far from the initial configuration, and Figures 1.4c) and d) show respectively the corresponding flow field and streamlines in the simulation domain. These results reveal the emergence of large structures in the flow, that move in a chaotic way. They can be compared to the experimental work of Aranson and coauthors [147], who have shown that patterns of chaotic large-scale flows emerge in a monolayer film of *Bacillus subtilis* bacteria above a certain concentration. In Figure 1.5 we have reported the evolution with increasing concentration of the mean velocity, *i.e.* the mean value of the modulus of the velocity in the domain. It shows that the collective flow speed can be highly increased by hydrodynamic interactions in moderate to dense suspensions, up to one order of magnitude, which is consistent with experimental observations [147]. Above a certain concentration it decreases due to congestion in dense suspensions. The emergence of the congestion phenomena is observed in experiments with a critical value of the concentration which is much larger than in our simulations : this is due to the two-dimensional modelling that leads to a more constrained collective response than in the three-dimensional setting. Figure 1.5 also shows that the collective dynamics of micro-swimmers drastically depend on the type of propulsion and on the geometry. In fact, above a certain concentration, the curves representing mean velocity for both swimmer types diverge in the case of elongated particles, and collective

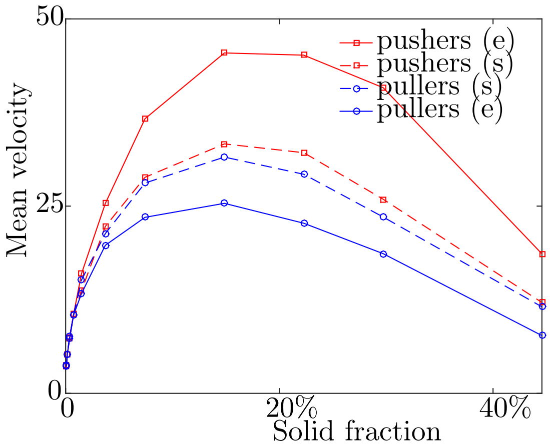

FIGURE 1.5 – Mean velocity (in $\mu\text{m}\cdot\text{s}^{-1}$) of the suspension for pushers and pullers : from dilute suspensions to dense suspensions. Two populations of swimmers : (e) ellipsoidal swimmers, (s) spherical swimmers.

velocities become much larger for pushers than for pullers. Theoretically there is no consensus whether cell elongation is necessary for collective motion. But experiments with spherical motile bacteria *Serratia marcescens* do exhibit collective dynamics and correlated coherent motion [127]. Our results also show evidence that sphericity of the bacteria does not alter the emergence of coherent structures even at moderate concentrations.

Rheological properties

A relevant issue in complex flows is the study of the rheological properties of a fluid, that characterize its resistance to gradual deformation by shear stress or tensile stress. The fluid's viscosity is defined through the relation between the strain rate and the viscous stress. A fluid is said to be Newtonian when the relationship is linear. In this case, the viscosity μ can be expressed as :

$$\mu = \frac{(\underline{\underline{\sigma}} \cdot \mathbf{n}) \cdot \boldsymbol{\tau}}{2(\mathbb{D}(\mathbf{u}) \cdot \mathbf{n}) \cdot \boldsymbol{\tau}}, \tag{1.9}$$

where $\underline{\underline{\sigma}}$ is the stress applied on the fluid and $\mathbb{D}(\mathbf{u})$ the strain rate tensor, p the pressure. For non-Newtonian fluids, where the relationship is not linear, it is not possible to define a constant viscosity μ. Typically, the quantity defined by (1.9) will depend on the type of flow considered, and it will vary with time. However, one can still characterize the response of the fluid to some particular forces. We focus on the study of the so-called shear-viscosity, which characterizes the response of the fluid when confined between two parallel rigid plates with a steady relative shear motion. In this case one can measure the shear stress, which is defined as the average force applied by the fluid on the plates per surface unit in response to this shear :

$$F = \frac{\int_\Gamma (\sigma \cdot \mathbf{n}) \cdot \boldsymbol{\tau}}{2L},$$

where Γ denotes the surface of the two plates, L denotes the length of each plate, $\mathbf{n}$ is the normal vector Γ pointing outward and $\boldsymbol{\tau}$ is the tangential vector on Γ opposed to the shear flow. In the case where the fluid is Newtonian, the flow is uniform in the x direction and linear in the y

direction. Following relation (1.9), the viscosity is then equal to the ratio of the shear stress to the shear rate. This definition is simply extended to the case of a suspension, and an apparent viscosity is defined as

$$\mu_{\text{app}}(t) = \frac{F}{\dot{\gamma}}, \tag{1.10}$$

where $\dot{\gamma}$ denotes the shear rate. The apparent viscosity is likely to vary in time, depending on the instantaneous configuration of the particles. Therefore one usually considers the effective viscosity :

$$\mu_{\text{eff}} = \lim_{T \mapsto +\infty} \frac{1}{T} \int_0^T \mu_{\text{app}}(t)\,\mathrm{d}t. \tag{1.11}$$

The effective viscosity of a suspension of passive spherical particles in a fluid of viscosity μ depends on its volume fraction ϕ. In the dilute regime, where $\phi \ll 1$ so that particles do not interact, the effective viscosity is well described by Einstein's relation

$$\mu_{\text{eff}} \approx \mu_0(1 + \alpha\phi), \tag{1.12}$$

where α is known as Einstein's coefficient (see for instance [9]) and depends on the dimension and on the elongation of entities. The linear dependency with respect to volume fraction is due to the fact that, in this regime, the total effect of the particles on the viscosity is equal to the sum of individual contributions. Beyond the dilute regime, particles interact and thus simple addition of contributions is no more valid. Work in the semi-dilute regime has focused on finding coefficients for the higher order terms in ϕ in a polynomial development of the form : $\mu_{\text{eff}} \approx \mu_0(1 + \alpha\phi + \beta\phi^2 + \dots)$.

In the case of active suspensions, the measurement or computation of the effective viscosity is particularly interesting, since different phenomena can arise depending on the type of motion. Elongated pusher-like swimmers, for instance, tend to decrease the effective viscosity [76], while spherical ones have no rheological signature [77, 84]. The different studies have shown that three ingredients are needed in order for self-propelled swimmers to produce a rheological signature : propulsion, elongation and hydrodynamic interactions. Our numerical simulations confirm these results. We have computed the effective viscosity in active suspensions of pusher- and puller-like swimmers using 2D simulations in which shear is imposed through non homogenous Dirichlet conditions and periodic boundary conditions are imposed on the left and right boundaries. Figure 1.6 shows the effective viscosity computed in simulations of pushers, pullers and passive particles, for concentrations up to little less than 45% volume fraction.

We can give a simple explanation of these results. Our simulations have shown that, in a planar shear flow, a single active particle (pusher or puller) rotates with the same angular velocity as a passive particle of same shape, while performing an ellipsoidal trajectory with characteristics depending on its individual velocity. The contribution to apparent viscosity due to its activity depends on the orientation of the force dipole. The contribution of an active particle to apparent viscosity is maximal when the dipole of propulsion forces is against the flow, and it is minimal when this dipole helps the flow. But since the time spent by a particle in each orientation is symmetric with respect to the neutral position (when the dipole is oriented parallel to the walls and apparent viscosity is equal to the passive case), the contribution to viscosity due to the activity vanishes when averaging over one period. Thus we obtain the same effective viscosity as in the passive case. In the dilute regime, since effective viscosity is a result of the sum of contributions of each particle, self-propulsion has no impact on the rheology of the

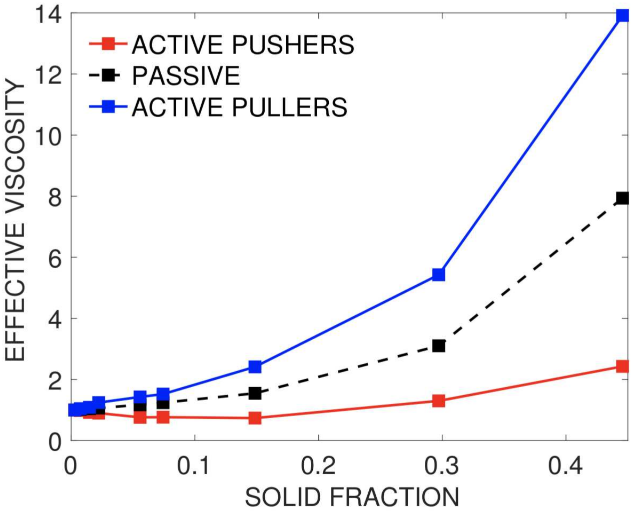

Figure 1.6 – Cubic fit of the effective viscosity with respect to the concentration in a suspension of pushers and pullers.

suspension. Beyond the dilute regime, hydrodynamic interactions disrupt the rotational behavior of individual swimmers. However, in the absence of a particular alignment of the active particles in the flow, the orientation of the population remains isotropic when averaging in time, and thus the effective viscosity remains the same as in the passive case. In fact, when the swimmers are spherical, activity of the particles has no impact on the effective viscosity. This is no longer true when the particles are elongated. Indeed if we look at the probability density function (pdf) of particle orientations obtained for the simulations with elongated particles we can see that the symmetry with respect to the neutral orientation is broken in the case of active and elongated particles. Due to interactions with the other particles, the latter tend to align in the flow at an orientation that maximizes their contribution to apparent viscosity in the case of pullers, and minimizes this contribution in the case of pushers. Thus effective viscosity is enhanced in the first case, and diminished in the second case.

Least-squares polynomial regression allows us to fit a polynomial of any degree to numerical data of the form $(\phi^{(1)}, \mu^{(1)})$, $(\phi^{(2)}, \mu^{(2)})$,..., $(\phi^{(N)}, \mu^{(N)})$. Thus we derive the expression of the effective viscosity with respect to the solid fraction ϕ as :

$$\mu_{\text{eff.}} \simeq \mu_0(1 + \alpha\phi + \beta\phi^2 + \gamma\phi^3 + ...).$$

Figure 1.6 shows the cubic fit obtained for the effective viscosity with respect to concentration in passive, pusher and puller suspensions. Table 1.1 provides the coefficients of the polynomial of order 3.

We have also investigated how the effective viscosity evolves when the ratio between activity of the micro swimmers and shear rate changes. For that purpose we introduce a non-dimensional number that characterizes the shear flow in presence of micro-swimmers :

$$\Phi = \frac{f_p}{\mu s},$$

$\eta_{\text{eff.}}$	α	β	γ
passive	$+4.3$	-21.8	$+105.6$
pushers	-5.4	$+26.2$	-15.5
pullers	$+9.8$	-32.9	$+170.3$

Table 1.1 – Coefficients of the mean-least-squares fit describing how the effective viscosity relates to the solid fraction

where f_p is the magnitude of the propulsion force, μ is the viscosity of the fluid and s the speed of the plates. For low values of the propulsion-shear ratio, the effective viscosity in pusher (resp. puller) suspensions decreases (resp. increases) in a non-linear way. But above a certain ratio, the effective viscosity stagnates, which is consistent with [76].

1.5 Chemotactic aspects

Bioconvection is an important issue for understanding the collective dynamics of microswimmers. In a suspension that is not saturated in oxygen, bacteria swim towards the fluid-air interface which is rich in oxygen. Since bacteria are about 10% denser than water, accumulation at the interface results in an unstable gradient under the effect of competition with gravity, thus creating convective dynamics. In a horizontal meniscus, these stratifications evolve into hydrodynamic instabilities described by plumes moving bacteria from the surface to the bottom.

We were particularly interested in two experiments [53, 150] presenting bioconvection dynamics in a suspension of *B. subtilis*. These experiments show in particular the influence of the geometry of the drop. Bacteria swim to the free surface and, under the influence of gravity, slide along the meniscus towards the bottom or fall back towards the bottom within unstable columns. A persistent hydrodynamic vortex reinforces the advection of oxygen in the suspension.

Run and tumble model

Bacteria like *E. Coli* perform chemotaxis by alternating two basic behaviours : a more or less linear motion called a run, and a highly erratic motion called tumble, the purpose of which is to reorient the cell (see [10]). Run times are typically much longer than the time spent tumbling, and they are closely related to the surrounding environment. In fact, when bacteria move in a favorable direction (i.e. in the direction of a nutrient) the run times are increased ; on the contrary, they are decreased when the direction is not favorable. These bacteria are too small to detect instantaneously spatial differences in the concentration of an attractant at their own length scale. Therefore they measure if they are going in the right direction by doing several successive evaluations of the concentration in time. The effect of alternating these two modes of behavior, and in particular, of increasing the run length when moving in a favorable direction, is that a bacterium executes a three-dimensional random walk with drift in a favorable direction when observed on a sufficiently long time scale [139, 121, 104, 8, 57, 103].

E. coli, for instance, have an average tumbling frequency of $\lambda = 1\ s^{-1}$. Denoting by c the concentration of the chemical attractant considered, the tumbling frequency can be described [104, 139] by :

$$\lambda(c) = \lambda_0 \left(1 - \int_{-\infty}^{t} c(s)\, R(t-s)\, \mathrm{d}s \right),$$

where λ_0 is the average tumbling frequency and R is a kernel that models the "memory" of the bacterium. Different kernel choices are used in the literature to model the memory effect. We have used a simplified model for the tumbling frequency that reads :

$$\lambda(c) = 1 - \varepsilon\, \phi \left(\frac{\mathrm{D}c}{\mathrm{D}t} \right), \tag{1.13}$$

were $\frac{\mathrm{D}c}{\mathrm{D}t}$ is the Lagrangian derivative of c along the trajectory of the bacterium, and ϕ is the sign function.

Although the swimming directions before and after a tumble are correlated, with a mean angle between both directions of $\sim 60°$ [10], we neglect this fact and in our model the bacterium randomly chooses a new orientation angle θ after each run.

Oxygen dynamics

In [49] we have considered oxygen as the only chemoattractant in the bacteria's environment. The dynamics of the oxygen concentration c are described by the following equation :

$$\frac{\partial c}{\partial t} + \mathbf{u} \cdot \nabla c - D_c\, \Delta c = -g(c, B), \tag{1.14}$$

where D_c is the oxygen diffusion coefficient, $\mathbf{u}$ the fluid velocity and $-g(c, B)$ is the sink term accounting for the oxygen consumption by the bacteria [150]. This term can be written as follows :

$$g(c, B) = \kappa\, f(c)\, \chi_B,$$

where κ is the volumic consumption rate (in oxygen molecules per second per volume of bacteria), χ_B is the characteristic function for the "bacterial" domain, and $c \to f(c)$ modulates this rate, going to 1 when c is large, but vanishing as c is smaller than a critical value. The motion of the bacteria is also related to the oxygen concentration since bacteria which do not consume enough oxygen loose their capacity of self-propulsing [150]. Therefore, the intensity of the self-propulsion force f_p is modulated by the so-called motility function $r(c)$ which is equal to unity at large c and vanishes rapidly for c below the motility cutoff c^*.

In order to simulate tumbling for each bacterium, we need to time-discretise a Poisson process with variable intensity (*i.e.* the frequency of tumbling λ). For that purpose, we set $\Delta t_T > 0$ a fixed time-step, and we define P_T the probability of a bacterium to tumble at least one time during Δt_T. This probability can be computed and depends on the values of Δt_T and λ :

$$P_T(\lambda, \Delta t_T) = 1 - \exp(-\lambda\, \Delta t_T)\ . \tag{1.15}$$

Now, for each bacterium, the frequency of tumbling λ varies in time following (1.13). Therefore, the value of P_T also varies in time, depending on the sign of the lagrangian derivative of the concentration $\mathrm{D}c/\mathrm{D}t$ evaluated by the bacterium along its trajectory. After each time-step Δt_T, each bacterium performs a random reorientation (a tumble) with probability :

$$P_T(c) \ = 1 - \exp\left(- \left(1 - \varepsilon\, \phi \left(\frac{\mathrm{D}c}{\mathrm{D}t} \right) \right)\ \Delta t_T \right)\ .$$

Note that with this procedure we neglect the fact that there can be more than one reorientation during Δt_T. But this has no influence on the result as long as we neglect correlation between the directions before and after tumbling.

The hydrodynamic model is coupled to the individual run and tumble model just described. In practice, each bacterium is animated by a rigid movement determined by the hydrodynamic model. But it reorients itself with the frequency $\lambda(t)$ and depends on the sign of the gradient of the oxygen concentration along its trajectory. During the tumbling phase, a bacterium randomly reorients itself.

The simulation presented in Figure 1.7 shows hydrodynamic instability due to the density gradient (non-zero buoyancy bacteria). Initially the medium is saturated with oxygen ; under the effect of the oxygen consumption by bacteria, an oxygen gradient appears between the fluid-air interface and the bottom of the drop ; columns of bacteria form under the effect of gravity, dragging the bacteria to the bottom. In addition, bacteria are trapped at the bottom : the concentration being low, their propulsion force is almost zero. However recirculations lead to an oxigen supply of the bottom, and that allows temporarily trapped bacteria to access the interface again.

1.6 Conclusion

Defining a simple biomimetic micro-swimmer model, we have designed a numerical strategy to perform direct simulations of active suspensions in 2D, from the dilute to the dense regime. Based upon the determination of the exact fluid-structure interaction (through the strong coupling between the Stokes equations and Newton's law), our numerical investigations have focused on the hydrodynamic interactions with a limited or large number of micro-swimmers of different type (pushers or pullers) and different geometrical properties (ellipsoidal or spherical bodies). Our model allows to investigate the influence of critical parameters on the dynamics, such as the type of motility, the elongation of the micro-swimmers, their concentration and the intensity of the propulsion force. The method readily adapts to dense suspensions and allows to determine the complex behaviour of a dense active suspension, reproducing large-scale coherent structures observed in experiments and allowing to investigate the rheological signature. Our results provide strong evidence for the pure hydrodynamic origin of collective swimming. The next important step is the extension to 3D simulations, in order to be able to make quantitative comparisons with experiments. For that purpose, the same model can be used but the numerical strategy must be adapted so that iterative methods can be used efficiently to solve the linear system associated to the Stokes problem.

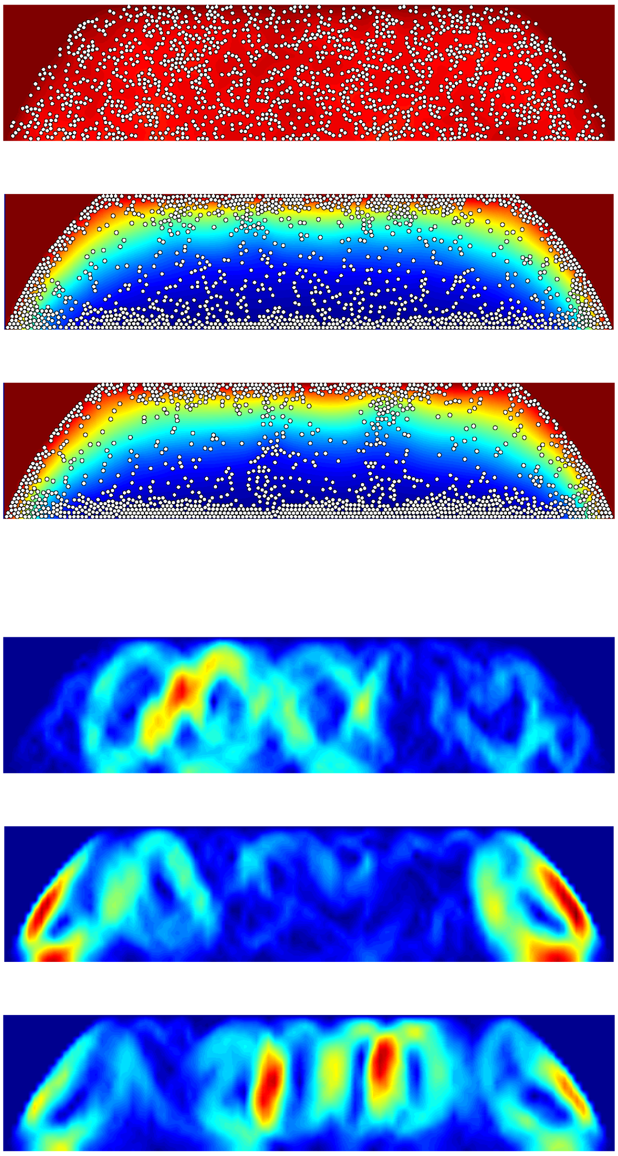

FIGURE 1.7 – Dense suspension, oxygen distribution (left) and modulus of the fluid velocity (right) in a drop domain at different time steps $t_n = n\Delta t$. From top to bottom : $n = 3$, 200, 350.

Chapitre 2

Modeling of cilia-driven fluid flows.

The work presented in this chapter deals with the modeling and numerical simulation of cilia-driven fluid flows. The results presented have been obtained during the PhD thesis of Loic Lacouture (LMO, Université Paris-Sud, october 2012-june 2016), that I have co-directed with Sébastien Martin (MAP5, Université Paris Descartes) and Bertrand Maury (LMO, Université Paris Sud). Our objective is to develop a numerical tool for the simulation of large forests of cilia beating in a viscous fluid, allowing to study the emergence of collective dynamics and the dependence of certain parameters like the cilia density and the viscosity of the fluid. The approach adopted in this work is to consider the "one-way" fluid-structure interaction, that means that the motion of the cilia is prescribed and we do not solve the action of the fluid on the structures. These are modeled as 1*-dimensional manifolds immersed in the* 3*-dimensional space, and their action on the fluid is taken into account by considering Dirac line forces in the fluid. This model is a first step towards a "two-ways" model in which the full fluid-structure interaction is solved.*

2.1 Introduction

In this chapter we are interested in the modeling of active fluids in which the activity is due to thin structures called cilia, that beat in coordinated waves. Motile cilia are slender protuberances that project from the much larger bodies of eukaryotic cells ; these use them either for locomotion or to simply move liquid over their surface. Active cilia are present in many biological flows, as for instance in the internal ear or in the brain [155]. They are also responsible for the locomotion of several micro-organisms as for instance the microalgae *Chlamydomonas* mentioned in the previous chapter. A very interesting example of such a fluid is the bronchial mucus, a thin liquid layer lining the interior of the airways. It protects the human lung against dehydration and inhaled particles, like dust or allergens. In the mechanical process of mucociliary clearance, mucus traps aspirated particles and is then itself evacuated from the lung by the coordinated action of cilia lining the lung bronchi. Preserving the lung from inhaled impurities is necessary, since they could obstruct the bronchi and limit the exchange area for oxygen and carbon dioxide. Fortunately, the lung airways are clean in healthy individuals [90], but under pathological conditions, mucus characteristics and mucociliary clearance efficiency can be altered. For instance, due to a modification of the viscosity of the mucus or a degradation of cilia, ciliary motion can become ineffective. It is therefore important to understand better some of the mechanisms involved in mucociliary clearance, in particular the emergence of the collective dynamics and their impact on the efficiency of the mucus transport.

Our approach is microscopic, that means that we model the cilia individually and solve the action of each cilia on the flow. We aim at developing a model capable of simulating large forests of cilia, reproducing the collective dynamics arising in ciliated systems. The complexity of the process when considering cilia-driven fluid flows is high : a high amount of cilia, possibly different fluid layers, several interfaces, several scales. Although a wide variety of works can be found in the literature, the numerical simulation of such flows remains at present time a challenge. One of the main difficulties is the modeling of the activity of cilia ; in fact, how the internal ciliary engine affects the ciliary beat form remains an open question. That is why most of the works focus on the flow fields produced by cilia with given beat pattern and frequency. In the work presented in this chapter we also adopt this approach : the fluid-structure interaction considered is "one-way", that means that the motion of the cilia is prescribed and we do not solve the action of the fluid on the structures. This model is a first step towards a "two-ways" model in which the full fluid-structure interaction is solved, with a reduced computational cost allowing to simulate large forests of cilia. A further step towards such a model is presented in chapter 3, where we focus on the modelling of the activity of the cilia and the numerical resolution of the complete three-dimensional fluid-structure interaction.

Let us now say a few works on the literature concerning the "one-way" modeling of mucociliary transport. Many works use a continuum representation of the airway surface liquid as a traction layer, with a continuous distribution of forces or velocities [143, 56, 117, 112], replacing the forest of cilia by an active porous medium or a prescribed velocity at the bottom layer. They focus on different aspects affecting mucociliary clearance, like for instance the role of the geometry of the airway tree. These works present interesting multiscale approaches but they do not allow to investigate the emergence of collective dynamics.

Another approach consists in representing the cilia individually. Representing each structure as a three-dimensional body immersed in the fluid domain involves a considerable computational effort to represent the fluid-body interface. An option in order to reduce this cost can be to use a fictitious domain approach (see for instance [30]). However the amount of cilia in simulations remains limited, due to the high computational cost induced by the representation of the structure's thickness. Due to their slenderness, the action of individual cilia can be represented by a centerline distribution of point forces in the fluid, leading to a combination of singular "Stokeslet" solutions. This idea was initially developed in studies such as [102] and [63], and then further developed in other works [74, 75]. The distribution of point forces is derived from the prescribed beat pattern using different methods [63, 102], and particular "Stokeslet" solutions are chosen depending on the boundary conditions. The approaches also differ by the level of detail of the model : accuracy of the boundary condition at the surface of the cilia, consideration of the properties of the different layers in which the cilia beat, cilia in the transversal direction [111], [30].

In the present work, and in order to reach a high computing efficiency, we avoid size constraints by working in the asymptotic limit of infinite slenderness : the thin structures are modeled as 1-dimensional manifolds immersed in the 3-dimensional space, and their action on the fluid is taken into account by considering Dirac line forces in the fluid. The motion of the cilia is prescribed and the distribution of forces along the cilia must be deduced from their prescribed motion, and this is done using the *slender-body theory* approximation [37]. This leads to a Stokes problem with singular source term, which is well defined in the finite element framework, but the convergence rate of classical finite element methods is slowed down by the singularity. However, the optimal order can be recovered by considering any subdomain that excludes the singularity, as we have proven in [12] and [11]. Nevertheless, we use a numerical method that allows to recover the optimal convergence rate on the whole domain. The numerical model developed is applied to the simulation of very large forests of bronchial cilia, and we investigate the emergence of the collective dynamics.

2.2 One-way modeling of the fluid-structure interaction.

Cilia are slender bodies that beat very quickly in a viscous fluid. In mucociliary transport for instance, the ratio between the cross-sectional radius of the cilia and their length is $\frac{a}{L} \sim \frac{0.1}{6}$, and their beating frequency is about $f = 15$ Hz. We have chosen to take advantage of the geometry of the structure and work in the asymptotic of infinite slenderness, that is when the ratio between the thickness and the length of the structure $\epsilon = \frac{a}{L}$ vanishes. Keeping the force exerted by each section of the body constant when ϵ vanishes allows to conserve the action of the structure on the fluid, while the velocity of the fluid becomes infinite at the centerline of the slender body. Our model thus consists of the Stokes equations governing the dynamics of a viscous fluid, with in the source term a line distribution of forces along a 1d curve representing the thin structure. In order to ease the computations, the line distribution of forces is approached by a sum of punctual forces distributed along the structure, as illustrated in Figure 2.1.

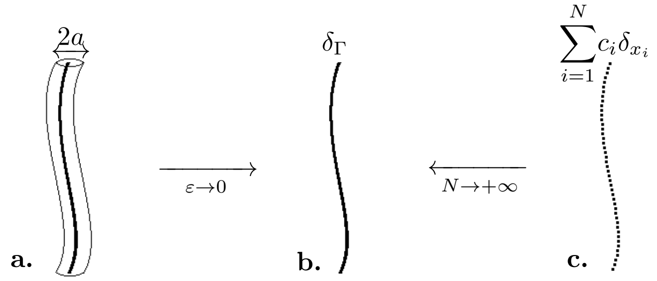

FIGURE 2.1 – Modeling ot the slender body : **a.** For a cylindrical slender body of radius a, the volumic force is of order ε^{-2}, such that the total force stays constant when ε tends to 0. **b.** At the limit where ε vanishes, the body becomes a $1d$ curve with a line distribution of forces. **c.** The line distribution of forces is approached by a sum of N punctual forces distributed along the 1d curve.

We refer the reader to [94] for an analysis of the convergence of the solution to the Stokes problem with a constant volumic force on the 3D structure, represented by a curved cylinder, to the solution of the asymptotic model when ϵ vanishes. This convergence result has been established in weak Sobolev spaces.

Another issue is how to define the distribution of forces induced by the cilia on the fluid. A complete model would consist in a mechanical model for the structure coupled to the fluid equations, so that both the action of the structure on the fluid and the retroaction of the fluid on the structure are taken into account. However, modeling the mechanics of active thin structures like the bronchial cilia for instance is a difficult task, since the underlying internal dynamics are not well understood. Besides, since the solution of the Stokes problem with a line dirac distribution is singular, the coupling between a 1d model for the cilium and the 3d model for the fluid is not trivial. Further work is necessary to give a clear mathematical sense to such a coupling, so that the velocity of the structure can be computed in a straightforward way. That is why in this work, we do not address the problem of the construction of the mechanical model, and we consider that the force distribution is given. More precisely, we consider that the motion of each cilium is known and allows to deduce a force distribution.

In order to deduce the distribution of forces along the thin structure from its movement, we use the so-called slender-body theory, based on asymptotic expansions when the ratio ϵ between the thickness and the length of the body vanishes. Cox [37] established an asymptotic expansion of the force at each point of the structure. If $\boldsymbol{\xi}(.,t)$ is a parametrization of the position of the structure at time t in curvilinear coordinates, the expression of the force at the point of curvilinear abscissa s is

$$\mathbf{f}(s,t) = \frac{2\pi\mu}{\ln(L/a)} \left(2\mathbb{I}_3 - \frac{\dot{\boldsymbol{\xi}}(s,t) \otimes \dot{\boldsymbol{\xi}}(s,t)}{\|\dot{\boldsymbol{\xi}}(s,t)\|^2} \right) \mathbf{u}_{\text{str}}(s,t) + O(\frac{1}{(\ln(L/a))^2}), \tag{2.1}$$

where $\dot{\boldsymbol{\xi}}$ is the derivative of $\boldsymbol{\xi}$ relative to s and $\mathbf{u}_{\text{str}}$ is its derivative relative to t :

$$\dot{\boldsymbol{\xi}}(s,t) = \frac{\partial \boldsymbol{\xi}}{\partial s}(s,t) \text{ and } \mathbf{u}_{\text{str}}(s,t) = \frac{\partial \boldsymbol{\xi}}{\partial t}(s,t).$$

Relation (2.1) has been established in [37] by confronting two different approaches : an inner expansion that consists in studying the fluid velocity near the slender body, seen as an infinite cylinder, and an outer expansion considering the flow far from the slender body seen as a zero-thickness body.

We consider a list of cilia $i \in [\![1, M]\!]$, immersed in a bounded domain $\Omega \subset R^d$, where d is the dimension, filled with a viscous fluid, and we denote by $\boldsymbol{\xi}_i(s,t)$ the parametrization of their motion. The resulting mathematical problem is the following :

$$\left\{ \begin{array}{rcll} -\text{div}(\mu\nabla\mathbf{u}) + \nabla p & = & \sum\limits_{i=1}^{M} \big(\sum\limits_{n=1}^{N} \delta_{\boldsymbol{\xi}_i(s_n,t)}\, \mathbf{f}_i(s_n,t) \big) & \text{on } \Omega, \\ \text{div}(\mathbf{u}) & = & 0 & \text{on } \Omega, \\ \mathbf{u} & = & 0 & \text{on } \partial\Omega, \end{array} \right. \tag{2.2}$$

where N is the number of punctual forces composing each slender body and $\mathbf{f}_i(s_n,t)$ is the force it exerts at time t on point $\xi_i(s_n,t)$. For the sake of simplicity we consider here homogeneous Dirichlet boundary conditions, which correspond from the physical point of view to no-slip conditions of the fluid at the boundaries of the domain Ω. However, other boundary conditions will be considered in the numerical simulations (periodic and slip BC).

By linearity of the Stokes equations, studying Problem (2.2) consists in studying the same problem with a single point force :

$$\left\{ \begin{array}{rcll} -\mu\triangle\mathbf{u} + \nabla p & = & \delta_{\mathbf{x}_0}\mathbf{f} & \text{on } \Omega, \\ \text{div}(\mathbf{u}) & = & 0 & \text{on } \Omega, \\ \mathbf{u} & = & 0 & \text{on } \partial\Omega, \end{array} \right. \tag{2.3}$$

where $\mathbf{f} \in \mathbb{R}^d$.

The solution of the Stokes problem with a dirac mass in the source term is well known in the particular case where the domain is unbounded and the solution vanishes at infinity. It is often called “Stokeslet” [34] and, for $x_0 = 0_{\mathbb{R}^d}$, it is defined as follows in dimension 2 :

$$\begin{aligned} \mathbf{u}_\delta(\mathbf{x}) &= \frac{1}{4\pi\mu}\left(-\ln\|\mathbf{x}\|\mathbb{I}_2 + \frac{\mathbf{x}\cdot{}^t\mathbf{x}}{\|\mathbf{x}\|^2}\right)\cdot\mathbf{f} \quad \in \mathbb{R}^2, \\ p_\delta(\mathbf{x}) &= \frac{\mathbf{x}\cdot\mathbf{f}}{2\pi\|\mathbf{x}\|^2} \quad \in \mathbb{R}. \end{aligned} \tag{2.4}$$

In dimension 3, the “Stokeslet” is defined by

$$\begin{aligned} \mathbf{u}_\delta(\mathbf{x}) &= \frac{1}{8\pi\mu}\left(\frac{\mathbb{I}_3}{\|\mathbf{x}\|} + \frac{\mathbf{x}\cdot{}^t\mathbf{x}}{\|\mathbf{x}\|^3}\right)\cdot\mathbf{f} \quad \in \mathbb{R}^3, \\ p_\delta(\mathbf{x}) &= \frac{\mathbf{x}\cdot\mathbf{f}}{4\pi\|\mathbf{x}\|^3} \quad \in \mathbb{R}. \end{aligned} \tag{2.5}$$

When the domain is bounded, Problem (2.3) has a unique weak solution $(\mathbf{u}, p) \in W^{1,q}(\Omega)^d \times \mathbb{L}_0^q(\Omega)$ for all $q \in [1, 2[$ in dimension $d = 2$, and for all $q \in [1, 3/2[$ in dimension $d = 3$. Actually, the solution can be built by using a suitable lift procedure which consists in adding to $(\mathbf{u}_\delta, p_\delta)$ a correction term $(\mathbf{w}, \pi) \in H^1(\Omega)^d \times \mathbb{L}_0^2(\Omega)$ which satisfies the following problem :

$$\left\{ \begin{aligned} -\triangle\mathbf{w} + \nabla\pi &= 0 && \text{in } \Omega, \\ \operatorname{div}(\mathbf{w}) &= 0 && \text{in } \Omega, \\ \mathbf{w} &= -\mathbf{u}_\delta(\cdot - \mathbf{x}_0) && \text{on } \partial\Omega. \end{aligned} \right.$$

Then, the solution is given by :

$$\begin{aligned} \mathbf{u}(\mathbf{x}) = \mathbf{u}_\delta(\mathbf{x}) + \mathbf{w}(\mathbf{x}) &= \frac{1}{4\pi}\left(-\ln\|\mathbf{x}\|\mathbb{I}_2 + \frac{\mathbf{x}\cdot{}^t\mathbf{x}}{\|\mathbf{x}\|^2}\right)\mathbf{F} + \mathbf{w}(\mathbf{x}), \\ p(\mathbf{x}) = p_\delta(\mathbf{x}) + \pi(\mathbf{x}) &= \frac{\mathbf{x}\cdot\mathbf{F}}{2\pi\|\mathbf{x}\|^2} + \pi(\mathbf{x}). \end{aligned}$$

2.3 Analysis of the finite element method for elliptic problems with singular source terms

An important issue for numerical purposes is that the solution of the elliptic problem (2.3) does not have the classical regularity $H_0^1(\Omega)^d \times \mathbb{L}^2(\Omega)$ in dimensions 2 and 3. Thus, standard results on the convergence rates of the finite element method do not hold. Actually, several authors have shown that the convergence rate for the Laplace equation with singular source terms over the whole domain is suboptimal. In [137] for instance, Scott proved an a priori estimate of order $2 - \frac{d}{2}$ in L^2-norm, where $d = 2$ or 3 is the dimension, regardless of the order of the finite element. Interestingly, optimality is recovered when one considers local errors, that means an error computed on a sub-domain of Ω which excludes the singularity.

In [12], we have proven a quasi-optimal convergence result (up to a logarithmic factor) in local H^s norm, for $s \geq 1$, on a family of quasi-uniform meshes in dimension 2 of space for a punctual Dirac, and in dimension 3 for a Dirac along a 1D curve. This result applies to a wide class of finite-element methods and beyond, including Lagrange and Hermite finite elements and wavelets. In the particular case of linear Lagrange finite elements, we proved optimal convergence in the local H^1 norm. Our results were obtained using the Nitsche and Schatz local error estimates, a weak version of the Aubin-Nitsche duality lemma, and a discrete inf-sup condition. The results were initially obtained for the Laplace problem and published in [12], then for the Stokes problem and published in [11]. At the same time, Köppl and Wohlmuth [92] showed the optimal convergence in local L^2-norm for the Lagrange finite element method (the result is quasi-optimal for the $P1$-element). Their proof is based on different arguments.

Thus, if one is interested in what happens far from the singularity, the standard finite element method may be sufficient. However, one can still recover optimal convergence rates on the whole domain by solving a regular annexe problem, as shown in the next section.

2.4 Numerical method

In order to improve the convergence rate of the finite element method applied to an elliptic problem with singular right hand side, several authors have proposed to use locally refined meshes near the singularity [5, 38]. But using graded meshes increases the complexity of the meshing and the computational cost, even if the mesh is refined only locally, especially if there are several Dirac measures in the right-hand side. In [58], Eriksson developed a numerical method to solve the Laplace problem with singular source term and recover the optimal convergence rate : the numerical solution is searched in the form $u_0 + v_h$, where u_0 is a known function containing the singularity of the solution, and v_h is the numerical solution of a smooth problem. Since the solution of the smooth problem has classical H^1 regularity, the standard finite element method converges with optimal rates. This method has been extended to the Stokes problem in [93] and is applied in this work to solve problem (2.2). The approach fits in the class of subtraction methods, used in several contexts like electroencephalography and more recently for the simulation of blood flow in microvascular networks [152].

Let us briefly detail the principle of this subtraction method. We consider problem (2.3) for $\mathbf{x}_0 = 0_{\mathbf{R}^d}$:

$$\left\{\begin{array}{rcll} -\mu\triangle\mathbf{u} + \nabla p &=& \delta_0\mathbf{f} & \text{on } \Omega, \\ \operatorname{div}(\mathbf{u}) &=& 0 & \text{on } \Omega, \\ \mathbf{u} &=& 0 & \text{on } \partial\Omega, \end{array}\right. \tag{2.6}$$

where $\mathbf{f} \in \mathbb{R}^d$. The fundamental solution $(\mathbf{u}_\delta, p_\delta)$ of the Stokes problem (2.6) contains the whole information on the singularity of the solution $(\mathbf{u}, p)$ located at $\mathbf{x}_0$. In order to extract this singularity, we define a regular bump function χ that is equal to 1 in some small open ball centered in $\mathbf{x}_0$, and 0 outside a slightly bigger open ball centered in $\mathbf{x}_0$, *i.e.* for $0 < a < b < d(\mathbf{x}_0, \partial\Omega)$, $\chi \in H^{2+k}(\mathbb{R}^d)$, $\chi_{|B(x_0,a)} = 1$ and $\chi_{|B(x_0,b)^c} = 0$.

By constructing the functions $\mathbf{u}_0 = \chi\mathbf{u}_\delta$ and $p_0 = \chi p_\delta$, we define $\mathbf{g}$ and h as

$$\mathbf{g} = -\mu\triangle\mathbf{u}_0 + \nabla p_0 - \delta_{\mathbf{x}_0}\mathbf{F}, \tag{2.7}$$

$$h = \operatorname{div}\,\mathbf{u}_0. \tag{2.8}$$

By construction of $\mathbf{u}_\delta$, p_δ and χ, $supp(\mathbf{g}) \subset \mathcal{R}_a^b(\mathbf{x}_0)$ and $supp(h) \subset \mathcal{R}_a^b(\mathbf{x}_0)$, where $\mathcal{R}_a^b(\mathbf{x}_0)$ is the ring centered around $\mathbf{x}_0$, of internal radius a and external radius b. Since $\mathbf{u}_\delta$ and p_δ are analytic on $\Omega \setminus \{\mathbf{x}_0\}$, the regularity of functions $\mathbf{g}$ and h directly depends on the regularity of function

χ, namely $\mathbf{g} \in H^k(\Omega)$ and $h \in H^{k+1}(\Omega)$. Finally, it only remains to correct the terms $\mathbf{u}_0$ and p_0 by solving the regular elliptic problem

$$\left\{ \begin{array}{rcll} -\mu\triangle \mathbf{v} + \nabla q &=& -\mathbf{g} & \text{in } \Omega, \\ \text{div } \mathbf{v} &=& -h & \text{in } \Omega, \\ \mathbf{v} &=& 0 & \text{on } \partial\Omega, \end{array} \right. \tag{2.9}$$

and the solution of Problem (2.6) is given by

$$(\mathbf{u}, p) = (\mathbf{u}_0 + \mathbf{v}, p_0 + q) = (\chi \mathbf{u}_\delta + \mathbf{v}, \chi p_\delta + q),$$

where $\mathbf{u}_0$ and p_0 are explicitly known functions and $(\mathbf{v}, q)$ is the solution of Problem (2.9).

Now, denoting $(\mathbf{v}_h, q_h)$ the numerical solution of Problem (2.9), we can construct an approximation of the solution of Problem (2.6), namely $\mathbf{u}_h = \mathbf{v}_h + \mathbf{u}_0$ and $p_h = q_h + p_0$. This solution satisfies

$$\begin{array}{ll} \|\mathbf{u} - \mathbf{u}_h\|_{H^s(\Omega)} = \|\mathbf{v} - \mathbf{v}_h\|_{H^s(\Omega)}, & \text{for } 0 \leqslant s \leqslant k+1, \\ \|p - p_h\|_{H^s(\Omega)} = \|q - q_h\|_{H^s(\Omega)}, & \text{for } 0 \leqslant s \leqslant k. \end{array}$$

In that way, we switch from the numerical computation of the solution of a singular problem with a punctual force in source term (with a poor convergence rate) to the numerical computation of the solution of a regular problem with an optimal convergence rate, at any required precision in terms of regularity.

For practical aspects of the implementation of this method, as for instance possible choices for the function χ and the corresponding expressions of the functions $\mathbf{g}$ and h, we refer the reader to [93]. Let us however note that the substraction method can be extended to more general boundary conditions (Dirichlet, Neumann and periodic boundary conditions), non-constant viscosity (as long as this viscosity can be represented by a piecewise constant function), and Dirac distributions along 1d curves as source term.

2.5 Application to mucociliary transport in the lung

The model and the numerical method presented in the previous sections have been used for the simulation of mucociliary transport. Three different fluid layers are involved in this process : a thin sol layer known as the periciliary liquid [90], commonly called PCL ; mucus, a visco-elastic fluid secreted by the respiratory epithelium [95], and air. Mucus is a viscoelastic fluid, therefore a non-Newtonian fluid model should be considered. Nevertheless, the relaxation time is very high, which means that at the scale of the cilia beat, the elastic energy of the fluid is insignificant with regard to the viscous resistance As a consequence, it is reasonable to model mucus as a Newtonian fluid. And since both mucus and the PCL are viscous at the scale of the cilia, we solve the Stokes equations in both layers. Furthermore, it has been observed that the interface between the PCL and mucus layers is almost flat and does not vary in time for a given beating frequency. Therefore we use a bi-fluid model with constant and horizontal interface for the PCL and the mucus layers, and particular boundary conditions at the upper boundary of the domain in order to take into account the mucus/air interface. Moreover, we neglect the effect of tidal breathing and cough upon clearance, and we intend to add this effects to our model in future work. We also neglect the effect of gravity, because at the micrometric scale, the force of gravity

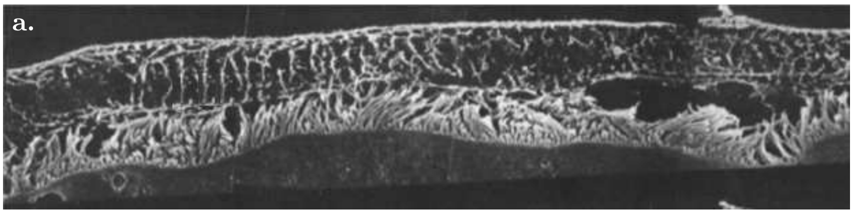

Figure 2.2 – Section of cultured rabbit tracheal epithelium examined by scanning electron microscopy, modified from [136].

ρg and of buoyancy $\Delta\rho$g are insignificant.

Let us now focus on the motion of bronchial cilia. Active research has been devoted to the study of the motion of bronchial cilia, since the pioneering work by Lucas [107]. These very slender structures whose length is about 6 μm and radius is 0.1 μm are fixed on the epithelial cells in the bronchi. They beat in the periciliary layer, where viscosity is much lower than in the mucus, at an average frequency of 15 Hz depending on the characteristics of the environment. Since mucus and PCL are viscous fluids at the scale of a cilium, a symmetric movement under time reversal of the cilium would not allow for a positive net transport of the mucus. Thus, the motion of the cilium is different during the recovery stroke and the effective stroke. According to Sanderson and Dirksen [135], the effective stroke is two or three times faster than the recovery stroke, and cilia may penetrate the overlying mucus during the faster phase. Besides, cilia that propel mucus coordinate into a metachronal wave, which wavelength is of the order of a hundred of cilia, that is around 30 μm, and that propagates in the opposite direction of mucus transport. It is believed that coordination of the beating into a metachronal wave arises during the recovery stroke and is due to hydrodynamic interactions between the cilia. Changes in the viscosity of the medium, in the length or in the spacing of the cilia may therefore have a deep influence on the characteristics of the metachronal wave.

Parametrization of the Cilia motion

Since the present model is based on a prescribed motion of cilia, we need to define a parametrization of this movement. We use the parametrization established by Fulford and Blake in [64], based on the Fourier series decomposition of the beat of one cilium described by Sanderson and Sleigh in [136]. The authors also proposed an extension of the parametrization to the movement of a whole forest of cilia, via two parameters that represent respectively the distance ℓ_0 between two cilia and the wavelength λ of the metachronal wave. It is based on the assumption that the metachronal wave propagates in the direction of the cilia beat, although experiments show that activity is also propagated in the transversal direction. However this approximation is classical and experiments [68] show that increasing viscosity causes the metachronal wave to become more and more orthoplectic (*i.e.* in the direction of mucociliary transport). In the simulations presented in this work, this assumption has also been made, but the model allows to prescribe a methachronal wave with arbitrary direction.

Figure 2.3 shows the beat of a cilium obtained using this parametrization and allows to observe a good correspondance with the description made by Sanderson and Sleigh in [136]. The cilium crosses the interface between the mucus and the peryciliary layer (PCL) only during the effective stroke and not during the recovery stroke. This feature is known to be important in order to guarantee an efficient mucus transport.

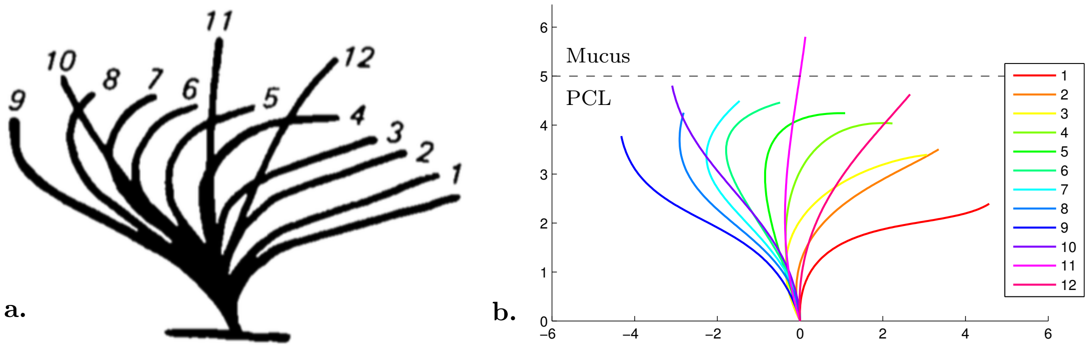

FIGURE 2.3 – Traces of a cilium during one period of its beat. **a.** Description made by Sanderson and Sleigh [136]. **b.** Parametrization established by Fulford and Blake [64].

We have drawn in Figure 2.4 a section of a forest in the direction x. The propagation of the metachronal wave (to the left on the picture) is in the opposite direction of mucus transport (to the right).

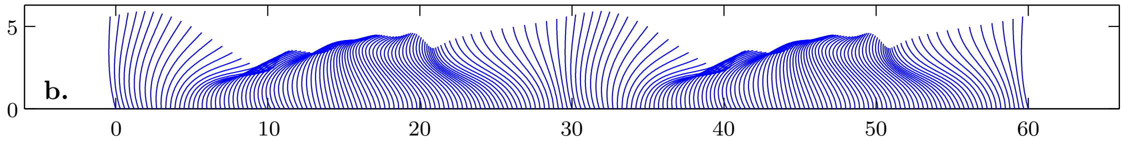

FIGURE 2.4 – Drawing of a section of a forest obtained with the parametrization established by Fulford and Blake [64].

Bifluid model

We use a bifluid model in which the viscosity is prescribed and defined through the piecewise constant function

$$\mu(x, y, z) = \begin{cases} \mu_1 & \text{if } z \leqslant h_0, \\ \mu_2 & \text{if } z \geqslant h_0, \end{cases}$$

where h_0 is the height of the periciliary layer.

The distribution of forces exerted by the cilia on the fluid, denoted by $\mathbf{f}_i(s_n, t)$ in (2.2), is retrieved from their prescribed movement using relation (2.1). Now in the case of a two-viscosity fluid this relation, based on the slender-body theory described by Cox [37], is no longer valid. However Fulford and Blake [63] established the expression of the distribution of forces along a slender body which straddles an interface. At the first order (in the regime $\ln(L/a)^{-1}$ tends to zero) and far from the interface, the expression of the force is the same as for constant viscosity. Close to the interface, more precisely at a distance smaller than the radius a of the body, relation (2.1) is no more valid. In our case, however, we discretize the distribution of forces along each cilium by a list of punctual forces, and we will see that the distance between two punctual forces is three times the radius a. Therefore, we neglect the correction arising from the variable viscosity fluid and we consider expression (2.1) for the forces along the whole cilium.

Domain and boundary conditions

Since the dimension of the computational domain considered is negligible compared to the size of the bronchiole (in the third generation, the length is of about 8 m, compared to a radius of 3mm), we can reasonably neglect the curvature of the bronchiole in our model. Therefore we consider a rectangular computational domain Ω, with the bottom corresponding to the lining of the bronchi, that is the epithelium/PCL interface, and the top corresponding to the mucus/air interface. At the bottom we impose a no-slip boundary condition ($\mathbf{u} = 0$), while at the top of the box we prescribe so-called free-slip conditions :

$$\begin{cases} \mathbf{u} \cdot \mathbf{n} = 0 & \text{kinematic condition,} \\ (\boldsymbol{\sigma} \cdot \mathbf{n}) \cdot \boldsymbol{\tau} = 0 & \text{dynamic condition,} \end{cases}$$

where $\mathbf{n}$ is the normal vector, $\boldsymbol{\tau}$ the tangential vector and $\boldsymbol{\sigma}$ the constraint tensor. Prescribing this kinematic condition means that we assume that the particles of fluid do not cross the mucus/air interface, so that this interface remains flat and constant during the whole simulation, which is a reasonable assumption with regard to the experimental results available. The dynamic condition implies that we neglect friction of the air layer. More complex boundary conditions could be considered in order to take into account the effect of the airflow on the mucus layer, as for instance a prescribed shear stress (see for instance [112] and [117]. Finally, the box we consider is seen as a window focused on a part of a bronchus, and mucociliary transport goes on outside this box. Therefore it is natural to impose biperiodic boundary conditions in both directions.

Computational aspects and physical parameters

This numerical model has been implemented in the finite element solver CAFES (Cartesian Finite Element Solver) [60], which is written in C/C++ and uses the 4Q1/Q1-finite element to solve a class of problems for which a solver on a Cartesian grid is needed. The library PETSc is used for the parallel structure of matrices and vectors, as well as the parallel solvers for the linear systems. In all simulation presented in this section, convergence in space has been checked. Therefore we do not specify the mesh size.

Before presenting results, let us comment on the values of the physical parameters. By linearity of the Stokes equations, and since the intensity of the force $\mathbf{f}_i$ is proportional to the viscosity of the fluid, we observe that, for a prescribed movement of the cilia (that is for a given parametrization $\boldsymbol{\xi}_i(\cdot, t)$), if $(\mathbf{u}, p)$ is the solution of problem (2.2) for $\mu = 1$, then the couple $(\mathbf{u}, \mu p)$ is solution of the problem for any arbitrary value of μ. This remark leads us to consider a viscosity $\widetilde{\mu} = 1$ in all computations : in order to recover physical values, the velocity field is kept the same and the pressure is multiplied by the physical viscosity μ. In the case of the bi-fluid model, the observation is the same : the velocity field only depends on a non-dimensional value which is the ratio between both viscosities $r_\mu = \mu_{mucus}/\mu_{PCL}$.

Table 2.1 resumes the data related to the cilia, as given in [64]. These parameters are the ones used in all the simulations (unless otherwise stated). The simulations should present the time evolution of the flow field. In our model the movement of the cilia is prescribed, and it is periodic (the period T is $1/f$). Due to the instantaneousness of the Stokes equations, the results are also periodic, and therefore the simulation of one unique period is sufficient. The time step $\triangle t$ is taken equal to $T/20$. In all the simulations presented in this paper, the number of punctual forces composing each cilium is 20, and the mesh size is sufficiently small so that we can assume

Length of a cilium	L	6 μm
Cross-sectional radius	a	0.1 μm
Beat frequency	f	15 Hz
Cilia spacing	ℓ_0	0.3 μm
Metachronal wavelength	λ	30 μm

Table 2.1 – Summary of data for cilia in the lung, from [64].

that the solution is not far from convergence.

Results

We have chosen to show the results of three simulations, in order to illustrate the emergence of collective dynamics in the active fluid. Figure 2.5 shows the 3-dimensional flow generated by a small patch of cilia (15 cilia in each direction) in a constant-viscosity fluid, during the effective stroke (left) and during the recovery stroke (right). As expected, the velocity of the mucus layer is high during the effective stroke, whereas it is low and in the opposite direction during the recovery stroke, leading to an average flow over one period which is non-zero, and thus to a net transport of the mucus outside. In this configuration, the global dynamics observed are nearly the sum of the individual dynamics. But when increasing the amount of cilia beating in the box, collective dynamics emerge. Figure 2.6 illustrates the flow produced by a forest of cilia that fills

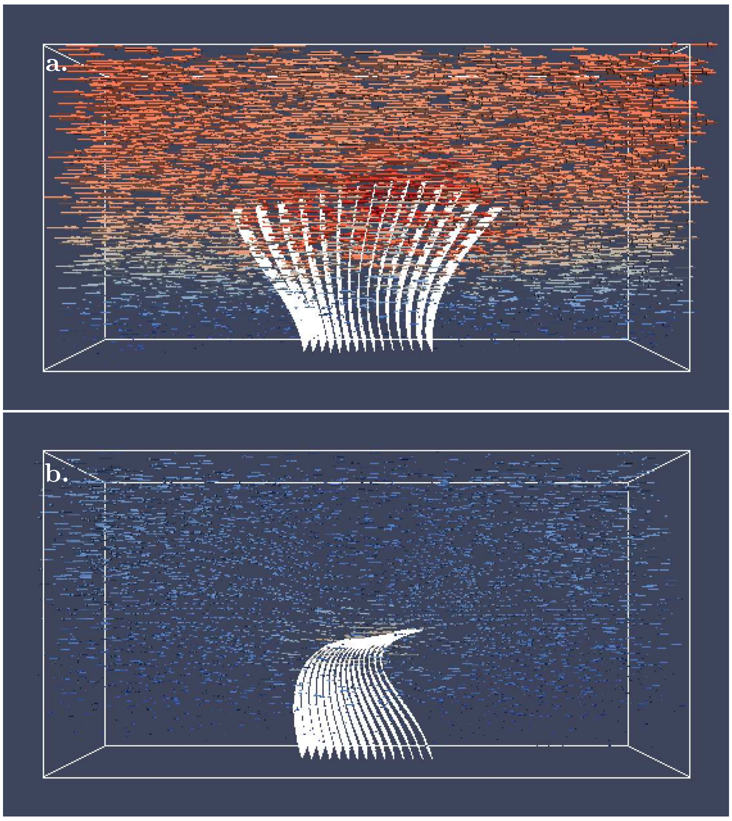

Figure 2.5 – 3D-Simulation of a patch of cilia in a constant-viscosity fluid. **a.** Effective stroke ($t = T/20$ s). **b.** Recovery stroke ($t = T/2\triangle t$ s).

the whole domain : a 153 × 51 array of cilia has been considered and the size of the domain is exactly the length of one metachronal wave. The results show a flow which is constant in time, up to a translation at the velocity of the metachronal wave. A more efficient mucus transport emerges from the collective movement of the high number of cilia. However, the flow in the mucus layer is not uniform : recirculations result in a loss of energy and therefore a sub-efficiency of the mucus transport. Figure 2.7 illustrates the flow produced by a whole forest of cilia in a two-layer

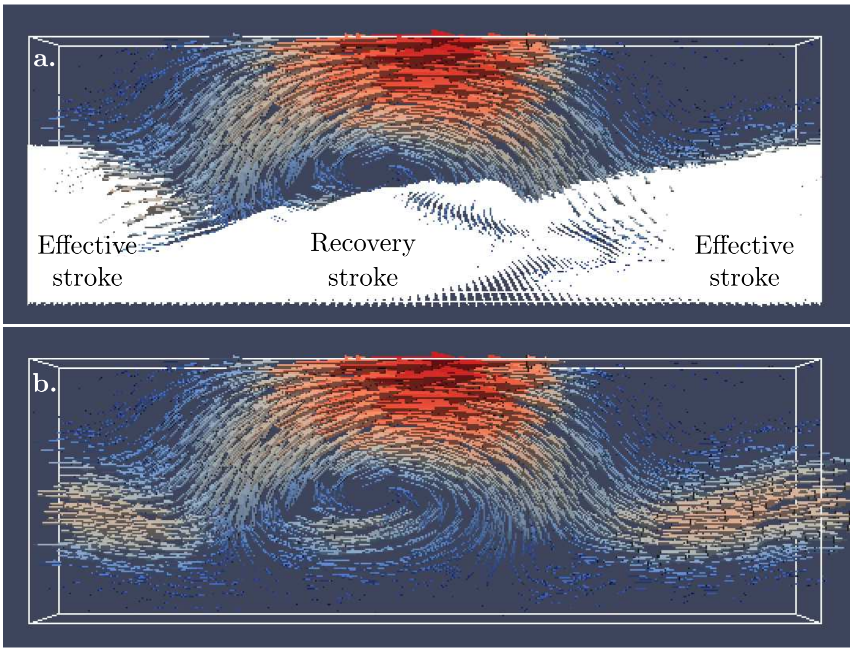

Figure 2.6 – 3D-Simulation of a whole forest of cilia in a constant-viscosity fluid. **a.** Drawing with the cilia. **b.** The same flow drawn without the cilia.

fluid where the ratio between the viscosity in the mucus and the viscosity in the periciliary layer is $r_\mu = 50$, as measured in the experiments [98, 143]. In this case the flow is uniform and has no vertical component. The mucus is transported at a near constant velocity, like a block “sliding” over the periciliary layer. Moreover, in the periciliary layer, the horizontal velocity grows linearly. The high viscosity in the mucus allows for a more efficient transport, and it is an essential ingredient in the process.

We have investigated the impact of the density of cilia on the transport efficiency. Our results show that the average velocity of the mucus decreases linearly with the density of cilia up to a certain limit, as expected due to the linearity of the Stokes equations. However, under a certain value of the cilia density, the flow is no longer constant in time. Moreover our results show that, when cilia density is high, the fact that they reach the mucus is not necessary to obtain important mucus velocities ; however it becomes essential when the density is low. In the latter case, if cilia do not enter the mucus, there is no net transport of the mucus layer, and only a bit of periciliary layer is propelled. This result is consistent with experimental observations [142, 145].

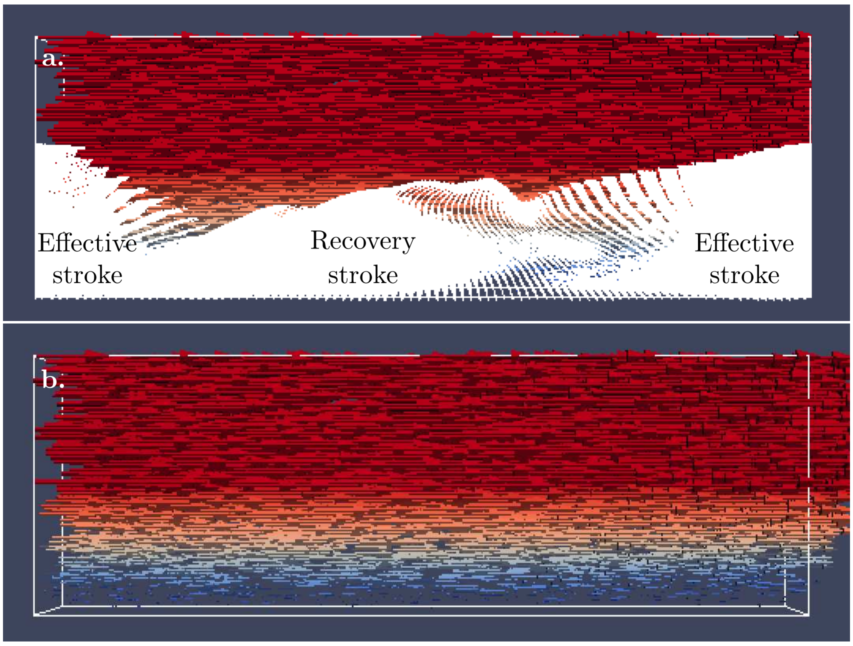

FIGURE 2.7 – 3D-Simulation of a whole forest of cilia in a bi-fluid. **a.** Drawing with the cilia. **b.** The same flow drawn without the cilia.

Chapitre 3

An active fluid-structure interaction model.

This chapter deals with the direct simulation of active fluids driven by cilia, based on the resolution of the complete fluid-structure interaction between the viscous fluid and the active cilia, in order to fully include the hydrodynamic interactions. The results presented have been obtained during the PhD thesis of Fabien Vergnet (LMO, Université Paris Sud, october 2015 - june 2019), that I have co-directed with Sébastien Martin (MAP5, Université Paris Descartes) and Bertrand Maury (LMO, Université Paris Sud). Unlike the model presented in Chapter 2, in which the cilia motion is prescribed, the model developed in this work is based on the strong coupling of a $3d$ *elasticity model for the cilium and the Stokes equations for the fluid, and the feedback of the fluid is accurately taken into account.*

3.1 Introduction

The objective of the work presented in this chapter is the *direct simulation* of the interaction of active cilia with a viscous fluid, based on the numerical resolution of the fundamental equations governing both the fluid (Stokes equations) and the structures (elasticity model), in order to include exhaustively hydrodynamic interactions. The fine resolution of this interaction is essential to understand better the individual motion of cilia, and how it leads to the collective dynamics observed in these active fluids. Of course, such a model will not allow to simulate large forests of cilia, because the computational cost will be prohibitive. However, we consider this model as a further step towards the development of a reduced model which solves the "two ways" fluid-structure interaction in active fluids, without the limiting hypothesis of a prescribed motion. Besides, this model will be very useful to obtain reference solutions to be compared to the solutions of the reduced model.

Eukaryotic cilia are elongated deformable structures with a typical diameter between 0.1 and 0.3 μm, and a length that ranges from 5 μm in the lung [15], to 80 μm (in mice spermatozoon). Beats are generated by the axoneme, a rod inside cilia composed of nine doublet microtubules arranged in a circle around a central pair of microtubules and held together by three sets of protein cross-links. As in the movement of muscles during contraction, the basis for axonemal movement is the sliding of protein filaments relative to one another. In cilia, the filaments are the doublet microtubules. Axonemal bending is produced by forces that cause sliding between pairs of doublet microtubules. The active sliding occurs all along the axoneme, so that the resulting bends can be propagated without damping. The precise nature of the spatial and temporal control mechanisms regulating the various ciliary beats is still unknown [21].

In the previous chapter we presented a model that, like often in the approaches considered up to now, is based on the prescription of the motion of the cilia. Now this motion is driven by internal motors, leading to dynamics that depend on the interaction with the fluid [155] ; the dynamics will therefore be different depending on the viscosity of the fluid, but also whether it is at rest or not. In particular, it is known that bronchial cilia interact when they are at a sufficiently small distance and synchronize their beats in order for the mucociliary transport to be more efficient. In vitro experiments on rabbit bronchial epithelial cells show the emergence of a metachronal wave in a direction opposite to the flow, beyond a certain density of cilia [16, 68]. The way in which cilia interact is subject to discussion ; but the emergence of this synchronization is believed to result mainly from hydrodynamic forces.

Some authors have worked on the numerical simulation of active fluids based on the individual representation of the active bodies and the modeling of their internal activity. But they are often based on a truncated resolution of the Stokes equations, using approximation methods based on estimates of hydrodynamic interactions. Using Green functions associated with Stokes equations, one method consists in solving an integral equation for the velocity field of a cilia and its contribution to the average velocity field [144]. Other techniques are based on the construction of a relationship between hydrodynamic forces and the velocity of a rigid object in a viscous fluid, like the Stokesian dynamics method initiated by Brady & Bossis [18].

In [109] Machin proposed the first model of internal deformation for eukaryotic cilia. The cilium is considered as a 1d elastic filament immersed in a viscous fluid, whose action on the structure is given by the resistive force theory. The internal activity of the cilium is modeled by adding an active bending moment distributed all along the structure : it traduces the action of elements on each side of the structure that induce a deformation of the cilium by contracting and elongating. The model has been progressively improved and complexified by other authors, like for instance [20, 22, 106], using a more realistic geometry of the internal structure of a cilium. These models allow to obtain motions that are similar to those observed on cilia.

Dillon and coworkers [52], and later [156] and [108], tried to model the entire internal structure of eukaryotic cilia, representing the microtubules and the proteins involved in the mechanism. But the description is discrete and does not make sense at the continuous level. In [74, 75], the cilia activity is also modeled by shear forces, with a scenario based on experimental data and it is three-dimensional. The velocity and pressure in the fluid are obtained using the Stokeslets method and the feedback of the fluid on the cilia comes from the Slender body theory. In [118], the author considers a 3d model in which the force scenario linked to the action of the strands of dynein is imposed and the fluid problem is more detailed, solved directly with the method of finite volumes. In these works, the deformations of the structures observed are fairly close to the actual cilia deformations and synchronization effects are observed. Finally, a completely different approach is to let cilia adapt their deformations in order to find the most energy-efficient beat, as for instance in [96].

We have chosen to model the active cilia using a continuous and macroscopic model that does not rely on a description of the internal structure, but rather on a phenomenological representation of activity. We consider a three-dimensional elasticity model in which the activity of the cilia is taken into account through an active stress tensor. This model is presented in the first section of this chapter. Then, we describe the fluid-structure interaction problem and in section 3 we briefly explain how the problem is solved numerically using a finite element method on a moving mesh that fits the interface at each time step. Section 4 is devoted to the presentation of the numerical results, and in the last section we develop a new fictitious domain approach that can be used to solve the fluid-structure interaction problem.

3.2 An active structure model

We have developed a model for the motion of active cilia that is inspired on models popularised in bio-mechanics in the context of biological tissues [119]. As far as we know they have never been used to model active eukaryotic cilia. These are represented in two or three dimensions and their interaction with the surrounding fluid is described at the fluid-structure interface through physical transmission conditions : continuity of the velocity field and the normal component of the surface stresses. The structure is described by a nonlinear 3d hyper-elasticity model, in which the internal activity is taken into account by adding an active component to the passive stress tensor usually derived from the strain energy.

We consider an open bounded domain $\Omega_s \subset \mathbb{R}^d$, with $d = 2, 3$, that represents the undeformed elastic medium. We denote by $\mathbf{d}_s \in \mathbb{R}^d$ the time-dependent displacement of the structure, defined in Ω_s at each time $t > 0$, by E the tensor of non-linear deformations (or Green-Lagrange strain tensor) and by F the gradient of deformations :

$$E(\mathbf{d}_s) = \frac{1}{2}\left(\nabla \mathbf{d}_s + \nabla \mathbf{d}_s^t + \nabla \mathbf{d}_s \nabla \mathbf{d}_s^t\right),$$

$$F(\mathbf{d}_s) = Id + \nabla \mathbf{d}_s.$$

For simplicity we assume that the elastic medium follows the Saint Venant-Kirchhoff law, thus the second Piola-Kirchhoff stress tensor writes as follows in the undeformed solid field (Lagrangian formulation) :

$$\Sigma(\mathbf{d}_s) = 2\mu_s E(\mathbf{d}_s) + \lambda_s \mathrm{Tr}(E(\mathbf{d}_s))\mathrm{Id},$$

where μ_s and λ_s are Lamé's parameters. The elasticity parameters are usually given by means of Young's modulus E_s, which represents the stiffness of the medium, and Poisson's ratio ν_s, which represents its compressibility, with the following formulas :

$$\mu_s = \frac{E_s}{2(1+\nu_s)}, \qquad \lambda_s = \frac{E_s \nu_s}{(1+\nu_s)(1-2\nu_s)}.$$

The internal activity of the structure is described using an active-stress tensor Σ^* that is supposed to depend only on time and space. Finally, since cilia live in a low Reynolds number regime, we neglect inertial terms. Then, in absence of external forces, the elasticity model writes, in lagrangian formulation, for $t > 0$:

$$\begin{cases} -\nabla \cdot \left(F(\mathbf{d}_s(t))\left(\Sigma\left(\mathbf{d}_s(t)\right) - \Sigma^*(t)\right)\right) & = \; 0, \quad \text{in } \Omega_s, \\ \left(F(\mathbf{d}_s(t))\left(\Sigma(\mathbf{d}_s(t)) - \Sigma^*(t)\right)\right) \cdot \mathbf{n} & = \; 0, \quad \text{on } \partial\Omega_s \setminus \Gamma_s, \\ \mathbf{d}_s(t) & = \; 0, \quad \text{on } \Gamma_s, \end{cases} \tag{3.1}$$

where Γ_s is the boundary where the structure is anchored, and where the displacement is therefore nil.

At each time $t > 0$, the physical domain $\Omega_s(t)$ occupied by the elastic medium can be defined through a regular mapping $\phi : \Omega_s \times \mathbb{R}^+ \to \mathbb{R}^d$, such that $\Omega_s(t) = \phi(\Omega_s, t)$. This mapping depends on the displacement $\mathbf{d}_s(t)$ and satisfies :

$$\phi(\cdot, t) = \mathrm{Id} + \mathbf{d_s}(t) \quad \text{in} \quad \Omega_s.$$

The effect of the active-stress tensor Σ^* can be interpreted as an additional body force that acts on the structure and writes $\nabla \cdot (F(\mathbf{d}_s)\Sigma^*)$. Note that, although inertial terms are neglected, the time-dependent active-stress tensor introduces a time dependency into the problem, which is therefore not static.

Model for the active-stress tensor

We follow the active-stress approach used in the context of biological tissues like arteries and muscles. The geometric arrangement of the active components of the tissue can be averaged in order to exhibit a macroscopic fiber-like structure. Then, the approach consists in traducing the active behavior of the tissue by local elastic deformations in the direction of the tissue fibers. In our case, this amounts to traduce the bending dynamics inside a cilium by elastic deformations in the direction of the microtubules, which induce a bending deformation.

We consider a reference configuration Ω_s which is a straight vertical cylinder of finite length, and we suppose that the structure is anchored at its bottom boundary Γ_s. Defining by $\mathbf{e}_a$ the unit vector field in the direction of the microtubules (which is constant in the reference configuration), the active stress tensor is then given by

$$\Sigma^*(t, x) = S_a(t, x)\mathbf{e}_a \otimes \ \mathbf{e}_a, \quad t \geq 0, \quad x \in \Omega_s,$$

where $S_a(t, x)$ is a scalar function called the *activity scenario*, which only depends on the time and the material position in the reference configuration.

At a given point x and a given time t, if $S_a(t, x)$ is positive the structure locally stretches, whereas if it is negative it contracts. Since it is anchored at the bottom, the local expansion or shrinking of the medium will induce the bending of the whole structure. Thus, if the activity scenario is well-chosen, this model enables to easily reproduce biomimetic self-induced deformations of elongated elastic structures. For a more detailed description of the model and the possible activity scenarios, see [151].

Figure 3.1 shows the motion obtained solving problem (3.1) with a particular activity scenario, which will be used to perform the two-dimensional numerical simulations of the fluid/active-structure interaction shown at the end of this chapter. The resulting cilium beat is not symmetric under time reversal, with an effective stroke followed by a recovery stroke with different deformations. The scenario is parametrized by its beating frequency and the intensity of the internal activity.

3.3 The fluid-structure interaction problem

We consider an open bounded domain $\Omega \subset \mathbb{R}^d$, typically a d-dimensional box, such that $\Omega_s \subset \Omega$ and $\Omega_s(t) \subset \Omega \ \forall t > 0$. The structure is anchored at the bottom of the domain, and immersed in a viscous fluid that occupies the whole box, so that the time-dependent fluid domain considered at each time $t > 0$ is $\Omega_f(t) = \Omega \setminus \overline{\Omega_s(t)}$. The fluid-structure interface at time $t > 0$ is denoted by $\Gamma_{fs}(t)$, *i.e.* $\Gamma_{fs}(t) = \partial\Omega_f(t) \cup \partial\Omega_s(t)$, while the undeformed interface is denoted by

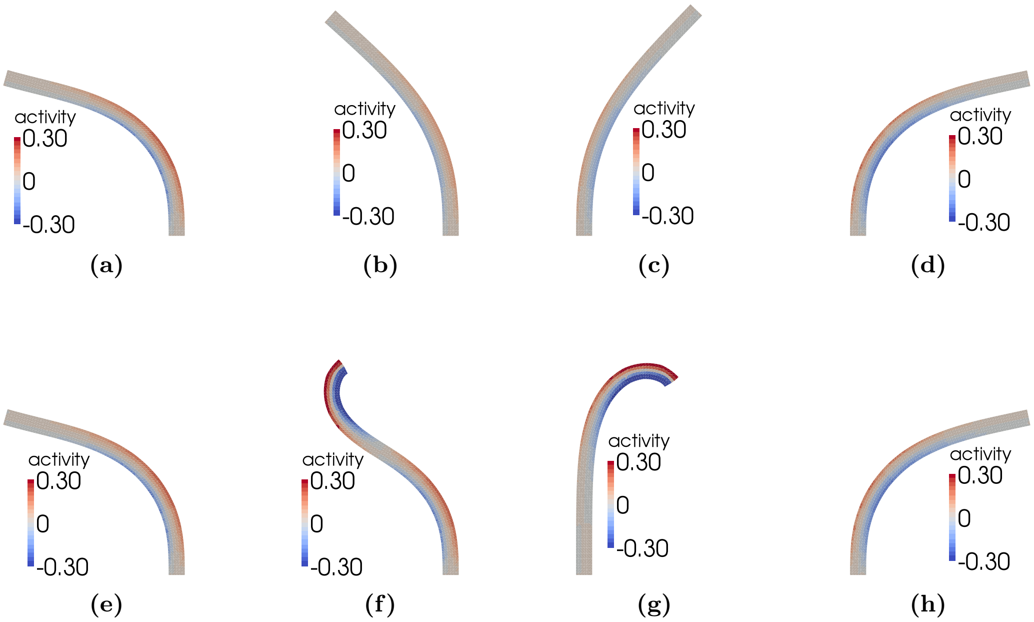

(a) (b) (c) (d) (e) (f) (g) (h)

FIGURE 3.1 – Elongated structure subjected to an internal activity inducing cilia-like deformations at different times.

Γ_{fs}. The fluid problem is governed by the Stokes equations :

$$\begin{cases} -\nabla \cdot (\sigma(\mathbf{u}(t), p(t))) & = & \mathbf{f}_f(t), \quad \text{in } \Omega_f(t), \\ \nabla \cdot \mathbf{u}(t) & = & 0, \qquad \text{in } \Omega_f(t), \end{cases} \tag{3.2}$$

where $\mathbf{u}$ denotes the velocity of the fluid, p the pressure field, $\sigma(\mathbf{u}, p)$ the fluid stress-tensor and $\mathbf{f}_f$ the external forces. We consider a Newtonian fluid, thus the stress-tensor writes :

$$\sigma(\mathbf{u}, p) = 2\mu\mathbb{D}(\mathbf{u}) - p\mathrm{Id},$$

where $\mathbb{D}(u) = \frac{1}{2}(\nabla\mathbf{u} + \nabla\mathbf{u}^t)$ is the strain tensor (or symmetric gradient of $\mathbf{u}$) and Id denotes the identify operator in $\mathbb{R}^d$.

The fluid problem is written in the Eulerian frame, that means in the physical fluid domain $\Omega_f(t)$ at each time $t > 0$, whereas the structure problem (3.1) is written in the Lagrangian frame, *i.e.* in the fixed reference configuration Ω_s. Both problems are coupled through the boundary conditions at the fluid-structure interface, traducing the continuity of the velocities and of the normal constraints. In order to write these conditions in the same Lagrangian frame, that means on the fluid-structure interface in the undeformed configuration, we need to introduce some mathematical objects.

Let us recall the function $\phi(t) : \Omega_s \to \mathbb{R}^d$, that maps Ω_s into $\Omega_s(t)$. This function can be extended to the whole domain Ω in a regular function $\phi(t) : \Omega \to \mathbb{R}^d$ satisfying the following relations at each time $t > 0$:

$$\phi(\Omega, t) = \Omega \quad \text{and} \quad \phi(\Omega_f, t) = \Omega_f(t), \quad \text{where } \Omega_f = \Omega \setminus \overline{\Omega_s}. \tag{3.3}$$

Such an extension is constructed in practice when using an ALE (Arbitrary Lagrangian Eulerian) method to solve the fluid-structure problem numerically. For instance, one can solve an elliptic problem (typically a Laplace equation or the equations of linearized elasticity) in the fluid domain with Dirichlet boundary conditions leading to the satisfaction of relation (3.3).

Using such a mapping, we can define the fluid velocity and the pressure field on the undeformed fluid-structure interface Γ_{fs} as follows :

$$\mathbf{w}(t) = \mathbf{u}(t) \circ \phi(\cdot, t) \quad \text{and} \quad q(t) = p(t) \circ \phi(\cdot, t) \quad \text{on } \Gamma_{fs}.$$

We denote by $\pi(\mathbf{w}, q)$ the fluid stress-tensor in the reference configuration (see for instance [151]).

The transmission boundary conditions at the fluid-structure interface Γ_{fs} (in the reference configuration) then write :

$$\mathbf{w}(t) = \frac{\partial \mathbf{d_s}(t)}{\partial t} \quad \text{and} \quad (F(\mathbf{d}_s(t))\,(\Sigma(\mathbf{d_s}(t))) - \Sigma^*(t)) \cdot \mathbf{n}_s - \pi(\mathbf{w}(t), q(t)) \cdot \mathbf{n}_s = 0 \quad \text{on } \Gamma_{fs}. \tag{3.4}$$

Boundary conditions must also be added on the other boundaries of the fluid domain, depending on the physical configuration considered. In the following we will consider homogeneous Dirichlet boundary conditions for simplicity.

The system of coupled partial differential equations obtained has been studied mathematically by Vergnet in [151]. The author proves the existence and uniqueness of weak solutions to the stationary problem, resulting from the time discretization of the equations, provided the internal activity of the structure is small enough. For the quasi-static problem, when fluid domains and structure evolve in time, he proves the existence and uniqueness of strong local solutions in time, provided the data of the problem are sufficiently small.

3.4 Numerical resolution of the fluid-structure interaction

The numerical method used to solve the fluid/active-structure interaction problem (3.1-3.2-3.4) is based on a finite element method on conformal meshes, that means that the mesh moves and fits the fluid-structure interface at each time step. Both problems are solved in a strongly coupled way using an iterative algorithm in order to avoir numerical instabilities [28].

For that purpose, the equations are first time-discretized using an Euler scheme to approximate the time derivative of the displacement in (3.4). The fluid and structure domains at a given time step are then entirely determined by the displacement of the structure at the previous time step. The non-linearity of the structure equation is treated implicitly.

Then, the problem is written into a variational form that strongly couples the fluid and structure equations. The boundary conditions at the fluid-structure interface (3.4) are treated as follows : the continuity of the normal constraints is prescribed as a natural condition, whereas the continuity of velocities is prescribed as an essential condition. Thus, the variational formulation obtained at time t^n is posed on a constrained functional space for the fluid velocity and the structure displacement, in which the constraint is the continuity of the velocities at the fluid-structure interface Γ_{fs}. More precisely we search the approximation of the velocity $\mathbf{u}^n$ and of the displacement ${\mathbf{d_s}}^n$ at each time $t = t^n = n\Delta t$ in :

$$V^n = \left\{ (\mathbf{u}, \mathbf{d_s}) \in V_f^n \times V_s \;/\quad \mathbf{u} \circ \phi^n = \frac{\mathbf{d_s} - {\mathbf{d_s}}^{n-1}}{\Delta t} \quad \text{on } \Gamma_{sf} \right\}, \tag{3.5}$$

where

$$V_f^n = \left\{ \mathbf{u} \in H^1(\Omega_f^n)^d \;/\; u = 0 \text{ on } \partial\Omega_f^n \setminus \Gamma_{fs}^n \right\},$$
$$V_s = \left\{ \mathbf{d_s} \in H^1(\Omega_s)^d \;/\; d_s = 0 \text{ on } \partial\Omega_s \setminus \Gamma_{fs} \right\},$$

and where ϕ^n maps Ω_s into Ω_s^n and Ω_f into Ω_f^n.

An internal discretization of this variational formulation is difficult because the finite element functions should satisfy the constraint ; thus standard finite element solvers cannot be used. Besides, it would lead to a monolithic resolution of the problem, that means the fluid and structure equations must be solved instantaneously. In order to relax the constraint in V^n, the problem is rewritten into a saddle-point formulation, with a Lagrange multiplier associated to the continuity constraint. The saddle-point problem is solved using an iterative Uzawa algorithm (see for instance [4]), that allows to deal with each problem (fluid and structure) independently. The non-linear elasticity problem is solved on the reference configuration, since the problem is written in Lagrangian formulation. The non-linearity is treated through a Newton method that leads to iteratively solve a linear problem, for which a classical first order finite element solver is used. The fluid problem is written in the Arbitrary Lagrangian Eulerian frame [86], and solved on a mobile mesh that fits to the physical fluid domain at each time step and is conformal to the fluid-structure interface. The ALE description consists in defining arbitrarily the velocity of the mesh inside the fluid domain, with the only constraint that it must fit to the physical boundaries at each time step. In this way it prevents significant distortions of the computational mesh that would arise if using a purely Lagrangian approach, while preserving the clear delineation of interfaces. Still, since in our approach the mesh in the fluid must perfectly fit to the mesh in the structure, strong distortions can occur occasionally, and then the fluid domain must be remeshed, but this only happens sometimes. We refer to [151] for a more detailed description of the numerical procedure.

This method has been implemented in by F. Vergnet in the finite element software FEniCS [105]. Some preliminary 2d results have been obtained so far. Figure 3.2 shows the result of a simulation of one cilium beating in a viscous flow, with the activity scenario shown in Figure 3.1.The computational domain is a $2D$ box of size $10\mu m \times 20\mu$m, the undeformed cilium has length 6.5μm and radius 0.2μm. The parameters of the elasticity model are $E_s = 10^6$pN$\cdot\mu$m^{-2} and $\nu_s = 0.49$, and the fluid viscosity is 0.01pN$\cdot\mu$m^{-2}. Other simulations have shown that, as expected, when increasing the viscosity of the fluid, the displacement of the cilium decreases. Figure 3.3 shows the result of the simulation of two cilia modeled with the same activity scenario, but with a phase shift. They interact via the fluid and the emerging beating pattern is completely different from the one obtained for a single cilium, and it strongly depends on the value of the phase shift. We now wish to investigate more deeply the influence of the different parameters of the model (phase shift, distance between two cilia, viscosity of the PCL and the mucus layer . . .) on the interaction between 2 or more cilia. However, three-dimensional simulations must be performed in order to obtain realistic results.

The numerical method presented in this section allows for a very accurate resolution of the

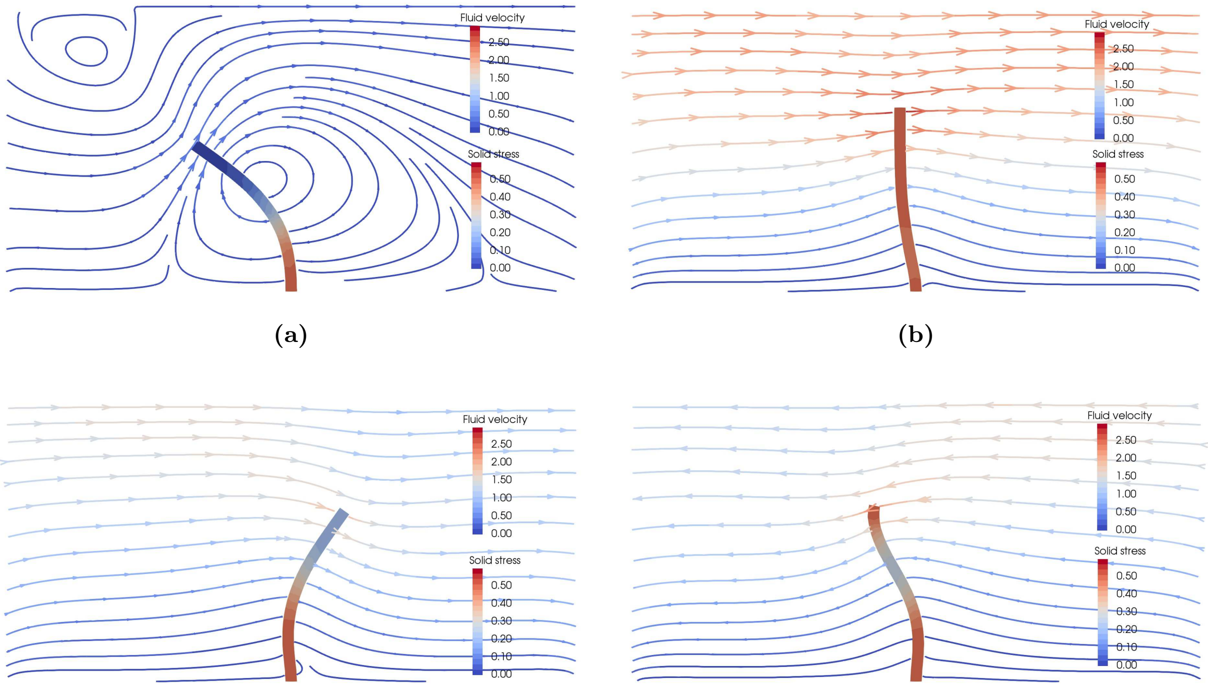

(a) (b)

(c) (d)

Figure 3.2 – One cilium beating in a viscous fluid of viscosity $\mu_f = 0.01$ pN·μm·s at different times between $t = 1$s and $t = 2$s. The activity scenario is the one illustrated in Figure **??**.

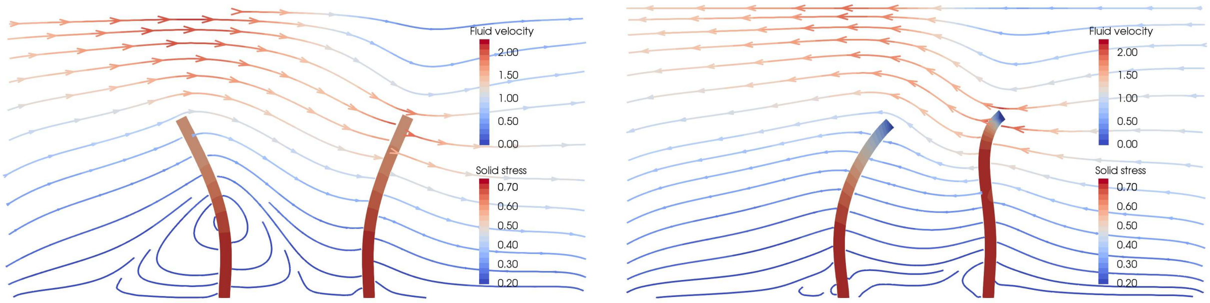

(a) (b)

Figure 3.3 – Two cilia beating in a viscous fluid of viscosity $\mu_f = 0.01$ pN·μm·s at $t = 78$s and $t = 0.83$s. The activity scenario for both cilia is the one illustrated in Figure **??**, with a phase shift of 0.075s.

fluid-structure problem, since the mesh is conformal to the fluid-structure interface and the finite element method applied to each stationary problem converges at the optimal order at each time step. However, it has a high computational cost : the Uzawa method needs a large amount of iterations, and at each iteration a Stokes problem on a large and complex domain must be solved (the elasticity problem is solved rapidly because the mesh is small, due to the small size of the structure). A lower cost method must be investigated, and this is the purpose of the last section of this chapter, in which we develop a fictitious-domain method that allows to use an unfitted, fixed and structured mesh for the fluid problem, while preserving the optimal order of convergence of the finite element method.

3.5 A fictitious domain method for elliptic transmission problems

In this section we present the numerical method developed in [47] for elliptic transmission problems. It is a method of the fictitious domain type, based on a control approach. Our aim was to develop such a method for the resolution of the fluid-structure problem, in order to be able to use an unfitted, fixed and structured mesh for solving the fluid problem, while preserving the optimal order of convergence of the finite element method. In [47], we describe the construction of the method in details and analyse it essentially at the continuous level ; the numerical analysis at the discrete level will be done in a future work.

Fictitious domain methods (see for instance [122, 7, 157, 13]) allow to solve problems in complex geometries using methods that are only adapted to simple geometry domains containing the complex one. In the framework of transmission problems, they allow to use meshes that do not fit the interface where the transmission conditions must be prescribed. In both cases, they give access to simple approximation methods that are well suited to rectangles and boxes, with efficient solvers such as Fast Fourier transform, Fast Poisson and Helmholtz solvers, multigrid, . . ., easy to parallelize and also well suited to fast domain decomposition. In addition, they allow to use fixed meshes although the interface may vary in time, and thus prevents from generating a new mesh at each time step. However these methods often do not converge with optimal order in space (see [69], because the mesh does not fit the boundary or the interface. Some methods overcome this problem [3], but this comes with an additional cost, and it is not always straightforward to adapt them to deformable moving materials.

In this work we develop a fictitious domain method based on a control formulation. This approach was initially developed in [6] to solve boundary value problems in complex geometries, for instance a box containing an obstacle, and adapted in [59] to solve the interaction between a viscous fluid and rigid particles. The idea is to extend the problem inside the obstacle and look for a right-hand side with compact support in the obstacle such that the solution satisfies the boundary conditions on its boundary. The problem can then be discretized on a non-conformal and fixed mesh, and solved using a classical finite element method that converges with optimal order in space. Besides, it is rather simple to implement ; in fact it leads to a least-square formulation of the boundary or transmission condition, for which gradient methods are well adapted. In [47], we have extended this approach to the solution of elliptic transmission problems using unfitted meshes. This “smooth extension” method is described for a simple “toy problem”, namely the Laplace transmission problem, and then applied to the Stokes transmission problem and the linear fluid-structure interaction problem. Besides recovering the optimal order, another advantage of this method is that it allows to decouple the problems involved and solve them independently on different meshes. For instance when applied to a fluid-structure interaction, it allows to, on one hand, solve a fluid problem in the whole domain on a structured mesh that does not fit the interface, and on the other hand solve accurately the elasticity problem on an independent mesh that only covers the structure. The method is therefore particularly adapted to transmission problems involving several small domains included in a bigger one, for instance bubbles in a fluid, rigid and deformable particles in a fluid or problems of conductivity and elasticity of non-homogeneous materials.

The Laplace-Laplace transmission problem

We consider a rectangular domain $\Omega \subset \mathbb{R}^d$, with $d = 2, 3$, divided in two subdomains $\Omega_1 \subset \Omega$ and $\Omega_2 \subset \Omega$ with Lipschitz boundaries, such that $\Omega_1 \cup \Omega_2 = \Omega$, $\Omega_1 \cap \Omega_2 = \emptyset$ and the interface $\Gamma = \partial\Omega_1 \cap \partial\Omega_2$ is not empty. We are interested in solving a Laplace problem

$$-\mu\Delta u = f \quad \text{in } \Omega,$$

with discontinuous coefficients $\mu = \mu_1\chi_{\Omega_1} + \mu_2\chi_{\Omega_2}$ and $f = f_1\chi_{\Omega_1} + f_2\chi_{\Omega_2}$, where $\mu_i \in \mathbb{R}_*^+$, $f_i \in L^2(\Omega_i)$ and χ_{Ω_i} denotes the characteristic function associated to Ω_i, for $i = 1, 2$. This problem can be rewritten as a Laplace problem with transmission conditions on Γ, that is find $u_1 : \Omega_1 \to \mathbb{R}$ and $u_2 : \Omega_2 \to \mathbb{R}$ such that

$$\begin{cases} -\mu_1\Delta u_1 & = f_1 \quad \text{in } \Omega_1, \\ -\mu_2\Delta u_2 & = f_2 \quad \text{in } \Omega_2, \\ u_1 & = u_2 \quad \text{on } \Gamma, \\ \mu_1\nabla u_1 \cdot \mathbf{n} & = \mu_2\nabla u_2 \cdot \mathbf{n} \quad \text{on } \Gamma, \\ u_1 & = 0 \quad \text{on } \partial\Omega_1 \setminus \Gamma, \\ u_2 & = 0 \quad \text{on } \partial\Omega_2 \setminus \Gamma. \end{cases} \tag{3.6}$$

In order to solve this problem using a finite element method, we can write the following variational formulation : find u in $H_0^1(\Omega)$ such that

$$\int_\Omega \mu\nabla u \cdot \nabla v = \int_\Omega fv \quad \forall v \in H_0^1(\Omega). \tag{3.7}$$

This variational problem admits a unique solution in $H_0^1(\Omega)$, whose components $u_1 = u_{|\Omega_1}$ and $u_2 = u_{|\Omega_2}$ have H^2 regularity on their associated domains Ω_1 and Ω_2 [4]. However, the solution u presents a jump in its normal derivative on Γ, and it is therefore not of regularity H^2 on the whole domain Ω. Thus, if one discretizes the domain Ω by a mesh that does not fit the interface Γ, the convergence rate of the finite element method is degraded. Indeed, classical convergence results do not apply, and in practice the method only converges with order $1/2$ in H^1-norm, independently of the order of the finite elements (the optimal convergence rate of an internal approximation when using piecewise linear elements is 1 in H^1-norm and 2 in L^2-norm). When the mesh fits the interface, the discontinuity is reconstructed accurately and the optimal order is recovered.

The smooth extension method provides a way to circumvent the degradation of the convergence rate using an unfitted mesh. Furthermore, it allows to deal with each problem involved independently.

The smooth extension method : continuous framework

The idea of the method is to replace, at the continuous level, problem (3.6) by the following Dirichlet and Neumann problems : let g be a function in $L^2(\Omega_2)$, find $u_{1,g}$, $u_{2,g}$ solving

$$\begin{cases} -\mu_1 \Delta u_{1,g} & = f_1 + g\chi_2 \quad \text{in } \Omega, \\ u_1 & = 0 \quad \text{on } \partial\Omega, \end{cases} \tag{3.8}$$

and

$$\begin{cases} -\mu_2 \Delta u_{2,g} & = f_2 \quad \text{in } \Omega_2, \\ \mu_2 \nabla u_2 \cdot \mathbf{n} & = \mu_1 \nabla u_1 \cdot \mathbf{n} \quad \text{on } \Gamma, \\ u_2 & = 0 \quad \text{on } \partial\Omega_2 \setminus \Gamma. \end{cases} \tag{3.9}$$

It is straightforward to prove that if $g \in L^2(\Omega_2)$ is such that the solution of problem (3.8-3.9) satisfies $u_{1,g} = u_{2,g}$ on Γ, then $u_{1,g}{}_{|\Omega_1} = u_1$ and $u_{2,g} = u2$, solutions of the initial problem (3.7).

The advantage is that problems (3.8) and (3.9) can be discretized independently. In fact, the first one is posed on the whole domain Ω and does not depend on the solution of the second problem ; thus it can be solved on a fixed and structured mesh that does not fit the interface. The second problem is posed on subdomain Ω_2 and can be solved on an independent mesh. Besides the practical advantage of decoupling the transmission problems, a standard finite element discretization of each problem will converge at the optimal order.

Such a function g exists under quite weak assumptions ; in fact, if there exists a smooth extension $\overline{u_1}$ of u_1 to the whole domain Ω such that $\overline{u_1} = 0$ on $\partial\Omega$, then $g = -\mu_1 \Delta \overline{u_1}$ in Ω_2 is admissible. We have shown in [47] (**Theorem 4.5**) that, if $u_1 \in H^2(\Omega_1)$ and if Γ and $\partial\Omega$ have at least $\mathcal{C}^2$-regularity in the neighborhood of their intersection, there exists an extension of regularity $H^2(\Omega)$ that satisfies the homogeneous Dirichlet conditions on the boundary of Ω. And since the extension is not unique, the control term g is not unique.

Then, introducing the cost function $J : L^2(\Omega_2) \to \mathbb{R}^+$ defined by :

$$J(g) = \frac{1}{2} \int_\Gamma |u_{1,g} - u_{1,g}|^2,$$

where $(u_{1,g}, u_{2,g})$ is the solution of problem (3.8-3.9), the initial transmission problem can be reformulated as a control problem : find $g \in L^2(\Omega_2)$that minimizes J. In fact, we have the following equivalence :

$$g = argmin_{q \in L^2(\Omega_2)} J(q) \quad \Leftrightarrow \quad (u_{1,g}{}_{|\Omega_1}, u_{2,g}) \text{ is the solution of problem (3.7).}$$

The smooth extension method thus consists in reformulating the transmission problem (3.7) as a *PDE-constrained optimization problem*, that can be solved using a gradient method. In [47] we use the *adjoint method* [88] to find an explicit formula of the gradient of the cost function J, necessary to construct the gradient method. For that purpose we introduce the Lagrangian corresponding to our constrained optimization problem, the constraint being that $(u_{1,g}, u_{2,g})$ is the solution of problem (3.8-3.9). The adjoint method consists in computing the gradient by solving two boundary value problems : for a particular value of $g \in L^2(\Omega_2)$, $\nabla J(g)$ is computed by solving the "direct" problem (3.8-3.9) for this value of g, and the adjoint problem on the Lagrange multipliers associated to the constraint. The adjoint problem is a Laplace problem with a singular right-hand side involving $(u_{1,g}, u_{2,g})$: find $(\lambda_{1,g}, \lambda_{2,g})$ such that

$$\begin{cases} -\mu_2 \Delta \lambda_{2,g} & = 0 \quad \text{in } \Omega_2, \\ \nabla \lambda_{2,g} \cdot \mathbf{n} & = (u_{1,g} - u_{2,g})\ \delta_\Gamma \quad \text{on } \Gamma, \\ \lambda_{2,g} & = 0 \quad \text{on } \partial\Omega_2 \setminus \Gamma, \end{cases} \tag{3.10}$$

and

$$\begin{cases} -\mu_1 \Delta \lambda_{1,g} & = f_g \quad \text{in } \Omega, \\ \lambda_{1,g} & = 0 \quad \text{on } \partial\Omega, \end{cases} \tag{3.11}$$

where δ_Γ is the dirac measure along Γ and $f_g \in H^{-1}(\Omega)$ is defined by

$$< f_g, v >= \int_{\Omega_2} \mu_1 \nabla \lambda_{2,g} \nabla v_{|\Omega_2} - \int_\Gamma (u_{1,g} - u_{2,g}) v \quad \forall v \in H_0^1(\Omega).$$

The *algorithm* presented in [47] to implement the smooth extension method is the following :

Choose an initial guess $g = g_0$ defined on Ω_2 for the control term.
While $|J(g)| > \epsilon$:

1. Compute the solution $(u_{1,g}, u_{2,g})$ of problem (3.8-3.9) ;
2. Compute the solution $(\lambda_{1,g}, \lambda_{2,g})$ of the adjoint problem (3.10-3.11) ;
3. Compute the gradient $\nabla J(g) = \lambda_2 - \lambda_{1|\Omega_2}$;
4. Update the control g using $\nabla J(g)$, depending on the optimization method chosen.

Finite element discretization

In [47] we have solved the Laplace transmission problem using the smooth extension method and standard finite elements to approximate the continuous functional spaces. This involves the approximation of three problems :

1. the Laplace problem (3.8)-(3.9), defined on Ω and Ω_2 resp. ;
2. the adjoint problem (3.10)-(3.11), defined on Ω_2 and Ω resp. ;
3. the minimization problem $g = argmin_{q \in L^2(\Omega_2)} J(q)$.

The numerical analysis of the convergence of the finite element discretization of the global problem is therefore not straightforward, and we aim to do it in a future work. We have performed several numerical tests that confirm that the method converges at the order 2 in the L^2-norm and at order 1 in the H^1-norm when using piecewise linear finite elements. Figure 3.4 shows the numerical solution obtained for a Laplace transmission problem. The reference solution (computed on a very fine mesh) is compared to the solution obtained with the smooth extension method. In [47] we also show a test case that illustrates the fact that even when the solution to the continuous problem is less regular than $H^2(\Omega)$ on each subdomain (because of the geometry of the domain or the regularity of the right-hand sides), the Smooth Extension method can still be applied and shows a converge rate that is the same than the classical Finite Element method with conformal meshes.

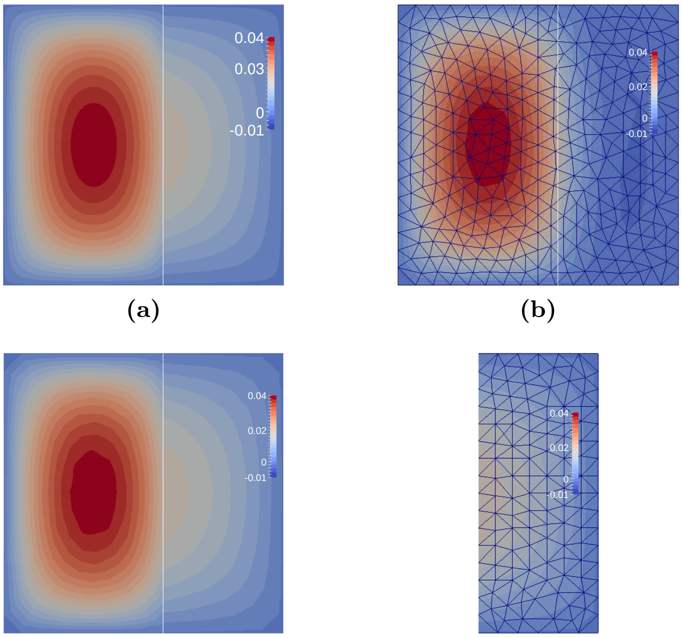

(a) **(b)**

(c) **(d)**

Figure 3.4 – Numerical solution for the Laplace transmission problem with $\mu_1 = 1$, $\mu_2 = 10$, $f_1 = 1$ and $f_2 = 1$. (a) Reference solution. (b) Field $u_{1,g}$. (c) Superposition of fields $u_{1,g}$ and $u_{2,g}$.

Regarding the computational cost, recovering the optimal convergence order comes with an additional cost : it requires the resolution of an optimization problem using an iterative method, and at each iteration one has to solve two boundary-value problems. However, the boundary value problems posed on Ω can be solved using a fast and parallel solver on a structured mesh. In addition, the operators involved are the same at each iteration of the optimization algorithm and at each time step, since they do not depend on the position of the interface ; thus, if the problem evolves in time, the operators defined on Ω do not change. The associated matrices can therefore be constructed once and for all at the beginning of the simulation, and their condition number is not degraded. Besides, an iterative method must often be used anyway to solve transmission problems in a strongly coupled way, as for instance in the case of a fluid-structure interaction problem. For all these reasons this method can allow for a considerable gain in the computational cost of the resolution of such problems. This gain remains to be investigated and quantified.

Application to other transmission problems

In [47] we have detailed the application of the smooth extension method to a Stokes transmission problem and a fluid-structure transmission problem. In the first case, the additional advantage of the method is that it allows to reconstruct the physical jump in pressure through the interface, while the classical finite element method with unfitted meshes does not (even with conformal meshes, if the pressure is not approximated by discontinuous finite element functions). In addition, if the position of the interface changes, the big domain (Ω) does not have to be remeshed. Figure 3.5 shows the numerical solution obtained for a Stokes transmission problem. Both the velocity (upper figure) and the pressure (lower) fields are plotted. We compare the solution

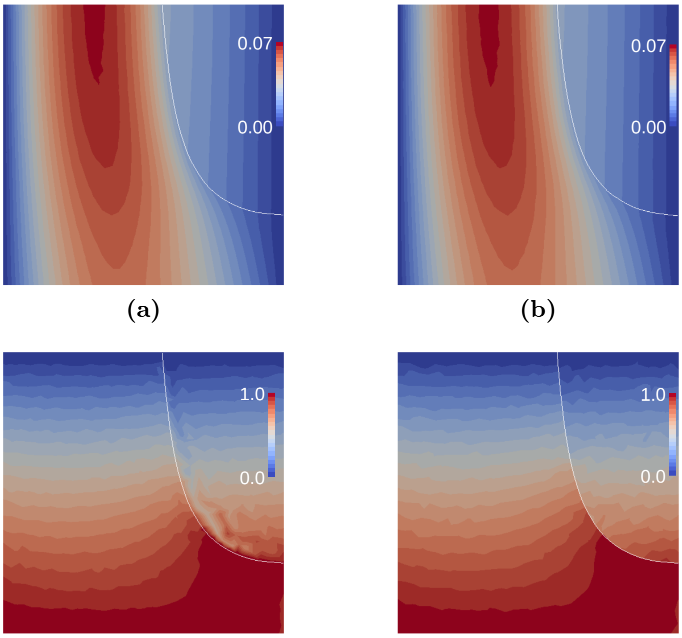

(a) **(b)**

(c) **(d)**

FIGURE 3.5 – Numerical solution for the Stokes transmission problem with $\mu_1 = 1$, $\mu_2 = 10$, $f_1 = (1, 0)$ and $f_2 = (1, 0)$. (a) Velocity field obtained with a classical FE method on a conformal mesh. (b) Velocity field obtained with the smooth extension method on a non-conformal mesh. (c) Pressure field obtained with a classical FE method on a conformal mesh. (d) Pressure field obtained with the smooth extension method on a non-conformal mesh.

computed using a conformal mesh (left) with the solution obtained with the smooth extension method on a non-conformal mesh (right). Both solutions are similar but the smooth extension method allows to well reproduce the physical jump in pressure.

In [47] the Smooth Extension Method is also applied to a linear fluid structure interaction problem. The fluid problem is solved in the Eulerian frame on a fixed mesh (thus no remeshing is needed), whereas the elasticity equations are solved in the Lagrangian frame on an independent mesh. We consider a test case where an elastic beam, anchored at the bottom of the domain, is bended in a shear flow. The solution obtained with the Smooth Extension Method (SEM) is in agreement with the solution computed on a conformal mesh using the numerical method described in section 3.4. We show how with the SEM method it is possible to coarsen the fluid mesh while maintaining the same amount of mesh elements in the structure, in order to reduce the computational cost.

Chapitre 4

Some inertial flows with free or moving boundaries

While the previous chapters concern active low Reynolds flows, where inertial effects can be neglected, this chapter deals with non-active inertial flows. It is the result of several collaborations, most of which are interdisciplinary. Inertial flows have completely different properties since the governing equations are nonlinear and convective terms must be taken into account. However, what these works have in common with the previous ones is that they concern flows with free or moving boundaries, and the numerical tools to deal with the moving interfaces are similar. The first section concerns free surface flows in domains that only move in the vertical direction, as for instance water waves in closed basins. I have been working on this subject since my Phd, that dealt with the three-dimensional hydrostatic model for free surface flows, and in particular its resolution in the Telemac-3D software developed at the Laboratoire National d'Hydraulique et Environnement (LNHE), EDF (Electricité de France). The collaboration with EDF has been pursued, especially with the Phd of P. Quemar that I have co-directed with Emmanuel Audusse and Olivier Lafitte (Laboratoire LAGA, Université Paris 13), on the analysis and improvement of the Telemac-3d software. The first work presented in this section results from a collaboration with Luca Bonaventura and Fausto Saleri (MOX, Politecnico di Milano), and deals with a reduced model for free surface flows [42]. When the ratio between the vertical and longitudinal scales is small enough, the so-called Shallow Water approximation is usually introduced, and the three-dimensional equations are reduced to a two or one dimensional system. In order to properly account for friction and eddy viscosity effects, we have asymptotically derived the section-averaged shallow water model usually applied in river and open channel hydraulics up to the second order in the vertical/longitudinal length ratio, starting from the three-dimensional Reynolds-averaged Navier-Stokes equations for incompressible free surface flows. Next, I give some hints on different ways to solve free surface flows numerically. In particular, I briefly describe the algorithm used in the Telemac3d software, which has been analyzed by P. Quemar during his Phd, and I comment on the advantages and drawbacks. Section 2 concerns the numerical study of a new oscillatory instability that has been observed experimentally by B. Semin and coworkers (Laboratoire FAST, Université Paris Sud) on a cylinder confined in an inertial flow. In order to help understanding the underlying mechanism, we have performed numerical simulations using a finite element method on a moving mesh which is conformal to the geometry of the cylinder at each time step. This method allows to achieve a good accuracy and the instability is well reproduced [140]. The last section concerns a collaboration with researchers from the IR4M (Imagerie par Résonance Magnétique Médicale et Multi-Modalités) laboratory at Université Paris Sud, on the characterization of blood flow in the aorta by combining numerical simulations and magnetic resonance imaging data [89].

4.1 The free surface Navier Stokes equations.

Let us introduce the incompressible Navier-Stokes equations governing the motion of a Newtonian fluid with constant density ρ in a moving domain denoted by $\Omega(t)$ at each time $t \geq 0$:

$$\left\{ \begin{aligned} \frac{\partial \mathbf{u}}{\partial t} + (\mathbf{u} \cdot \nabla)\mathbf{u} - \frac{1}{\rho}\nabla \cdot \big(\underline{\underline{\sigma}}(\mathbf{u}, p)\big) &= \mathbf{g}, \\ \nabla \cdot \mathbf{u} &= 0, \end{aligned} \right. \tag{4.1}$$

where $\mathbf{u}$ and p are the velocity and pressure fields, and $\underline{\underline{\sigma}}$ is the total stress tensor

$$\underline{\underline{\sigma}} = \nu(\nabla \mathbf{u} +^t \nabla \mathbf{u}) - p\mathbf{I}.$$

The domain's boundary can be decomposed into a free surface boundary denoted by $\Gamma_S(t)$, and an impervious boundary (walls) denoted by $\Gamma_W(t)$. In order to simplify the presentation we do not consider open boundaries here. The general dynamic conditions at the free surface boundary are :

$$\sigma \cdot \mathbf{n} = -p_e \mathbf{n} - \kappa \frac{\mathbf{n}}{R}, \tag{4.2}$$

where R is the radius of curvature of $\Gamma_S(t)$, κ the surface tension coefficient and p_e the external pressure. For a viscous fluid, imperviousness at the wall boundaries is described through a no-slip condition :

$$\mathbf{u} = 0. \tag{4.3}$$

In the next sections we will focus on the particular case of a flow whose free surface only moves in the vertical direction. This typically includes the case of water waves in a closed basin. We consider a model in which the free surface is supposed to be an “univoque” function of the horizontal plane, what rules out breaking waves.

Let ω be a fixed bounded region of $\mathbb{R}^{d-1}$ (with $d = 2$ or 3 the dimension of the problem). For any time t the domain $\Omega(t)$ is defined as follows :

$$\Omega(t) = \{(x, z) \in \mathbb{R}^d \ / \ x \in \omega \quad \text{and} \quad b(x) < z < \eta(x, t)\,\},$$

where η and b are two functions defined on ω describing respectively the free surface and the bottom. We will denote by h the water height :

$$h(x, t) = \eta(x, t) - b(x), \quad x \in \omega, \quad t > 0.$$

Particles at the free surface remain on it. Letting $(x(t), z(t))$ be the trajectory of a particle at the surface of the flow at time t, it satisfies : $z(t) = \eta(x(t), t)$ and

$$\frac{d}{dt}(\eta(x(t), t) - z(t)) = 0.$$

Thus, denoting by u the horizontal component of the fluid velocity and by w its vertical component, we have that

$$\frac{\partial \eta}{\partial t}(x, t) + u(x, z, t) \cdot \nabla \eta(x, t) = w(x, z, t), \qquad x \in \omega, \quad z = \eta(x, t). \tag{4.4}$$

This equation expresses the motion of the moving surface as a convection of the scalar function η defined on the two-dimensional domain ω, convected by the horizontal velocity $\mathbf{v}$ evaluated at the surface, with a source term equal to the corresponding vertical velocity w. Taking $\mathbf{n}$ the outgoing unit normal to the free surface, one can also express this kinematic condition as follows :

$$\frac{\partial \eta}{\partial t} = \mathbf{u} \cdot \frac{\mathbf{n}}{n_z} \qquad \text{on } \Gamma_S(t), \tag{4.5}$$

where n_z is the vertical component of the normal vector $\mathbf{n}$.

4.1.1 Asymptotic derivation of a section-averaged shallow water model

In environmental modeling of free surface flows, whenever the ratio between the vertical and longitudinal scales is small enough, the so-called *Shallow Water* approximation is usually introduced, in order to reduce the computational cost implied by the numerical solution of three-dimensional free surface flow equations. Models based on this approximation are extensively used to simulate various geophysical phenomena, such as rivers and coastal flows [61, 79], oceans and even avalanches [17], and they have been used in hydraulics for a very long time. When the viscosity is neglected and a rectangular channel section is assumed, the derivation of the one-dimensional Shallow Water system is classical, see e.g. [154]. However, this derivation is unsatisfactory, since viscosity effects are added *a posteriori* and the three-dimensional geometry is not arbitrary.

In [67], Gerbeau and Perthame formally derived, by asymptotic analysis, a one-dimensional viscous Saint-Venant system from the two-dimensional Navier-Stokes equations with molecular viscosity, linear friction boundary conditions and flat bathymetry. The effect of the viscosity was recovered in a one-dimensional friction term and in a one-dimensional diffusion term, both resulting from the derivation. The final system is a second order approximation – with respect to the ratio between the vertical and longitudinal scales – of the original two-dimensional model. Other systems have been derived in the same spirit [110, 132]. However, in order to simulate realistic river flows, three-dimensional geometries and turbulence phenomena must be taken into account. Thus, the Reynolds-averaged Navier-Stokes equations (RANS) on an arbitrary three-dimensional domain are a more appropriate starting point for the derivation of simplified systems.

In [42] we have chosen to proceed as in [67], extending the analysis to the three-dimensional Reynolds-averaged Navier-Stokes equations (RANS) with anisotropic Reynolds tensor for free surface flows in arbitrary geometry, with nonlinear friction boundary conditions entirely analogous to those actually used in practice in hydraulics applications. We consider a three-dimensional domain that represents a natural river whose depth tends to zero as the banks are approached. Such a domain is illustrated in Figure 4.1. But the same derivation can be made for channels with rectangular cross-section. We consider a turbulence model proposed by Levermore and Sammartino in [100], given through an anisotropic relationship between the stress tensor $\underline{\underline{\sigma}}$ and the strain-rate tensor $\mathbb{D} = \nabla \mathbf{u} + (\nabla \mathbf{u})^T$. This anisotropic stress tensor involves three viscosities μ_h, μ_v and μ_e that can be interpreted as the eddy viscosity relative to the horizontal shear motion, the eddy viscosity relative to the vertical shear motion, and the bulk viscosity relative to the expansion rate in the horizontal direction, respectively.

In a viscous flow, the velocity is zero on a solid wall, so that the so-called “no-slip” condition (4.3) should be applied. However, the boundary layer at the bottom is hardly ever resolved at typical resolutions of environmental models. Furthermore, it is necessary to describe in some

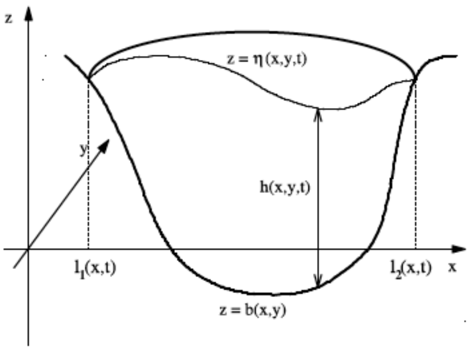

Figure 4.1 – Three-dimensional domain

approximate fashion the subgrid scale surface roughness. Thus, condition (4.3) is generally substituted by two boundary conditions assigned at a small distance Δz_r from the wall, which represents the typical length scale of the bottom boundary layer. The first boundary condition is a kinematic condition :

$$\mathbf{u}\cdot\mathbf{n} \;=\; 0 \qquad \text{at} \quad z = b(x,y) + \Delta z_r, \tag{4.6}$$

and the second one is a dynamic condition which accounts for friction effects :

$$(\frac{1}{\rho}\boldsymbol{\sigma_T}\cdot\mathbf{n})^T\cdot\mathbf{t} \;=\; -\alpha||\mathbf{u}||\mathbf{u}\cdot\mathbf{t} \qquad \text{at} \quad z = b(x,y) + \Delta z_r\,, \tag{4.7}$$

where $\alpha > 0$ is a dimensionless friction coefficient and $\mathbf{n}$ and $\mathbf{t}$ are, respectively, the outward normal and a matrix composed of two tangent vectors to the boundary. Condition (4.7) is indeed an assumption on the profile of the tangential velocity component along the direction normal to the bottom surface. A logarithmic wall law is usually assumed for tangential velocity near the bottom, see e.g. [131], so that a parabolic model is chosen for the vertical eddy viscosity, as well as a particular value of the friction coefficient α, depending on the value of Δz_r.

We have derived a section-averaged system that includes the effects of eddy viscosity and friction and whose unknowns are the section area $A = \displaystyle\int_{l_1}^{l_2} h(x,y,t)dy$ and the flow rate $Q = A(x,t)\bar{\bar{u}}(x,t)$, where $\bar{\bar{u}}$ is the average along the $y-$ and $z-$ direction of the longitudinal velocity component. If applied to channels with rectangular cross-section, this system is similar to the classical shallow water equations [131], except for the friction term. Indeed, our derivation shows that, in order to take into account effects up to the second order in the asymptotic parameter, the classical friction term should be corrected by a term which depends on the turbulent vertical viscosity. This conclusion is in agreement with [67] for two-dimensional flows with constant viscosity over a flat bathymetry. Indeed, if the vertical viscosity and friction coefficients are taken to be constant and the flow is homogeneous in the transversal direction, we retrieve the same friction correction. However, our derivation provides the expression of the friction correction term in a more general case, which includes turbulent flows, nonlinear friction boundary conditions and three-dimensional arbitrary geometry.

In particular, we have computed the correction term associated to a specific model for the vertical profile of turbulent velocity. For steady state open channel flows admitting analytic solutions of the three-dimensional as well as the simplified models, we have shown that the solutions computed including our correction term are much closer to those of three dimensional models than those of the standard shallow water model. If empirical friction closures are introduced, as commonly done in computational hydraulics (see e.g. [32]), one obtains results very similar to those of our generalized friction term for steady state open channel solutions. Thus, the generalized friction term resulting from this derivation justifies *a posteriori* these empirical closures, while allowing to avoid the assumptions on local flow uniformity on which these closures rely. The friction correction term can be easily included in section averaged models such as the one proposed by Deponti *et al.* in [51]. Its use is also expected to ease the coupling of three- and one-dimensional free surface models in the framework of an integrated hydrological basin model.

4.1.2 Numerical resolution of the free surface Navier-Stokes equations

In this section we have chosen to detail some possible numerical algorithms to solve the free surface Navier-Stokes equations (4.1)-(4.4) introduced at the beginning of this chapter. The domain only moves in the vertical direction and an ALE approach is adopted, allowing to use a mesh that follows the free surface evolution in time. We consider a particular configuration where the lateral boundaries of the domain are made of perfectly vertical and fixed walls, and the bottom is fixed and impervious.

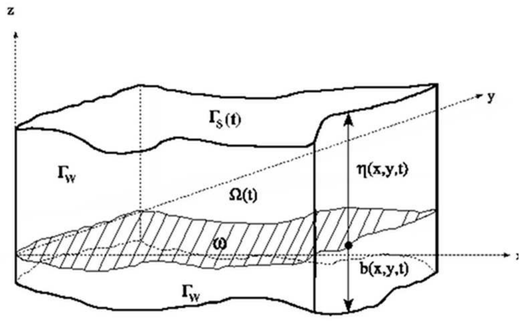

Figure 4.2 – The 3D domain and its boundaries.

The Arbitrary Lagrangian Eulerian (ALE) approach – see for instance [81, 149] – is a particular way of solving fluid flows in moving domains that has been adopted by many authors because of its great adaptability. It consists in defining a fitted mesh which follows the global motion of the fluid domain, at an arbitrary velocity which should be different from the fluid velocity, allowing for a continuous updating of the mesh. When the domain only moves in the vertical direction, it is appropriate to choose an arbitrary domain velocity $\mathbf{c}(\cdot,t) = (0,0,c(\cdot,t))$ defined on $\Omega(t)$ at each time $t \geq 0$ that only has a vertical non-zero component [43]. A very simple choice is to define :

$$c(\mathbf{x},t) = \frac{\partial \eta}{\partial t}(x,t)\frac{z-b(x)}{h(x,t)}, \quad t \geq 0, \quad \mathbf{x} = (x,z) \in \Omega(t). \tag{4.8}$$

This choice satisfies the consistency condition $\mathbf{c}(\cdot,t)\cdot\mathbf{n} = \mathbf{u}(\cdot,t)\cdot\mathbf{n}$ on $\partial\Omega(t)$ at each time $t \geq 0$, what ensures that the trajectory of the initial control volume corresponds to the physical time-space domain. It also prevents from any inversion of mesh elements during the simulation, since the ratio between the depth of each mesh layer and the total water height will remain constant in time. It is well-known in the atmospheric and oceanographic communities and referred to as the sigma transform or topography-following coordinate system [123, 91]. It allows to adopt a vertical discretization of the domain which at each time step follows the bathymetry and the free surface, as shown in Figure 4.3. Different CFD systems have been developed on this approach [79, 141].

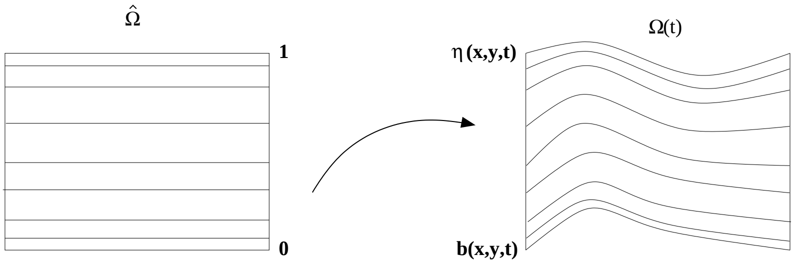

FIGURE 4.3 – Example of a discrete sigma-transform

From $\mathbf{c}$ it is possible to define ALE mappings between the domains $\Omega(t)$:

$$\begin{array}{rcl}\mathcal{A}(\cdot,t_1;t_2):\Omega(t_1) & \mapsto & \Omega(t_2)\\ \mathbf{x}_1 & \mapsto & \mathbf{x}_2=\mathcal{A}(\mathbf{x}_1,t_1;t_2),\end{array}$$

and for each time τ, we can define an eulerian field $\mathbf{q} : \{(t,\boldsymbol{x})/t \geq 0,\ \mathbf{x} \in \Omega(t)\} \mapsto \mathbb{R}^n$, $n \in N\backslash\{0\}$ in the ALE frame on the domain $\Omega(\tau)$ as follows :

$$\mathbf{q}_\tau(\boldsymbol{x},t) \ = \ \mathbf{q}(\mathcal{A}(\boldsymbol{x},\tau;t),t), \qquad \boldsymbol{x} \in \Omega(\tau), \quad t \in \mathbb{R}^+.$$

Conversely, any ALE field $\mathbf{q}_\tau : \Omega(\tau) \times \mathbb{R}^+ \mapsto \mathbb{R}^n$, $n \in N \setminus \{0\}$, can be defined in the Eulerian frame as follows

$$\mathbf{q}(\boldsymbol{x},t) \ = \ \mathbf{q}_\tau(\mathcal{A}(\boldsymbol{x},t;\tau),t), \qquad \boldsymbol{x} \in \Omega(t), \quad t \in \mathbb{R}^+. \tag{4.9}$$

Partial derivation with respect to time in (4.9) at $t = \tau$ gives :

$$\frac{\partial \mathbf{q}}{\partial t} = \frac{\partial \mathbf{q}_\tau}{\partial t} \ - \ \mathbf{c} \cdot \nabla \mathbf{q}. \tag{4.10}$$

The derivative $\dfrac{\partial \mathbf{q}_\tau}{\partial t}$ is an ALE time derivative ; it has two contributions : a transport term taking into acount the variation of $\mathbf{q}$ due to the displacement of the control volume at velocity $\mathbf{c}$, and an Eulerian time derivative term describing the temporal variations of $\mathbf{q}$.

Remark 1 *From a practical point of view, it is easier to discretize an ALE time derivative than an Eulerian time derivative on a mobile mesh. Actually, values of a discrete field q are associated to nodes whose coordinates vary in time, but whose numbering is fixed. If at time t node "i" has coordinates $\boldsymbol{x}_t$, and at time $t + \delta t$ its position is $\boldsymbol{x}_{t+\delta t}$, then values $q_i(t)$ and $q_i(t + \delta t)$ of q at this node are :*

$$q_i(t) = q(\boldsymbol{x}_t,t), \qquad q_i(t+\delta t) = q(\boldsymbol{x}_{t+\delta t}, t+\delta t).$$

The "natural" way of approaching the time derivative is therefore

$$\frac{q_i(t+\delta t)-q_i(t)}{\delta t} = \frac{q(\boldsymbol{x}_{t+\delta t},t+\delta t)-q(\boldsymbol{x}_t,t)}{\delta t} = \frac{q_t(\boldsymbol{x}_t,t+\delta t)-q_t(\boldsymbol{x}_t,t)}{\delta t} \approx \frac{\partial q_t}{\partial t}(\boldsymbol{x}_t,t),$$

which is an approximation of the ALE time derivative. In addition, in some situations, discretizing the eulerian time derivative makes no sense, since a point in the control volume at time t may not be inside at time $t+\delta t$.

We now introduce the notion of characteristics in the ALE formalism. Consider $\tau \geq 0$ and $\mathbf{x} \in \Omega(\tau)$. We introduce the ALE characteristic function $\mathbf{X}_\tau(\cdot;\tau,\mathbf{x}) : \mathbb{R}^+ \mapsto \Omega(\tau)$, defined on the domain $\Omega(\tau)$ as the solution of the following Cauchy problem :

$$\left\{ \begin{array}{rcl} \dfrac{\partial \mathbf{X}_\tau(s)}{\partial s} & = & (\mathbf{u}_\tau - \mathbf{c}_\tau)(\mathbf{X}_\tau(s),s), \quad \mathbf{X}_\tau(s) \in \Omega(\tau), \\ \mathbf{X}_\tau(\tau) & = & \boldsymbol{x}. \end{array} \right. \tag{4.11}$$

At each time s we can define

$$\mathbf{X}(s;\tau,\boldsymbol{x}) = \mathcal{A}(\mathbf{X}_\tau(s;\tau,\boldsymbol{x}),\tau;s) \tag{4.12}$$

the position at time s in $\Omega(s)$ of the pseudo-particle whose position at time τ is $\boldsymbol{x}$, and which is convected by velocity $\mathbf{u}-\mathbf{c}$.

We can write

$$\frac{d}{dt}(f_\tau(\mathbf{X}_\tau(t),t)) \; = \; \frac{\partial f_\tau}{\partial t}(\mathbf{X}_\tau(t),t) \; + \; \frac{\partial \mathbf{X}_\tau(t)}{\partial t} \cdot \nabla f_\tau(\mathbf{X}_\tau(t),t).$$

Therefore, at $t=\tau$, we have that :

$$\frac{d}{dt}(f_\tau(\mathbf{X}_\tau(t;\tau,\boldsymbol{x}),t)) \; = \; \frac{\partial f_\tau}{\partial t}(\boldsymbol{x},t) \; + \; (\mathbf{u}_\tau - \mathbf{c}_\tau)\cdot \nabla f_\tau(\boldsymbol{x},t),$$

what allows to write the momentum equation in (4.1) at time $t=\tau$ as follows :

$$\frac{d}{dt}\left(\mathbf{u}_\tau(\mathbf{X}_\tau(t;\tau,\boldsymbol{x}),t)\right) \; - \; \frac{1}{\rho}\nabla\cdot\left(\underline{\underline{\sigma}}(\mathbf{u}_\tau,p_\tau)\right) \; = \; \mathbf{g} \quad \text{in } \Omega(\tau). \tag{4.13}$$

This formulation of the convective term is well adapted to a discrete resolution using the characteristics method.

A simple algorithm

In [48], we describe how the software Freefem++ can be used to solve the free surface Navier-Stokes equations, using a classical finite element method and a simple time algorithm, and we provide two and three dimensional illustrations in the context of water waves. We use a semi-implicit, semi-Lagrangian approach to solve the free surface problem (4.1),(4.4). The advantage of this approach is that there is no CFL stability restriction on the time step, thus large time steps are tolerated and stationary state, when it exists, is reached quickly.

Let $\delta t > 0$ be the time step. We denote by $q^n(\cdot)$ the approximation at $t^n = n\delta t$ of the Eulerian field $q : \{(\mathbf{x}, t)/t \geq 0 \text{ and } \mathbf{x} \in \Omega(t)\} \mapsto \mathbb{R}$, and by $q^n_m(\cdot)$ the approximation at t^n of the ALE field $q_{t^m} : \Omega(t^m) \times \mathbb{R} \mapsto \mathbb{R}$. The approximated domain at time t^n is denoted by Ω^n.

We use the following first-order time algorithm : suppose that at some time t^n, the domain Ω^n and the fluid velocity $\mathbf{u}^n$ are known. The kinematic boundary condition at the free surface (4.5) suggests a naive way to move the boundary : the new value of the free surface η^{n+1} could be defined by

$$\eta^{n+1}(x) \;=\; \eta^n(x) \;+\; \frac{\delta t}{n_z}\,\mathbf{u}^n(x, \eta^n(x)) \cdot \mathbf{n}, \qquad x \in \omega, \tag{4.14}$$

where $\mathbf{n}$ is the outgoing unit normal to the free surface, and n_z its vertical component. This simple method is consistent from a kinematic point of view, but it leads to a scheme which is unstable in many applications. Indeed, condition (4.5) can be rewritten as a convection equation of the free surface function on ω, equation (4.4), for which an explicit centered scheme deriving from (4.14) would be unstable. Thus, we rather consider a time discretization of the free surface convection equation, which is solved using a 2D caracteristics method. Once the new free surface function is known, the domain can be updated through the following displacement of each point $\mathbf{x} = (x, z)$ in Ω^n :

$$\delta t c^n(\mathbf{x}) = (\eta^{n+1}(x) - \eta^n(x))\frac{z - b(x)}{h^n((x))}.$$

Remark 2 *The characteristics method being first order in time, it is easy to establish that the consistency relation* $\mathbf{c} \cdot \mathbf{n} = \mathbf{u} \cdot \mathbf{n}$ *on* $\partial\Omega(t)$ *holds at the first order.*

The approximation $\mathbf{u}^{n+1}$ of the velocity at time t^{n+1} on domain Ω^{n+1} is then given by the following semi-discrete scheme based on formulation (4.13) of the momentum equation :

$$\left\{\begin{array}{rcl} \mathbf{u}^{n+1} \;-\; \mathbf{u}^n_{n+1} \circ \mathbf{X}^n_{n+1} \;-\; \dfrac{\delta t}{\rho}\,\nabla \cdot \left(\underline{\underline{\sigma}}(\mathbf{u}^{n+1}, p^{n+1})\right) & = & \delta t\,\mathbf{g} \quad \text{in } \Omega^{n+1}, \\ \nabla \cdot \mathbf{u}^{n+1} & = & 0 \quad \text{in } \Omega^{n+1}, \end{array}\right. \tag{4.15}$$

where $\mathbf{X}^n_{n+1}(\boldsymbol{x})$ is the solution at time t^n of the following Cauchy problem :

$$\left\{\begin{array}{rcl} \dfrac{\partial \mathbf{X}_{n+1}(t)}{\partial t} & = & (\mathbf{u}^n_{n+1} - \mathbf{c}^n_{n+1})(\mathbf{X}_{n+1}(t)), \quad t \text{ in } [t^n, t^{n+1}] \\ \mathbf{X}_{n+1}(t^{n+1}) & = & \boldsymbol{x}, \qquad \boldsymbol{x} \in \Omega^{n+1}, \end{array}\right. \tag{4.16}$$

which is a first-order time-discretization of (4.11) in $[\tau - \delta t, \tau]$, for $\tau = t^{n+1}$.

As for the space discretization, a regular triangulation $\mathcal{O}_h$ of the horizontal domain ω is considered, and at each time step the free surface η^n is approximated by a piecewise linear function defined on this triangulation. The initial three-dimensional mesh $\mathcal{T}^0_h$ is obtained by piling up the horizontal mesh over N_z layers on the vertical from $z = b$ to $z = \eta^0$ (if $\mathcal{O}_h$ is a two-dimensional mesh made of triangles, then $\mathcal{T}^0_h$ is a prismatic mesh). The mesh is updated at each time step through the following displacement of each mesh node i :

$$\delta t c^n_h(\mathbf{x}^n_i).$$

The velocity and the pressure fields are approximated using a a pair of inf-sup stable finite element spaces ${X_h}^n \subset H^1(\mathcal{T}_h^n)^d$ and $M_h^n \subset L^2(\mathcal{T}_h^n)$. We chose for instance the classical P^1 Lagrange element for the pressure, and the P^2 Lagrange element or the so-called P^1-bubble element for the velocity. The corresponding pairs of finite element spaces are known to satisfy the "inf-sup" condition, which ensures the well-posedness of the discrete non-stationnary Stokes problem (see [125],[19]).

The difficulty when analyzing such a scheme is that the exact and approximated solutions are not defined in the same domain. In [113], Maury established a stability estimate on the global scheme, that relies on strong hypothesis on the regularity of the domain and the mesh at each time step. In addition, the field $\mathbf{u}^n$ used for the convection of the velocities is supposed to be projected on a space of fields with exactly vanishing divergence. In practice, this assumption does not seem to be required for stability.

The main drawback of this algorithm is that is does not preserve the global mass conservation exactly. Indeed, mass conservation is only satisfied at the first order in time and space. In the framework of the Phd of Pierrick Quemar [126], we have proposed an alternative algorithm that is exactly mass-conservative. Furthermore, we can prove stability under the same hypothesis on the regularity of the domain and the mesh, but without assuming that the velocity field is exactly divergence free. The idea of the algorithm relies on solving the free surface advection equation with an explicit scheme :

$$\frac{\eta^{n+1} - \eta^n}{\delta t}(x) \ + \ u^n(x, \eta^n(x)) \cdot \nabla \eta^n(x) \ = \ w^n(x, \eta^n(x)), \quad \text{for } x \in \omega, \tag{4.17}$$

so that, when integrating on ω, the term $\int_\omega u^n(x,\eta^n(x)) \cdot \nabla \eta^n(x) - w^n(x,\eta^n(x)) \,\mathrm{d}x = \int_{\Gamma_s^n} \mathbf{u}^n \cdot \mathbf{n} = \int_{\Omega^n} \nabla \cdot u^n$ vanishes, and the scheme ensures the exact global mass conservation. Since centered explicit schemes for convection equations are known to be unstable in many configurations, a Finite Element symmetric stabilization term in space is added (see for instance [24]). On the other hand, the convection term in the momentum equation is replaced by a consistent skew-symmetric term; this enables to prove a stability result without assuming that the velocity field is exactly divergence free (see [126]). However, the explicit treatment of the free surface advection introduces a CFL condition that imposes a restriction on the time step. Further work is necessary to develop a scheme which ensures global mass conservation without introducing a time step restriction.

The hydrostatic/non-hydrostatic pressure decomposition

In [126], P. Quemar compares the approach described previously with another approach to solve the free surface Navier-Stokes equations that has been widely used in academic and industrial environmental softwares like [79, 61, 25, 26]. In particular, he has worked on the analysis and improvement of the Telemac-3d software which solves the three-dimensional free surface Navier-Stokes equations for applications to environmental flows at the local scale (km). It allows to deal with laminar and turbulent flows using classical turbulent models, and the numerical algorithm is based on the finite element method.

The time algorithm used in Telemac-3d is based on a pressure decomposition into a hydrostatic pressure p_h and a dynamic pressure correction p_d, that takes advantage of the fact that the mesh is structured in the vertical direction :

$$p = p_h + p_d, \quad \text{with } p_h = \rho g(\eta - z).$$

With this decomposition, the free surface unknown η appears explicitly in the momentum equations, allowing to solve the problem with a numerical algorithm in which the velocity and the free surface are "strongly coupled" at the discrete level. Actually the equations are solved using a projection method in the spirit of the Chorin Temam method (see for instance [72]), that amounts to first solve a hydrostatic prediction step, in which the velocity and the free surface satisfy :

Hydrostatic prediction step

$$\left\{ \begin{array}{rcl} \dfrac{\tilde{u} - u^n}{\delta t} \; - \; \dfrac{\mu}{\rho}\Delta \tilde{u} \; + \; g\nabla\eta^{n+1} & = & 0 \quad \text{in } \Omega^n, \\[2ex] \dfrac{\eta^{n+1} - \eta^n}{\delta t} \; + \; \nabla \cdot \displaystyle\int_b^{\eta^n} \tilde{u}(x,s,t)ds & = & 0 \quad \text{in } \omega. \end{array} \right. \tag{4.18}$$

and

$$\left\{ \; \dfrac{\tilde{w} - w^n}{\delta t} \; - \; \dfrac{\mu}{\rho}\Delta \tilde{w} \; = \; 0 \quad \text{in } \Omega^n, \right. \tag{4.19}$$

and then correct the velocity using the dynamic pressure so that it becomes divergence free, by solving a Darcy problem in Ω^n :

Dynamic correction step

$$\left\{ \begin{array}{rcl} \dfrac{\mathbf{u}^{n+1} - \mathbf{u}^n}{\delta t} \; + \; \nabla p_d & = & 0, \\ \nabla \cdot \mathbf{u}^{n+1} & = & 0. \end{array} \right. \tag{4.20}$$

Here we have neglected the convection term for simplicity; this term is usually treated in an initial separate step, or integrated in the prediction step through a characteristics formulation. The prediction step corresponds to a time-discretization of the so-called hydrostatic model, that is valid whenever the ratio between the vertical and longitudinal scales is small enough. We analyzed equations (4.18) and its internal finite element approximation in [41]. The time and space discrete problem is well posed provided a discrete inf-sup condition is satisfied by the Finite Element spaces used to approximate the 3D variable u and the 2D variable η. A pair of finite elements that satisfy this condition on a mesh that is structured in the z-direction is the $P1$-Lagrange element defined on Ω^n for the velocity, and the P1-bubble element defined on ω for the 2D free surface η.

The reasons for which many authors proceed with this decomposition are the followings. On the one hand, this decomposition approach allows to deal with hydrostatic flows by only solving the prediction step. On the other hand, it allows to decrease the computational cost of the resolution; indeed, the procedure often used is based on an explicit treatment of the horizontal diffusion term on $\tilde{u}$ in (4.18). This, along with the structured configuration of the mesh in the vertical direction, allows to decouple η and $\tilde{u}$ in the hydrostatic step : the second equation in (4.18) can be rewritten into an equation involving only η, and $\tilde{u}$ is then recovered from η through the first equation. The computational cost is much lower since the equation involving only η is

2-dimensional, and the first equation only involves a mass-matrix to invert (and this matrix can be mass-lumped). Besides, the system obtained does not require to use finiteelements that satisfy the discrete inf-sup condition to admit a unique solution. Furthermore, the dynamic correction step consists in the resolution of a Darcy problem, which at its time can be treated by solving a Poisson problem on the pressure correction p_d, and then recover the velocity from p_d using the first equation in (4.20). Again, this allows to reduce the computational cost and does not require to use finite elements that satisfy the discrete inf-sup condition.

However this strategy, that essentially aims at decreasing the computational cost of the algorithm, has several important drawbacks.

— On the one hand, it implies a parabolic CFL restriction on the time step due to the explicit treatment of the horizontal diffusion term. This CFL condition writes :

$$\delta t \;\leq\; \frac{\rho}{\mu}\,\min((\Delta x)^2,(\Delta y)^2)$$

where Δx and Δy are the space steps in the x and y direction.

— Following Guermond and co-authors in [73], the use of finite elements that do not satisfy the inf-sup condition when solving the Navier-Stokes equations on a fixed domain with a projection method has a bad impact on the stability and accuracy properties of the scheme. In particular, it induces a lower limit on the time step :

$$Ch^{l+1} \;\leq\; \delta t,$$

where l is the degree of the element used for the velocity. An analysis similar to the one in [73] should be performed in order to extend their results to the case of the free surface Navier Stokes equations.

— On the other hand, it is well known (see for instance [73]) that the particular procedure to solve the Darcy problem by solving a Poisson problem on the pressure leads to a final velocity that is not divergence free, even in a weak sense. This has severe consequences on the stability of the algorithm ; thus, for instance in the Telemac software, another intermediate divergence-free velocity is computed and used to convect the velocities and other quantities at the next time step. The consistency of this procedure has not been analyzed.

— Lastly, the kinematic consistency condition ($\mathbf{u}\cdot\mathbf{n} = \mathbf{c}\cdot\mathbf{n}$) is not satisfied by the couple $\mathbf{u}^n$, η^n if computed in this way. In order to satisfy the consistency condition (in some sense), one should update the free surface at the end of each time step, by solving the convection equation (4.4) using the final velocity obtained.

Results

In [126], Pierrick Quemar has performed numerical tests using the finite element solver FreeFem++ [78] in order to compare the different approaches described previously. Here we report the results obtained for a two-dimensional test case in which a sloped free surface profile and zero velocities are imposed at the initial time, and the fluid is assumed to be not viscous : the total energy is therefore preserved and a continuous exchange of potential and kinetic energy takes place. We consider a closed basin with side $L = 10$m, equilibrium water depth $H = 10$m and constant bottom at $z = -10$m. The initial free surface profile is

$$\eta(x) = H + \eta_0 \cos(kx),$$

where $\eta_0 = 0.1$m and $k = \dfrac{\Pi}{L}$. When the free surface is horizontal, the whole potential energy has been exchanged into kinetic one. When the highest elevation is reached at one of the basin boundaries, the maximum potential and minimum kinetic energy state is achieved, just as at the beginning of the simulation.

A good approximation of the solution is provided by the small amplitude wave theory for the linearized equations – see for instance [40] :

$$\left\{\begin{array}{lcl} \eta &=& H + \eta_0 \ \cos{(kx)} \ \cos{(\omega t)}\,, \\ u &=& \omega \ \eta_0 \ \dfrac{\cosh{(k(z))}}{\sinh{(kH)}} \ \sin{(kx)} \ \sin{(\omega t)}, \\ w &=& -\,\omega \ \eta_0 \ \dfrac{\sinh{(k(z))}}{\sinh{(kH)}} \ \cos{(kx)} \ \sin{(\omega t)}, \end{array}\right. \tag{4.21}$$

with $\omega^2 = g\,k \tanh{(kH)}$.

The two-dimensional simulations are performed over $T = 60$ seconds, using a time step of successively $\delta t = 0.2$, 0.1, 0.05, 0.02 and 0.01s. 40 layers are used on the vertical direction and 40 nodes in the horizontal direction. When the "simple algorithm" is used, the velocity and pressure fields are discretized using respectively the P^1-bubble and the P^1 finite elements. But when the pressure decomposition approach is applied, both the velocity and the pressure are approximated by $P1$ finite elements, since the inf-sup condition is not necessary for the discrete problem to admit a unique solution. The solutions computed with the different algorithms for a time step $\delta t = 0.05$s are shown in figures 4.4 and 4.5, where they are compared to the quasi-analytic solution (denoted by *Analytic* in the legend). The curves denoted by *Characteristic* and *Current* are obtained with the two methods based on the "simple algorithm", the difference being that the first one uses a characteristics method to solve the convection equation on the free surface function η, and the second one uses an explicit scheme with a stabilization term. The other curves correspond to the results obtained with three methods based on the pressure decomposition : the curves denoted by *Hydro/No-Hydro* and *T3D-like* are obtained using two slightly different versions of the algorithm used in the Telemac-3d software, whereas the one denoted by *Hydro/No-Hydro + Kinematic* is obtained by the same algorithm but with an updating of the free surface at the end of each time step.

We observe that the results obtained with the methods that follow the "simple algorithm" are much better than the results obtained using the hydrostatic/non-hydrostatic pressure decomposition. In fact, the latter algorithm suffers from severe numerical diffusion, due to the different fractional steps. However, when updating the free surface at the end of each time step in order to satisfy the kinematic consistency condition ($\mathbf{u} \cdot \mathbf{n} = \mathbf{c} \cdot \mathbf{n}$ at the physical boundaries), the numerical diffusion is reduced. In all cases the period of oscillation is reproduced exactly, although it progressively gets slightly shorter when using larger time steps. Numerical estimation of convergence order in time and space orders suggest that the schemes based on the simple algorithm are first order in time as expected, whereas the schemes based on the pressure decomposition have an order in time less than one. Concerning the relative mass loss during the simulations, as expected only the method based on the simple algorithm and a characteristics method to advect the free surface does not preserve exactly the water mass conservation. The relative mass loss at $t = 10$s for a time step $\delta t = 0.05$s is of the order of 10^{-5}, and decreases when the time step

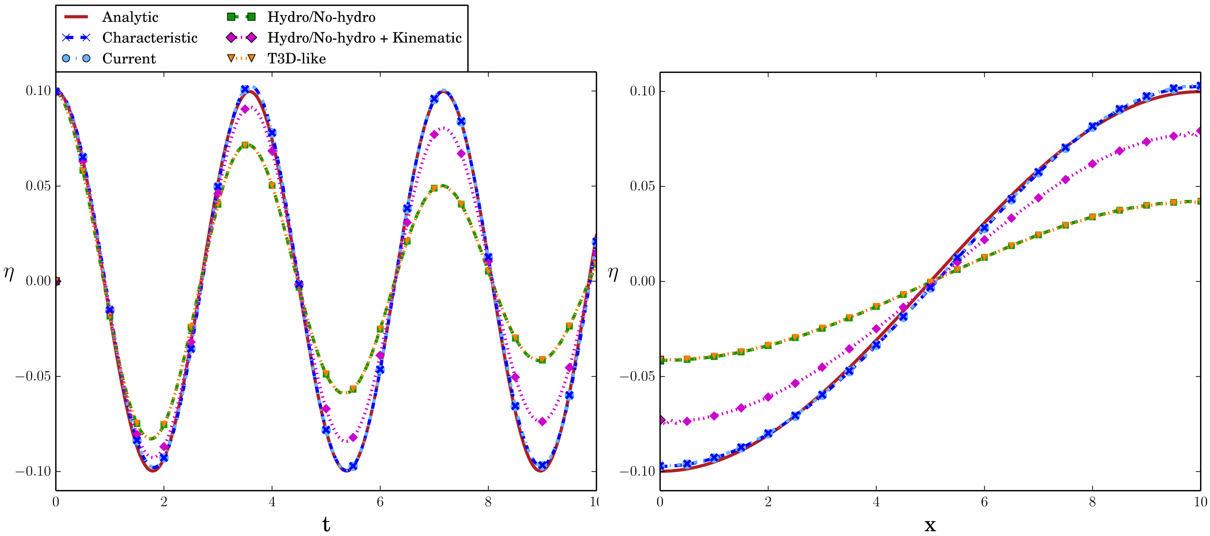

FIGURE 4.4 – Exact elevation (red full line) vs. computed elevation, at $x = 0.25$m as a function of time (left), and at $t = 9$s as a function x (right).

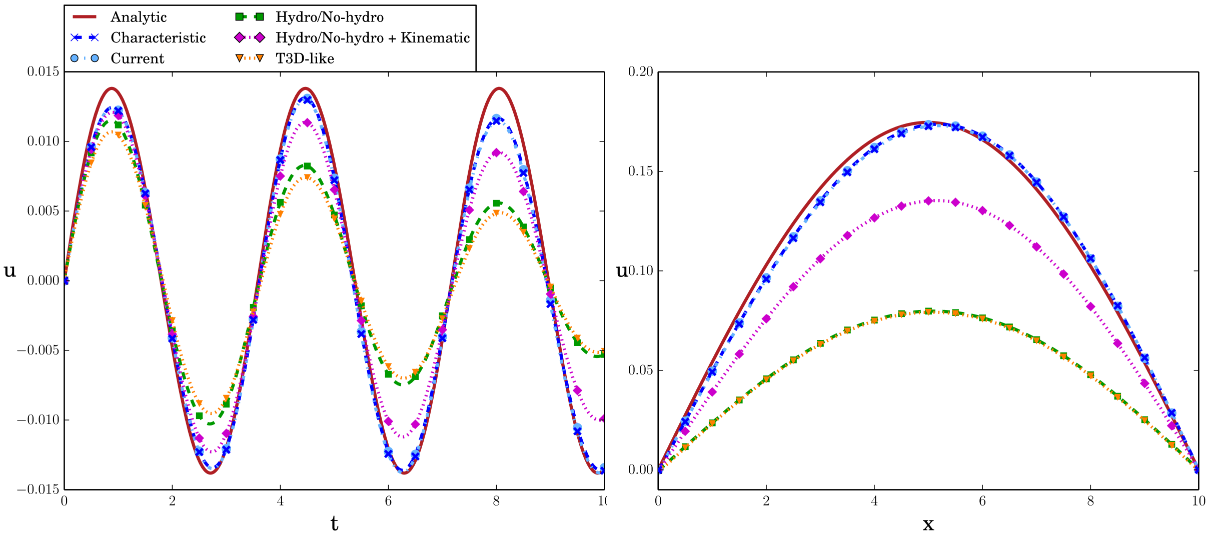

FIGURE 4.5 – Exact horizontal velocity (red full line) vs. computed velocity, at $x = 0.25$m as a function of time (left), and at $t = 9$s as a function x (right).

decreases.

We can also consider the three-dimensional counterpart of the two-dimensional test case presented previously. The two-dimensional domain is a square of side $L = 20$m, and the initial condition for the free surface is the following Gaussian shape function :

$$\eta(t=0) \;=\; H + 0.1 \exp\left(-0.25((x - L/2)^2 + (y - L/2.)^2)\right),$$

where $H = 1$. We consider a flat bottom, and the viscosity is 10^{-2}. Simulations are performed using a time step $\delta t = 0.01$, and the three-dimensional mesh has been obtained by piling up 10

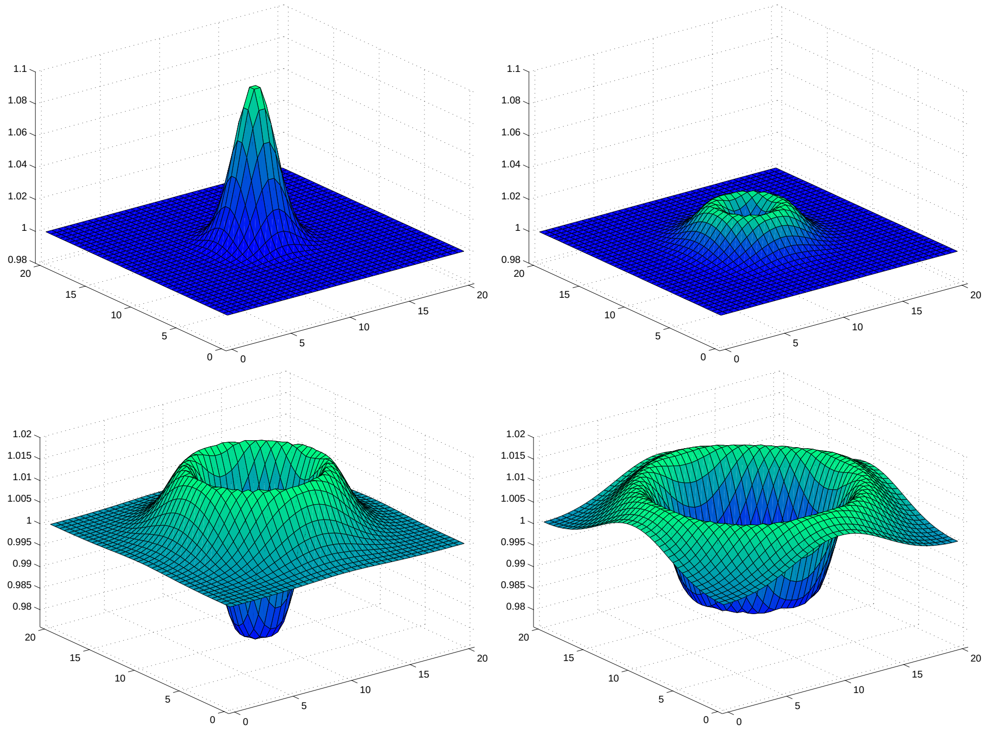

FIGURE 4.6 – Three-dimensional free surface at times $t = 0$s, $t = 0.33$s, $t = 0.66$s and $t = 0.99$s $t = 1.5$s, $t = 2$s, $t = 2.5$s and $t = 3$s.

layers of a two-dimensional mesh counting 3818 triangles and 1600 vertices. The velocity and pressure fields are discretized using P^2/P^1 Lagrange finite elements. Figure 4.6 represent the free surface at different times of the computation, using the "simple" algorithm approach.

4.2 New oscillatory instability of a confined cylinder in an inertial flow.

In [140] we report and analyze a new type of flow induced oscillation for a tethered cylinder in a highly confined geometry. This instability was experimentally observed by B. Semin and coworkers. In their experiment, the cylinder was only free to move in the direction towards the walls, and the oscillations appeared above a Reynolds number $Re \simeq 20$, much lower than the threshold for Bénard–Von Kármán vortex shedding behind a fixed cylinder in the same geometry, implying a different instability mechanism. Since the oscillations cannot be explained in a conventional manner, it is necessary to characterize the hydrodynamic forces that act on the cylinder. Moreover, it is essential to be able to analyze the dependence of the oscillations with respect to parameters like the Reynolds number and the cylinder density. This is why numerical simulation has been chosen as a complementary tool to study the system, allowing for the determination of the velocity and pressure fields and the computation of hydrodynamic forces.

The instability is studied both numerically and experimentally in [140] as a function of the Reynolds number Re (defined using the mean velocity and the aperture h) and of the density ρ_s of the cylinder, but my contribution essentially concerns the numerical part.

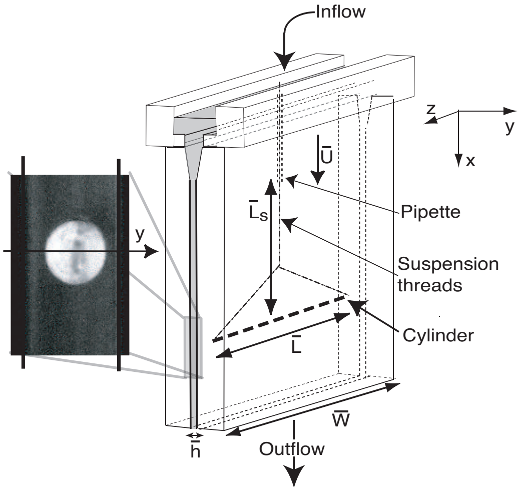

Figure 4.7 – Schematic view of the experimental setup.

Their experimental setup is shown in figure 4.7 : it consists of a Hele-Shaw cell made of two transparent parallel Plexiglass plates, inside which a fluid is flowing vertically downwards. The lateral sides of the cell are also transparent, allowing for the visualization in the gap of the cell. It has a constant aperture $\bar{h} = 4.9 \pm 0.1$ mm and width $\bar{W} = 90 \pm 0.1$ mm. Note that dimensional variables are displayed with an overbar ($\bar{W}$, $\bar{h}$...) in contrast with dimensionless ones. A Plexiglas cylinder is placed horizontally in the gap. Its density is close to that of water in order to reduce buoyancy effects. The ends of the cylinder are attached by nylon threads to a fixed suspension point located close to the inlet (see figure 4.7). The cylinder can only translate in the y direction and rotate around the x axis. Figure 4.8 shows a photography of the experimental result (a) for a fixed cylinder and (b) for a cylinder free to oscillate.

Since the oscillations of the cylinder are parallel to the plates, we consider two-dimensional simulations. A schematic view of the numerical configuration is shown on figure 4.9. The fluid is modeled using the incompressible Navier–Stokes equations with no-slip boundary conditions on the walls of the cell and on the surface of the cylinder (reduced to a disk in these two-dimensional simulations). A parabolic, constant-in-time, Poiseuille velocity profile is assumed at the inlet and a stress-free condition at the outlet. In most simulations, the motion of the cylinder is restricted to a rigid-body translation in the y direction (the cylinder is not allowed to rotate) ; it is then determined by the component along y of Newton's second law.

The numerical method is based on a variational formulation that strongly couples the fluid and rigid solid problems. This is essential for the stability of the numerical scheme that will be derived, especially when the differences of densities between the fluid and the solid become very small (see [28]). Fictitious domain methods allow to use unfitted meshes, but the use of a moving mesh that is conform to the fluid-structure interface at each time step allows to achieve higher accuracy. With a fixed grid, the amount of mesh grids would decrease dramatically near a wall when the cylinder approaches it. This would lead to a bad resolution of the hydrodynamic forces near the walls, which are essential to the oscillatory dynamics of the cylinder. Since we wish to reproduce the fine experimental results on the small oscillations of the cylinder, we use a moving grid, consistent with the motion of the cylinder. For that purpose we use an Arbitrary Lagrangian Eulerian (ALE) formulation of our problem, and we choose the arbitrary velocity of the domain to be consistent with the motion of the fluid domain's boundaries, and to vary

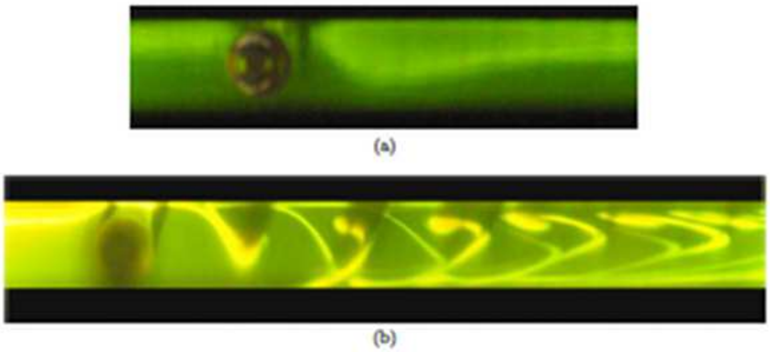
(a)
(b)

FIGURE 4.8 – Visualization of the flow for a fixed cylinder (a) and a free oscillating cylinder (b), for $Re = 50$.

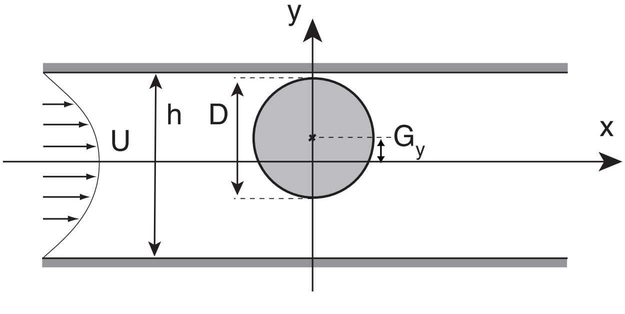

FIGURE 4.9 – Schematic two-dimensional representation of the numerical configuration.

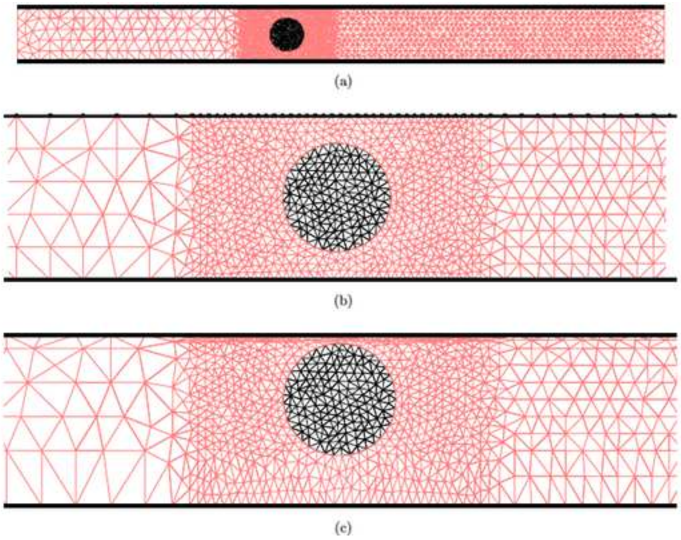

FIGURE 4.10 – Example of a mesh. (a) Initial mesh. (b) Zoom of the initial mesh. (c) Mesh after displacement.

linearly in the direction towards the walls, so that the amount of mesh grids on each part of the cylinder remains constant. Since the cylinder only moves in the y-direction, it is appropriate to choose an arbitrary domain velocity $\mathbf{c}(\cdot,t) = (0, c(\cdot,t))$ that only has a non-zero component in the y-direction (similarly to the free surface problem described in the previous section). We consider a triangulation $\mathcal{T}_h^0$ of the initial fluid domain (the cylinder is initially located at $y = 0$), and the vertical displacement of each mesh vertex with respect to its initial position is defined by the following piecewise linear function :

$$d_y(x,y,t) = \begin{cases} \frac{y_0(y+0.5)}{y_0-R+0.5} & \text{if} \quad -0.5 \le y \le y_0 - R, \\ \\ y_0 \quad \text{if} \quad y_0 - R \le y \le y_0 + R, \\ \\ \frac{y_0(y-0.5)}{y_0+R-0.5} & \text{if} \quad y_0 + R \le y \le 0.5. \end{cases}$$

Figure 4.10 shows an exemple of such a mesh and its displacement. The fluid and rigid problems are first discretized in time, and the variational formulation is then discretized in space using a Galerkin method. The constraint due to the rigid motion of the cylinder is handled by penalty [87], and that due to the threads by duality (the Lagrange multiplier is the tension of the threads). The advection term is treated using a method of characteristics in the ALE frame, as detailed in the previous section. The variational problem obtained is solved by means of the finite element solver FreeFem++ [78].

The instability is also observed in numerical simulations : if the Reynolds number is high enough, the cylinder oscillates spontaneously almost sinusoidally. For low Reynolds numbers, the cylinder moves to the center and then stays there motionless. The initial position of the cylinder has no influence on the amplitude and the frequency in steady state, which is consistent with the experiments. More quantitatively, the numerical results for amplitude and frequency are compared to the experimental results in Figure 4.11 (there is no adjustable parameter).

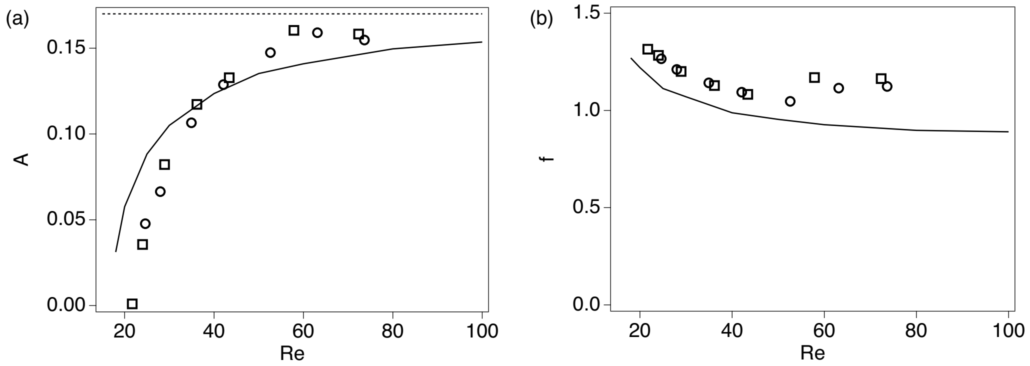

FIGURE 4.11 – Dimensionless amplitude A and frequency f measured experimentally and numerically at $\rho_s = 1.19$. ○ : experiments using water, □ : experiments using an aqueous natrosol solution, solid line : numerical results, dotted line : maximal possible amplitude of the oscillation.

The threshold values are in agreement to 20%, the values of the frequency also. The agreement between these results is acceptable and validates the numerical simulations, allowing to use them to study the mechanisms of instability. The gap for large flows can be explained by an experimental artefact : in this case, because of the elasticity of the threads, the cylinder also oscillates in the x direction. $3D$ effects can also play a role, especially the thin layer of fluid between the end of the cylinder and the side wall.

The characteristics of the oscillations, in both the permanent and transient regimes, are analyzed. The amplitude of the oscillations increases sharply with the Reynolds number above the threshold, but saturates because of the walls ; whereas the frequency grows linearly with Re (with no saturation), and decreases with the density of the cylinder. These features are observed both on the experimental and numerical results and remain qualitatively the same when the mass of the cylinder varies (quantitatively, Re_c decreases for high density cylinders).

The sinusoidal nature of the oscillations and the existence of a threshold suggest that the whole system may be described by a weakly non-linear dynamic system : the position of the cylinder satisfies a Van der Pol equation. This equation characterizes conveniently the dynamics of the system by a small number of physically meaningful parameters, which were determined numerically by forcing the oscillations to amplitudes and frequencies different from the free oscillations, and by computing the hydrodynamic forces acting on the cylinder. These parameters are a stiffness, a mass and a destabilizing term. The stiffness term has a purely hydrodynamic origin and results from the confinement of the flow. The mass term includes the mass of the cylinder (which may be equal to zero without suppressing the oscillations) and the added hydrodynamic mass. The frequency can be calculated using the stiffness and the total mass, providing an interpretation of the variation of the frequency with ρ_s. The third term is proportional to the velocity and determines the stability of the system. It results from tiny variations of the local pressure distribution in the region between the cylinder and the walls and involves a subtle balance between viscous and inertial effects, which cannot be explained by Bernouilli's theorem.

4.3 Characterization of blood flow in the aorta

The work presented in [89] is the result of a collaboration with researchers from the IR4M (Imagerie par Résonance Magnétique Médicale et Multi-Modalités) laboratory at Université Paris

Sud. They are interested in evaluating the dynamics of blood flow and cardiac function from cardiovascular images acquired by magnetic resonance. One of the aims of this work is to find a way to estimate the pressure in the artery in a non-invasive way, which is a recurrent and difficult question in this field, and we are therefore interested in the combined use of numerical simulations and imaging.

We have worked on a 1D model for blood flows in arteries, that is already well known in the literature. It is a system of hyperbolic conservation laws, similar to the Saint Venant equations, that describes blood flow in arteries and its interaction with wall motion. The artery is considered as a cylindrical compliant tube of length L and radius R ($R << L$).

The model derivation approach consists of integrating the Navier Stokes equations on a generic section S [62]. Some simplifying assumptions are made :

- the model assumes axisymetry ;
- the wall displacement is supposed to solely be in the radial direction ;
- pressure is assumed to be uniform in each section ;
- the axial velocity is predominant.

The unknowns are the section area $A(t,z) = \int_{S(t,z)} \mathrm{d}\Sigma$ and the flow rate $Q = \int_{S(t,z)} u_z \mathrm{d}\Sigma$, and the system writes :

$$\begin{cases} \dfrac{\partial Q}{\partial t} + \dfrac{\partial}{\partial z}\left(\dfrac{Q^2}{A}\right) + \dfrac{A}{\rho}\dfrac{\partial P}{\partial z} + K_r \dfrac{Q}{A} = 0 \\ \dfrac{\partial A}{\partial t} + \dfrac{\partial Q}{\partial x} = 0, \end{cases} \tag{4.22}$$

where K_r is the friction coefficient and ρ is the blood density. To close the system, a relation between the section area A and the pressure P is defined.

Although a three-dimensional (3D) model gives a more complete and realistic reproduction of the aortic flow, 1D models are able to describe the nonlinear flow behavior in large elastic vessels. These models are reasonably accurate, and they are widely used for aortic flow simulations. Their accuracy has been assessed by comparison with experimental data acquired in a tube phantom [14], in a distributed arterial model [2] and in vivo [130].

The pressure laws used in 1D model equations are determined experimentally with invasive measurements or estimated using optimization methods [55]. We propose to use a pressure law involving a single parameter, that can be measured in a non-invasive way. Under physiological conditions, the aorta section deformation is commonly assumed to be linked to the intravascular pressure by the aortic compliance. Aortic compliance establishes a linear relation between the pressure and the section area ; it represents the arterial wall's ability to deform in response to a pressure variation [36]. Also, it is clinically used and can be estimated non-invasively by measuring the pulse wave velocity (PWV) in magnetic resonance imaging (MRI). Hence, it provides a simple and non-invasive pressure law that can be applied in vivo and, as it includes compliance changes, is patient-specific. We use a pressure law based on the aortic compliance C which reflects arterial elasticity and can be determined non-invasively with MRI :

$$P - P_{ext} = \frac{A_0}{C}\left(\frac{A}{A_0} - 1\right).$$

In the limit of small displacements, this pressure law is equivalent to the commonly used linear law [62].

Using this pressure law, we couple the 1D model with realistic boundary conditions measured by MRI to estimate absolute pressure in the aortic segment. We used a classical second order finite volume scheme to solve the hyperbolic problem in conservative form. One of the difficulties we have encountered is the treatment of boundary conditions. Indeed, when it comes to make comparisons with experiments, the standard boundary conditions are no longer appropriate, and we must try to model as finely as possible what happens at the interfaces. The derived model was tested on a straight compliant phantom and computed pressure was compared to experimental pressure measurements recorded simultaneously with the MRI acquisition. The model was also tested on a real-sized compliant aortic phantom. Then, the model is used to estimate blood pressure on healthy volunteers. This work was published in a biomechanics journal. Our collaboration with IR4M researchers has then been pursued through the co-direction of Khalil Rachid's PhD [128], who has worked on the sensitivity analysis of the model's solutions to its various parameters, as well as the extension of our 1D model to compliance values that vary in time and space.

Travaux en cours et perpectives

Je décris à présent quelques travaux en cours et mes perspectives de recherche pour les prochaines années. A très court terme je souhaite finaliser une étude que je réalise en ce moment avec Sébastien Martin et Fabien Vergnet, en collaboration avec Sergio Chibbaro, physicien à l'Institut Jean Le Rond d'Alembert, et qui concerne une propriété très intéressante que nous avons observée dans nos simulations de suspensions actives de micro-nageurs : il s'agit de la brisure au niveau macroscopique de la symétrie temporelle des équations microscopiques, sans doute causée par les effects collectifs. Je souhaite également finir assez rapidement un autre travail en cours depuis quelques années en collaboration avec des médecins du Centre Hépato-Biliaire de l'Hôpital Paul Brousse ainsi qu'un biologiste de l'Université Paris Sud, sur la modélisation de l'impact sur le processus de régénération du foie de la circulation entérohépatique des acides biliaires. Ce travail s'inscrit dans un projet de collaboration plus large, impliquant aussi mon collègue du LMO Jean-Baptiste Lagaert, et portant sur le modélisation mathématique de la régénération du foie. Mon intérêt principal porte néanmoins toujours sur les fluides actifs, et j'ai à plus ou moins long terme plusieurs projets de développement autour de la modélisation et la simulation numérique de l'interaction entre un fluide visqueux et des cils actifs, et son application au transport muco-ciliaire. Je souhaite en particulier développer, à partir de nos travaux préalables sur le sujet, un véritable outil numérique pour la simulation directe efficace et robuste de fluides faisant intervenir un grand nombre de cils actifs. Ceci implique de réussir à faire un vrai couplage fluide-structure entre un modèle $3d$ *pour le fluide et* $1d$ *pour les cils, ce qui pose des problèmes à la fois au niveau mathématique et numérique. Enfin, un nouveau projet qui me tient très à coeur est en train de débuter avec des chercheurs du laboratoire BioMaps (Laboratoire d'imagerie biomédicale multimodale Paris-Saclay), spécialistes d'imagerie médicale, sur la modélisation de la perfusion tumorale. Notre objectif est de développer un modèle numérique capable de représenter, à partir d'images IRM, le réseau de vascularisation d'une tumeur et de résoudre l'écoulement fluide et le transport de l'oxygène dans les micro-vaisseaux et dans les tissus.*

Irréversibilité et chaos dans des suspensions actives

Les différences observées dans les simulations présentées au Chapitre 1 entre micro-nageurs de type "pusher" et "puller" semblent contredire le fait qu'un modèle est obtenu à partir de l'autre en inversant simplement les forces de propulsion. La linéarité des équations de Stokes impose alors que le champ de vitesses instantané pour une configuration donnée soit exactement le même, au signe de la vitesse près (qui est inversé). Pourtant, nous observons bien des différences de dynamique marquées au-delà d'une certaine concentration entre les deux types de nageur, notamment sur le module des vitesses collectives et la rhéologie (voir les figures 1.5 et 1.6).

L'invariance des lois de la mécanique par inversion du temps est l'une des propriétés les plus fondamentales du monde physique. L'existence d'une direction temporelle dans le comportement macroscopique fournit un paradoxe apparent dont l'explication constitue l'un des principaux objectifs de la mécanique statistique depuis Boltzmann [65, 33]. La complexité dans la relation entre la dynamique microscopique et les propriétés macroscopiques est telle que la nature de l'irréversibilité temporelle se prête encore au débat, notamment en ce qui concerne le rôle du chaos et du nombre de degrés de liberté. Les suspensions de particules autopropulsées que nous étudions au Chapitre 1 sont un exemple particulièrement intéressant de ce paradoxe, et nous cherchons à comprendre les mécanismes sous-jacents à cette rupture de la symétrie par inversion du temps.

Les trajectoires de micro-nageurs obtenues dans nos simulations (voir Fig. 1.4) montrent que la dynamique est hautement non triviale dans les deux cas, se caractérisant par des déplacements très irréguliers qui mettent en évidence l'interaction non linéaire entre les nageurs, aboutissant à un mouvement chaotique. Les différences observées suggèrent une rupture de la symétrie temporelle due au comportement collectif, puisque l'application de l'opérateur d'inversion temporelle sur les pushers individuels permet d'obtenir formellement la dynamique des pullers et inversement. Nous avons réalisé l'expérience numérique suivante : nous suivons une suspension de "pushers" dans le temps, et à l'instant t_0 nous inversons la dynamique avec une erreur d'arrondi de 10^{-16}. En principe, le système étant parfaitement réversible, il devrait revenir sur ses pas. Il s'avère qu'après un court laps de temps pendant lequel la dynamique est parfaitement inversée, le système rompt la symétrie temporelle. Le mouvement irrégulier présenté dans la figure 1.4 suggère que les nageurs sont sensibles à de légères perturbations des conditions initiales, un petit changement dans la position relative des particules produisant une forte réorganisation de toute la configuration. Nous avons quantifié cette sensibilité par une analyse statistique de la distance Euclidienne entre deux simulations :

$$\Delta(t) = \sqrt{\frac{1}{N}\sum_{i=1}^{N}(x_i^1(t) - x_i^0(t))^2 + (y_i^1(t) - y_i^0(t))^2},$$

où les deux simulations sont distinguées par ^{1} et ^{0} et font référence respectivement au cas perturbé et non perturbé. Nous imposons une perturbation initiale $\delta \mathbf{x} = 10^{-10}$ sur une seule particule, car cela devrait modifier toutes les trajectoires dû aux interactions hydrodynamiques. Pour les systèmes chaotiques, Δ croît de façon exponentielle en $|\delta \mathbf{x}| \exp(\lambda t)$, où λ est le premier exposant de Lyapunoff. Nos résultats préalables montrent que dans le cas de nageurs à forme allongée et pour des fractions de volume suffisamment élevées ($\phi > 3\%$), les deux espèces sont chaotiques, car l'exposant de Lyapunoff est positif. Nous nous attendons à ce que la forme ne joue aucun rôle dans le chaos, conformément à des résultats obtenus dans le cas passif [124, 116]. Mais nous sommes en attente de résultats numériques permettant de calculer les exposants de Lyapunoff dans le cas sphérique pour confirmer cette intuition. Deux mécanismes peuvent en principe conduire à un comportement aussi chaotique, les interactions hydrodynamiques à N corps et les interactions par contact. Nous avons néanmoins vérifié que nos résultats sont insensibles aux contacts en raffinant le pas de temps et le pas d'espace.

Nous espérons finaliser ce travail bientôt et soumettre nos résultats à une revue de physique.

Interaction Fluide-Cils

Nous avons plusieurs projets de développement autour de la modélisation et la simulation numérique de l'interaction entre un fluide visqueux et des structures fines actives, et de son application au transport mucociliaire.

D'une part, le travail décrit au Chapitre 3 autour du modèle de structure active et de la résolution numérique du problème fluide-structure doit être poursuivi. En l'état, le modèle développé permet d'obtenir des déformations proches de celles que l'on observe sur les cils bronchiques par exemple, et d'étudier de façon précise l'interaction d'un ou deux cils avec le fluide. Cependant, nous n'observons pas pour l'instant de réelle synchronisation des battements. Or il est connu que les cils synchronisent leurs battements de façon à rendre le transport mucociliaire plus efficace ; ce phénomène a en effet été observé dans des expériences [16, 68] à partir d'une certaine densité de cils. Il nous faut donc tout d'abord faire des simulations avec un plus grand nombre de cils pour déterminer si le modèle permet de reproduire cette synchronisation. Ensuite, nous souhaitons améliorer le modèle en faisant dépendre le scénario pour le tenseur des contraintes actives Σ^* des déformations de la structure, par exemple au travers du gradient du déplacement ∇d_s. En effet, plusieurs modèles discrets [52] considèrent les déformations locales de la structure dans la modélisation des contraintes de cisaillement internes, et permettent de mettre en évidence l'émergence d'une synchronisation. Le tenseur des contraintes actives s'écrirait alors

$$\Sigma^*(t,x,\mathbf{d_s}(t)) = S_a(t,x,\mathbf{d_s}(t))\,\mathbf{e}_a \otimes\; \mathbf{e}_a, \quad t \geq 0, \quad x \in \Omega_s,$$

où S_a est la fonction scalaire définissant le *scenario d'activité* du cil.

Nous souhaitons également continuer à travailler sur la méthode de prolongement régulier développée pour des problèmes elliptiques de transmission, et en particulier pour la résolution de problèmes fluide-structure. En particulier, nous comptons faire l'analyse numérique de la méthode de façon à justifier rigoureusement les ordres de convergence optimaux observés dans nos simulations. Par ailleurs, nous souhaitons utiliser des solveurs rapides et parallèles pour la résolution du problème fluide sur maillage structuré afin de tirer entièrement profit de la méthode. Enfin, il nous faut faire une étude comparative des différents algorithmes d'optimisation pour le problème de minimisation de la fonctionnelle sur lequel est basée la méthode.

L'implémentation de la résolution du problème en 3D est en cours, et les deux méthodes numériques présentées seront utilisées et comparées pour effectuer les simulations tridimensionnelles, qui sont les seules à pouvoir vraiment représenter la réalité physique. Une batterie de simulations devront alors être faites afin d'étudier la dépendance du mouvement des cils par rapport à la viscosité et l'épaisseur des différentes couches intervenant dans le transport mucociliaire : la PCL dans laquelle ils baignent et le mucus.

D'autre part, notre objectif est maintenant de développer à partir des travaux préalables décrits dans ce manuscrit (aux Chapitres 2 et 3) un véritable outil numérique pour la simulation directe efficace et robuste de fluides faisant intervenir un grand nombre de cils actifs. Le modèle 3d pour le cil est particulièrement coûteux. Il permet l'étude fine de l'interaction entre les structures mais des simulations avec un très grand nombre de cils ne sont pas envisageables. En outre, les effets de déformation tridimensionnels sont assez négligeables, un modèle complètement 3d ne semble donc pas nécessaire. Nous souhaitons donc simplifier le modèle élastique : les structures actives que sont les cils étant extrêmement fines, nous pouvons travailler dans l'asymptotique où le ratio entre l'épaisseur des cils et leur longueur tend vers 0. C'est l'approche que nous avons adoptée dans le travail présenté au Chapitre 2, où nous avons considéré un mouvement des cils imposé. Cette fois-ci nous souhaitons dériver un modèle asymptotique à partir du problème d'interaction fluide-structure 3d-3d complet, afin de prendre en compte l'effet du fluide sur les cils. On aboutira ainsi à un modèle élastique 1d pour les cils couplé aux équations 3d gouvernant le fluide. Ce couplage pose des questions difficiles à la fois du point de vue mathématique et numérique : en effet, des cils représentés par une courbe 1d interviennent dans les équations fluides à travers un terme source singulier, c'est-à-dire une mesure de Dirac le long de la courbe. Le champ de vitesse résultant de ces équations est alors discontinu le long des courbes représentant les cils, ce qui rend le couplage avec les équations portant sur le déplacement des structures non trivial. Notre objectif est donc de donner un sens mathématique à ce couplage et développer une méthode numérique efficace pour le résoudre, ainsi que valider l'approche 3d-1d par une analyse d'erreur par rapport aux calculs 3d-3d.

Par ailleurs, nous n'avons actuellement aucune méthode rigoureuse ou systématique pour paramétriser le tenseur des contraintes actives du cil ; nous construisons celui-ci de façon arbitraire, en nous basant sur les caractéristiques du mouvement des cils décrit dans les expériences [155]. Le travail que nous souhaitons entreprendre consiste donc également à estimer de façon rigoureuse la forme de ce tenseur, à partir des données disponibles dans la littérature sur le mouvement des cils dans une configuration donnée. Ceci revient donc à résoudre le problème inverse suivant : trouver le scénario d'activité optimal $S_a(t, \mathbf{x}, \mathbf{d_s}(t))$ qui minimise la fonctionnelle

$$J(S_a) = \frac{1}{2}||\mathbf{d}_s(S_a) - \mathbf{d}_{obs}||^2,$$

où $\mathbf{d}_s(S_a)$ est le déplacement du cil, solution du problème fluide-structure pour le scenario d'activité S_a, et $\mathbf{d}_{obs}$ désigne le mouvement du cil que l'on souhaite retrouver. Le scénario S_a devra être paramétrisé de façon à simplifier le problème inverse et se ramener à une estimation des paramètres intervenant dans cette paramétrisation.

Nous souhaitons également pouvoir prendre en compte certains ingrédients importants dans les phénomènes que nous étudierons. Par exemple, dans le cadre du transport mucociliaire, il serait intéressant de prendre en compte le comportement visco-élastique du mucus [16, 68]. Dans le cadre de notre approche, les effets élastiques peuvent être intégrés par un couplage du modèle de structure à un modèle d'écoulement non-newtonien de type Oldroyd. Dans ce cas, le tenseur des contraintes visqueuses $\Sigma = 2\mu\mathbb{D}(\mathbf{u})$ utilisé usuellement dans les équations de la mécanique des fluides pour modéliser des écoulements de Stokes est remplacé par un tenseur de contraintes visco-élastiques

$$\Sigma := 2\mu(1-r)\mathbb{D}(\mathbf{u}) + \sigma_e$$

avec $0 < r < 1$. Cela aboutit aux équations :

$$\begin{aligned} -\mu\Delta\mathbf{u} + \nabla p &= \mathbf{f}_{\mathrm{f}} + \mathrm{div}(\sigma_e), && \text{dans } \Omega_f(t), \\ \mathrm{div}(\mathbf{u}) &= 0, && \text{dans } \Omega_f(t), \end{aligned}$$

qui sont complétées par une loi de fermeture constitutive pour la contrainte élastique σ_e :

$$\lambda\left(\partial_t\sigma_e + \mathbf{u}\cdot\nabla\sigma_e + g_a(\nabla\mathbf{u}, \sigma_e)\right) + \sigma_e = 2r\mu\mathbb{D}(\mathbf{u}), \quad \text{dans } \Omega_f(t).$$

Ici λ est un temps de réponse élastique caractéristique du fluide et g_a est une forme bilinéaire associée à un ensemble de modèles dépendant d'un paramètre $a \in (-1, 1)$. Les résultats mathématiques associés à ce modèle sont désormais connus [101] et des algorithmes de résolution numérique peuvent être mis en œuvre, notamment en utilisant des techniques de splitting très simples [46] ; néanmoins le couplage fluide-structure associé à la mise en œuvre d'algorithmes de résolution numérique peut se révéler délicat du point de vue de la stabilité numérique.

Enfin, une fois cet outil numérique développé, et après validation par la comparaison avec les résultats expérimentaux disponibles dans la littérature, nous souhaiterions l'exploiter afin d'étudier de façon complète les comportements collectifs, et ainsi mieux comprendre les propriétés fondamentales des fluides biologiques étudiés. En effet, un tel modèle permettrait d'étudier l'impact des différentes caractéristiques du mucus, comme son épaisseur et sa viscosité, sur l'efficacité du transport mucociliaire, ainsi que celui d'éventuels défauts de motilité des cils, afin de caractériser un ensemble de pathologies respiratoires.

Modélisation mathématique de la régénération du foie

Une collaboration est en cours avec mon collègue du LMO Jean-Baptiste Lagaert et des médecins du Centre Hépato-Biliaire de l'Hôpital Paul Brousse, dont J.-C. Duclos-Vallée, ainsi qu'un biologiste de l'Université Paris Sud, Thierry Tordjmann, qui travaille sur des modèles expérimentaux liés aux problématiques des maladies du foie. Le but de cette collaboration est de développer des modèles mathématiques capables de mieux comprendre et prévoir la régénération du foie après hépatectomie, c'est-à-dire ablation d'une partie du foie malade. Le foie est un organe essentiel au fonctionnement de l'organisme, dont les fonctions ne peuvent être assurées par aucun autre organe, mais qui se régénère le plus souvent spontanément lorsqu'il est endommagé. Ainsi, une partie du foie peut être remplacée chirurgicalement : un donneur se voit retirer une partie de son foie qui est transplantée chez le malade. La transplantation hépatique est un succès si chacune des deux parties du foie se régénère alors en un foie complet. D'autre part, une hépatectomie peut être réalisée en cas de tumeur : la partie du foie malade est enlevée, en espérant que la partie saine se régénère. Dans ces deux types d'opérations chirurgicales, l'une des principales questions qui se posent est celle du « volume fonctionnel du foie ». Plus exactement, il faut pouvoir estimer le volume minimal du foie en-dessous duquel la survie du patient et la régénération de l'organe ne sont pas assurées. Cette notion de volume fonctionnel est essentielle, car elle détermine quelle partie du foie peut être réséquée et, dans le cas d'une transplantation, quel est le volume de foie à transplanter. Il est connu que le volume minimum vital est approximativement de 1% de la masse corporelle. Mais il serait important de pouvoir apporter une estimation plus fine et quantitative de ce volume minimal, en fonction de paramètres déterminants tels que l'état du foie restant par exemple.

Nous nous sommes intéressés dans un premier temps à l'étude de l'impact des acides biliaires sur la régénération du foie, car c'est le but des travaux expérimentaux de T. Tordjmann. Nous avons donc développé d'une part un modèle d'EDO pour la circulation entéro-hépatique des acides biliaires dans l'organisme, et d'autre part, un modèle simple d'EDO pour la croissance cellulaire après hépatectomie partielle. Les deux modèles sont évidemment couplés et nous sommes intéressés à étudier, grâce à ce modèle, l'impact d'une hépatectomie partielle sur cette circulation, car elle est jugée importante dans le processus de régénération du foie. Nous travaillons actuellement à l'estimation des paramètres du modèle que nous avons développé, à partir des données expérimentales disponibles. Nous utilisons pour cela une méthode déterministe, basée sur la minimisation d'une fonctionnelle coût qui mesure l'écart au sens des moindres carrés entre les résultats du modèle et les données. Pour minimiser cette fonctionnelle nous utilisons une méthode d'optimisation basée sur le gradient de cette fonctionnelle par rapport aux paramètres, qui lui est calculé grâce à une méthode de l'état adjoint.

D'autre part, nous souhaiterions développer un modèle de type EDP sur réseau pour la modélisation du foie. La structure élémentaire du foie, le lobule, serait représentée par un réseau sur lequel circulent le sang et la bile, et au sein duquel ont lieu les échanges de type synthèse et élimination de substances (comme par exemple les acides biliaires). Le but serait ensuite de déduire de ce modèle un modèle réduit (0D) qui puisse représenter les principales fonctions du foie au niveau d'un lobule. Ce modèle serait un premier pas vers le développement d'un modèle pour le foie entier, qui permettrait d'évaluer qualitativement l'impact sur les fonctions hépatiques de la suppression d'une partie des lobules, et de l'augmentation de leur taille ou nombre.

Modélisation de la perfusion tumorale

Il s'agit là d'un nouveau projet né de discussions avec des chercheurs du laboratoire BioMaps (Laboratoire d'imagerie biomédicale multimodale Paris-Saclay), Sébastien Jan et Fabien Rastello, spécialistes d'imagerie médicale, qui s'intéressent à la reconstruction de la vascularisation des tumeurs à partir d'images IRM et TEP (Tomographie à Emission de Positons). En effet, l'imagerie de la vascularisation tumorale est essentielle en cancérologie pour le suivi thérapeutique des nouvelles molécules qui ciblent la destruction des vaisseaux, afin d'entraîner l'asphyxie des tumeurs. Mais elle l'est aussi d'un point de vue plus fondamental, pour identifier les mécanismes biologiques sous-jacents entre néo-vascularisation, hypoxie et métabolisme tumoral. La modélisation mathématique des micro-écoulements apparaît comme un outil intéressant et complémentaire pour étudier le phénomène de perfusion tumorale. Il existe déjà des modèles de perfusion/oxygénation/diffusion dans la littérature [138, 27], mais la confrontation aux données expérimentales in-vivo reste difficile.

Notre objectif est donc de combiner les deux approches pour développer un modèle numérique capable de représenter, à partir des images, le réseau de vascularisation d'une tumeur et de résoudre l'écoulement fluide et le transport de l'oxygène dans les micro-vaisseaux et dans les tissus. D'une part, il nous faudra développer une méthode de reconstruction de la topologie vasculaire à partir des données expérimentales dont nous disposerons. D'autre part, nous développerons un modèle mathématique pour l'écoulement du sang dans les vaisseaux et l'oxygénation de la tumeur, prenant en compte le passage de l'oxygène du sang vers le tissu et la propagation dans le tissu.

Les données expérimentales dont nous disposerons proviendront en particulier de coupes histologiques de modèles de tumeurs développées sur des rongeurs au laboratoire BioMaps, mais aussi de données d'imagerie in-vivo effectuées par les chercheurs en physique médicale du même laboratoire.

Les tumeurs vascularisées ont des largeurs caractéristiques de l'ordre de plusieurs centimètres et la néo-vasculature est extrêmement dense : les plus petits vaisseaux fonctionnels ont des diamètres de l'ordre de 16 microns et on peut en dénombrer plus d'un millier par centimètre carré. Le modèle de vasculature utilisé devra être à même de gérer ces différences d'échelle et prendre en compte, éventuellement de façon phénoménologique, la complexité et le caractère parfois chaotique des réseaux vasculaires issus de l'angiogénèse. Il faudra donc considérer des modèles réduits d'arbres vasculaires. L'approche que nous avons choisie pour l'instant est une reconstruction sous la forme d'un réseau 1d de micro-vaisseaux, dont la localisation spatiale est déterminée par l'axe central des vaisseaux, l'option d'une reconstruction 3d nous semblant trop coûteuse et non justifiée de par les erreurs trop importantes que celle-ci induirait. Le tissu environnant est considéré comme un milieu poreux, et les équations de Darcy sont utilisées pour simuler l'écoulement dans l'espace extra-vasculaire. Le couplage entre l'arbre vasculaire et les tissus environnants est non-trivial car les échanges d'oxygène et autres molécules sont pris en compte par des termes source linéiques dans le modèle de tissu 3d, ce qui mène à une solution singulière et peut compliquer la résolution numérique (voir par exemple [39]). De plus, ces tissus sont très hétérogènes et la propagation de l'oxygène et des molécules dans les tissus sains et dans la tumeur diffèrent beaucoup. Des modèles de ce type existent déjà dans la littérature

[138, 27], mais nous souhaitons les améliorer, notamment en prenant en compte les propriétés rhéologiques particulières du sang dans des micro-canaux, ou encore l'adaptation de conditions limites plus appropriées [97]. Une approche par homogénéisation des échelles les plus fines dans l'arbre vasculaire pourra également être considérée [152] afin de diminuer les coûts de calcul.

Les résultats numériques obtenus avec ce modèle seront ensuite confrontés aux données expérimentales issues de l'imagerie par TEP et IRM, ce qui permettra l'estimation des paramètres, comme par exemple la perméabilité des vaisseaux et celle des tissus, et la validation du modèle.

Bibliographie

[1] N. Aguillon, A. Decoene, B. Fabreges, B. Maury, and B. Semin. Modelling and simulation of 2d stokesian squirmers. *ESAIM : Proceedings*, 38, 2012.

[2] J. Alastruey, A.W. Khir, K.S. Matthys, P. Segers, S.J. Sherwin, P.R. Verdonck, K.H. Parker, and J. Peiró. Pulse wave propagation in a model human arterial network : assessment of 1-d visco-elastic simulations against in vitro measurements. *J. Biomech.*, 44(12) :2250–2258, 2011.

[3] B. Alauzet, F. an d Fabrèges, M. Fernández, and M. Landajuela. Nitsche-xfem for the coupling of an incompressible fluid with immersed thin-walled structures. *Computer Methods in Applied Mechanics and Engineering*, 301 :300–335, 2016.

[4] G. Allaire and A. Craig. *Numerical analysis and optimization.* Oxford Science Publications, 2007.

[5] T. Apel, O. Benedix, D. Sirch, and B. Vexler. A priori mesh grading for an elliptic problem with Dirac right-hand side. *SIAM J. Numer. Anal.*, 49(3) :992–1005, 2011.

[6] C. Atamian, Q. Dinh, R. Glowinski, J. He, and J. Périaux. Control approach to fictitious-domain methods. application to fluid dynamics and electromagnetics. *Proceedings of the Fourth International Symposium on Domain Decomposition Methods for Partial Differential Equations, R. Glowinski, Y. Kuznetsov, G. Meurant, J. Périaux, and OB Widlund, eds., SIAM, Philadelphia*, pages 275–309, 1991.

[7] F. P. Baaijens. A fictitious domain/mortar element method for fluid structure interaction. *International Journal for Numerical Methods in Fluids*, 35(7) :743–761, 2001.

[8] R. N. Bearon and T. J. Pedley. Modelling run-and-tumble chemotaxis in a shear flow. *Bull. Math. Biol.*, 62(4) :775–791, 2000.

[9] M. Belzons, R. Blanc, J. L. Bouillot, and C Camoin. Viscosité d'une suspension diluée et bidimensionnelle de sphères. *C. R. Acad. Sci, Paris II*, 292 :939–44, 1981.

[10] H. C. Berg. *Random walks in biology.* Princeton University Press, 1983.

[11] S Bertoluzza, A. Decoene, L. Lacouture, and S. Martin. Local error analysis for the stokes equations with a punctual source term. *Numer Methods Partial Differential Eq.*, 2017.

[12] S Bertoluzza, A. Decoene, L. Lacouture, and S. Martin. Local error estimates of the finite element method for an elliptic problem with a dirac right-hand side. *Numerische Mathematik*, 2018.

[13] S. Bertoluzza, M. Ismail, and B. Maury. Analysis of the fully discrete fat boundary method. *Numerische Mathematik*, 118(1) :49–77, 2011.

[14] D. Bessems, C.G. Giannopapa, M.C. Rutten, and F.N. Van-de Vosse. Experimental validation of a time-domain-based wave propagation model of blood flow in viscoelastic vessels. *J.Biomech.*, 41(2) :284–291, 2009.

[15] J. R. Blake and G. R. Fulford. Mechanics of ciliary transport. *Physico. Chem. Hyd.*, 5 :401–411, 1984.

[16] J. R. Blake and H. Winet. On the mechanics of muco-ciliary transport. *Biorheology*, 17 :125–134, 1980.

[17] F. Bouchut, A. Mangeney-Castelnau, B. Perthame, and J.-P. Vilotte. A new model of Saint-Venant and Savage-Hutter type for gravity driven shallow water flow. *C. R. Acad. Sci. Paris. Ser. I*, 336, 2003.

[18] J. F. Brady and G. Bossis. Stokesian dynamic. *Ann. Rev. Fluid Mech.*, 20 :11–157, 1988.

[19] F. Brezzi and M. Fortin. *Mixed and hybrid finite element methods*, volume 15. Springer Series in Computational Mathematics, 1991.

[20] C. J. Brokaw. Bend propagation along flagella. *Nature*, 209(5019) :161–163, 1966.

[21] C. J. Brokaw. Bending moments in free-swimming flagella. *J. Exp. Biol.*, 53(2) :445–464, 1970.

[22] C. J. Brokaw. Computer simulation of flagellar movement. *Cell motility nd the cytoskeleton*, 53(2) :103–124, 2002.

[23] C. Bui, V. Lleras, and O. Pantz. Dynamics of red blood cells in 2d. *ESAIM : Proc.*, 28 :182–194, 2009.

[24] E. Burman, A Ern, and M. A. Fernández. Explicit runge-kutta schemes and finite elements with symmetric stabilization for first order linear pde systems. *SIAM J. Numer. Anal.*, 48(6) :2019–2042, 2010.

[25] V. Casulli. A semi-implicit finite difference method for non-hydrostatic, free-surface flows. *International Journal for Numerical Methods in Fluids*, 30(4) :425–440, 1999.

[26] V. Casulli and P. Zanolli. Semi-implicit numerical modeling of non-hydrostatic free-surface flows for environmental problems. *Mathematical and computer modelling.*, 36(9-10) :1131–1149, 2002.

[27] L. Cattaneo and P. Zunino. A computational model of drug delivery through microcirculation to compare different tumor treatments. *International Journal for Numerical Methods in Biomedical Engineering*, 30, 2014.

[28] P. Causin, J.-F. Gerbeau, and F. Nobile. Added-mass effect in the design of partitioned algorithms for fluid–structure problems. *Computer methods in applied mechanics and engineering*, 194(42-44) :4506–4527, 2005.

[29] S Chateau, J Favier, U. D'Ortona, and S. Poncet. Metachronal wave formation in 3d cilia arrays for mucus transport. *Journal of Fluid Mechanics*, 824 :931 – 961, 2017.

[30] R. Chatelin. Méthodes numériques pour l'écoulement de stokes 3d : fluides à viscosité variable en géométrie complexe mobile ; application aux fluides biologiques. *Thèse de doctorat de l'université Paul Sabatier, 197 pp.*, 2013.

[31] R. Chatelin and P. Poncet. A hybrid grid-particle method for moving bodies in 3D Stokes flow with variable viscosity. *SIAM J. Sci. Comput.*, 35(4) :925–949, 2013.

[32] V.T. Chaudry. *Open Channel Flows.* Prentice Hall, 1993.

[33] S. Chibbaro, L. Rondoni, and A. Vulpiani. *Reductionism, Emergence and Levels of Reality.* Springer, 2014.

[34] A. T. Chwang and T. Y.-T. Wu. Hydromechanics of low-Reynolds-number flow. II. Singularity method for Stokes flows. *J. Fluid Mech.*, 67 :787–815, 1975.

[35] L. H. Cisneros, R. Cortez, C. Dombrowski, R. E. Goldstein, and J. O. Kessler. Fluid dynamics of self-propelled microorganisms, from individuals to concentrated populations. *Exp. Fluids*, 43(5) :737–753, 2007.

[36] W. Conrad. Flow relationships in collapsible tubes. *IEEE Trans. Biomed. Eng.*, 16(4) :284–295, 1969.

[37] R. G. Cox. The motion of long slender bodies in a viscous fluid. Part 1. General theory. *J. Fluid Mech.*, 44 :791–810, 1970.

[38] C. D'Angelo. Finite element approximation of elliptic problems with Dirac measure terms in weighted spaces : applications to one- and three-dimensional coupled problems. *SIAM J. Numer. Anal.*, 50(1) :194–215, 2012.

[39] C. D'Angelo and A. Quarteroni. On the coupling of 1d and 3d diffusion-reaction equations. application to tissue perfusion problems. *M3AS*, 8(1481-1504), 2008.

[40] R.F. Dean and R.A. Dalrymple. *Water Wave Mechanics for Engineers and Scientists.* Prentice-Hall, Englewood CliVs, NJ, 1984.

[41] A. Decoene. *Hydrostatic model for three-dimensional free surface flows and numerical schemes.* PhD thesis, Université Pierre et Marie Curie, Paris VI, 2006.

[42] A. Decoene, L. Bonaventura, E. Miglio, and F. Saleri. Asymptotic derivation of the section averaged shallow water equations for river hydraulics. *M3AS*, 19(3), 2009.

[43] A. Decoene and J.-F. Gerbeau. Sigma transformation and ale formulation for 3d free surface flows. *Int. J. Numer. Meth. Fluids*, 59(4) :357–386, 2009.

[44] A Decoene, A. Lorz, S. Martin, B Maury, and M. Tang. Simulation of self-propelled chemotactic bacteria in a stokes flow. *ESAIM : Proceedings (Mathematical Modelling in Medicine)*, 30 :105–124, 2010.

[45] A. Decoene, S. Martin, and B. Maury. Direct simulation of self-propelled chemotactic bacteria. *Math. Model. Nat. Phenom.*, 6(5) :98–129, 2011.

[46] A. Decoene, S. Martin, and B. Maury. Direct simulation of rigid particles in a viscoelastic fluid. *Journal of Non-Newtonian Fluid Mechanics*, 260 :1–25, 2018.

[47] A. Decoene, S. Martin, and F. Vergnet. A smooth extension method for transmission problems. *Prépublication, 55 pages*, 2019.

[48] A. Decoene and B. Maury. Moving meshes with freefem++. *Journal of Numerical Mathematics*, 3-4(20) :195–214, 2012.

[49] A. Decoene, A. Lorz, S. Martin, B. Maury, and M. Tang. Local error analysis for the stokes equations with a punctual source term. *ESAIM : Proceedings (Mathematical Modelling in Medicine)*, 30 :105–124, 2010.

[50] B. Delmotte, E. Keaveny, F. Plourabou´ e, and E. Climent. Large-scale simulation of steady and time-dependent active suspensions. *J. Comput. Physics*, 2015.

[51] A. Deponti, G. Rosatti, and L. Bonaventura. An accurate and efficient semi-implicit method for section averaged free surface flow modelling. *Journal of Computational Physics, submitted*, 2008.

[52] R. H. Dillon, L. J. Fauci, C. Omoto, and X. Yang. Fluid dynamic models of flagellar and ciliary beating. *Ann. N. Y. Acad. Sci.*, 1101(1) :494–505, 2007.

[53] C. Dombrowski, L. Cisneros, S. Chatkaew, R. E. Goldstein, and J. O. Kessler. Self-concentration and large-scale coherence in bacterial dynamics. *Phys. Rev. Lett.*, 93 :098103, Aug 2004.

[54] K. Drescher, R. E. Goldstein, N. Michel, M Polin, and I Tuval. Direct measurement of the flow field around swimming microorganisms. *Physical Review Letters*, 105, 2010.

[55] L. Dumas. Inverse problems for blood flow simulation. *proceedings of ENGOPT*, 2008.

[56] S. Enault, D. Lombardi, P. Poncet, and M. Thiriet. Mucus dynamics subject to air and wall motion. *ESAIM : Proceedings*, 30 :125–141, 2010.

[57] R. Erban and H. Othmer. From individual to collective behavior in bacterial chemotaxis. *SIAM J. Appl. Math.*, 65(2) :361–391, 2004.

[58] K. Eriksson. Finite element methods of optimal order for problems with singular data. *Math. Comp.*, 44(170) :345–360, 1985.

[59] B. Fabrèges. *A smooth extension method for the simulation of fluid/particles flows.* PhD thesis, Université Paris Sud - Paris XI, 2012.

[60] Benoit Fabrèges. *A smooth extension method for the simulation of fluid/particles flows.* PhD thesis, Université Paris Sud - Paris XI, 2012.

[61] L. Fontana, E. Miglio, A. Quarteroni, and A. Saleri. A finite element method for 3D hydrostatic water flows. *Comput. Vis. Sci.*, 2(2-3) :85–93, 1999.

[62] L. Formaggia, D. Lamponi, and A. Quarteroni. One-dimensional models for blood flow in arteries. *Journal of engineering mathematics*, 47(3-4) :251–276, 2003.

[63] G. R. Fulford and J. R. Blake. Force distribution along a slender body straddling an interface. *J. Austral. Math. Soc. Ser. B*, 27(3) :295–315, 1986.

[64] G. R. Fulford and J. R. Blake. Muco-ciliary transport in the lung. *J. Theor. Biol.*, 121(4) :381–402, 1986.

[65] G. Gallavotti. *Nonequilibrium and Irreversibility.* Springer, https ://arxiv.org/pdf/1311.6448.pdf, 2014.

[66] D. Gérard-Varet and M. Hillairet. Regularity issues in the problem of fluid structure interaction. *Arch. Ration. Mech. Anal.*, 195(2) :375–407, 2010.

[67] J.-F. Gerbeau and B. Perthame. Derivation of viscous Saint-Venant system for laminar shallow water ; numerical validation. *Discrete and Continuous Dynamical Systems. Ser. B*, 1(1) :89–102, 2001.

[68] L. Gheber, A. Korngreen, and Z. Priel. Effect of viscosity on metachrony in mucus propelling cilia. *Cell Motil. Cytoskel.*, 39(1) :9–20, 1998.

[69] V. Girault and R. Glowinski. Error analysis of a fictitious domain method applied to a dirichlet problem. *Japan Journal of Industrial and Applied Mathematics*, 12(3) :487–514, 1995.

[70] R Glowinski. Finite element methods for incompressible viscous flow. *Handbook of Numerical Analysis.*, IX :363–427, 2003.

[71] R. Glowinski, T.W. Pan, T. I. Hesla, D. D. Joseph, and J. Périaux. A fictitious domain approach to the direct numerical simulation of incompressible viscous flow past moving rigid bodies : application to particulate flow. *J. Comp. Phys.*, 169 :363–427, 2001.

[72] J. Guermond, P. Minev, and J. Shen. An overview of projection methods for incompressible flows. *Computer methods in applied mechanics and engineering*, 195(44-47) :6011–6045, 2006.

[73] J.-L. Guermond and L. Quartapelle. On stability and convergence of projection methods based on pressure poisson equation. *International Journal for Numerical Methods in Fluids*, 26(9) :1039–1053, 1998.

[74] S. Gueron and K. Levit-Gurevich. Computation of the internal forces in cilia : application to ciliary motion, the effects of viscosity, and cilia interactions. *Biophysical Journal*, 74(4) :1658–1676, 1998.

[75] S. Gueron and K. Levit-Gurevich. A three–dimensional model for ciliary motion based on the internal 9+ 2 structure. *Proceedings of the Royal Society of London. Series B : Biological Sciences*, 268(1467) :599–607, 2001.

[76] V. Gyrya, K. Lipnikov, I. S. Aranson, and L. Berlyand. Effective shear viscosity and dynamics of suspensions of micro-swimmers from small to moderate concentrations. *J. Math. Biol.*, 62(5) :707–740, 2011.

[77] B. M. Haines, I. S. Aranson, L. Berlyand, and D. A. Karpeev. Effective viscosity of dilute bacterial suspensions : a two-dimensional model. *Phys. Biol.*, 5(4) :046003, 2008.

[78] F. Hecht, O. Pironneau, A. le Hyaric, and K. Ohtsuka. *FreeFem++ manual.* `http://www.freefem.org/ff++/`, 2010.

[79] J.-M. Hervouet. *Hydrodynamics of Free Surface Flows. Modelling with the Finite Element Method.* Wiley J., 2007.

[80] M. Hillairet. Lack of collision between solid bodies in a 2D incompressible viscous flow. *Comm. Partial Differential Equations*, 32(7-9) :1345–1371, 2007.

[81] T.J.R. Hugues. Lagrangian-eulerian finite element formulation for incompressible viscous flows. *Comput. Methods Appl. Mech. Engrg.*, 29 :329–349, 1981.

[82] T. Ishikawa and T. J. Locsei, J. T. Pedley. Development of coherent structures in concentrated suspensions of swimming model micro-organisms. *J. Fluid Mech.*, 615 :401–431, 11 2008.

[83] T. Ishikawa and T. J. Pedley. Diffusion of swimming model micro-organisms in a semi-dilute suspension. *J. Fluid Mech.*, 588 :437–462, 10 2007.

[84] T. Ishikawa and T. J. Pedley. The rheology of a semi-dilute suspension of swimming model micro-organisms. *J. Fluid Mech.*, 588 :399–435, 10 2007.

[85] T. Ishikawa and T. J. Pedley. Coherent structures in monolayers of swimming particles. *Phys. Rev. Lett.*, 100 :088103, Feb 2008.

[86] J. Donea J. Sarrate, A. Huerta. Arbitrary lagrangian-eulerian formulation for fluid-rigid body interaction. *Computer Methods and Applied Mechanics in Engineering*, 190 :3171–3188, 2001.

[87] J. Janela, A. Lefebvre, and B. Maury. A penalty method for the simulation of fluid-rigid body interaction. *ESAIM : Proc.*, 1 :115–123, 2005.

[88] M. Kern. *Numerical Methods for inverse problems.* ISTE Ltd and John Wiley and Sons Inc, 2016.

[89] M. Khalife, A. Decoene, F. Caetano, L. de Rochefort, E. Durand, and D. Rodriguez. Estimating absolute aortic pressure using mri and a one-dimensional model. *Journal of Biomechanics*, 13(47) :3390–3399, 2014.

[90] M. R. Knowles and R. C. Boucher. Mucus clearance as a primary innate defense mechanism for mammalian airways. *J. Clin. Invest.*, 109(5) :571–577, 2002.

[91] M. Kocyigit, R. Falconer, and B. Lin. Three-dimensional numerical modeling of free surface flows with non-hydrostatic pressure. *Int. J. Numer. Methods Fluids*, 40 :1145–1162, 2002.

[92] T. Köppl and B. Wohlmuth. Optimal a priori error estimates for an elliptic problem with Dirac right-hand side. *SIAM J. Numer. Anal.*, 52(4) :1753–1769, 2014.

[93] L. Lacouture. A numerical method to solve the Stokes problem with a punctual force in source term. *C. R. Mecanique*, 343(3) :187–191, 2015.

[94] L. Lacouture. Modélisation et simulation du mouvement de structures fines dans un fluide visqueux : application au transport mucociliaire. *Thèse de doctorat de l'université Paris-Sud.*, 2016.

[95] S. K. Lai, Y. Y. Wang, D. Wirtz, and J. Hanes. Micro- and macrorheology of mucus. *Adv. Drug Deliv. Rev.*, 61 :86–100, 2009.

[96] E. Lauga and C. Eloy. Shape of optimal active flagella. *Journal of Fluid Mechanics*, 730 :763–774, 2013.

[97] J. Lee and N. Smith. Theoretical modeling in hemdynamics of microcirculation. *Microcirculation*, 15(8) :699–714, 2008.

[98] W. L. Lee, P. G. Jayathilake, Zhijun Tan, D. V. Le, H. P. Lee, and B. C. Khoo. Mucociliary transport : effect of mucus viscosity, cilia beat frequency and cilia density. *Comput. & Fluids*, 49 :214–221, 2011.

[99] A. Lefebvre. Fluid-particle simulations with freefem++. *ESAIM : Proc.*, 18 :120–132, 2007.

[100] C.D. Levermore and M. Sammartino. A shallow water model with eddy viscosity for basins with varying bottom topography. *Nonlinearity*, 14(6), 2002.

[101] P.-L. Lions and N. Masmoudi. Global solutions for some Oldroyd models of non-Newtonian flows. *Chinese Ann. Math. Ser. B*, 21(2) :131–146, 2000.

[102] N. Liron and S. Mochon. The discrete-cilia approach to propulsion of ciliated microorganisms. *J. Fluid Mech.*, 75 :593–607, 1976.

[103] J. T. Locsei. Persistence of direction increases the drift velocity of run and tumble chemotaxis. *J. Math. Biol.*, 55(1) :41–60, 2007.

[104] J. T. Locsei and T. J. Pedley. Run and tumble in chemotaxis in a shear flow : the effect of temporal comparisons, persistence, rotational diffusion, and cell shape. *Bull. Math. Biol.*, 71(5) :1089–1116, 1986.

[105] A. Logg, K.-A. Mardal, and G. Wells. *Automated solutions of differential equations by the finite element method : The FEniCS book*, volume 84. Springer Science and Business Media, 2012.

[106] J. Lubliner and J. Blum. Model for bend propagation in flagella. *Journal of Theoretical Biology*, 31(1) :1–24, 1971.

[107] A. M. Lucas and L. C. Douglas. Principles underlying ciliary activity in the respiratory tract : II. A comparison of nasal clearance in man, monkey and other mammals. *Arch. Otolaryngol.*, 20(4) :518–541, 1934.

[108] S. Lukens, X. Yang, and L. Fauci. Using lagrangian coherent structures to analyze fluid mixing by cilia. *Chaos : An Interdisciplinary Journal of Nonlinear Science*, 20(1), 2010.

[109] K. Machin. Wave propagation along flagella. *Journal of Experimental Biology*, 35(4) :796–806, 1958.

[110] F. Marche. Derivation of a new two-dimensional viscous shallow water model with varying topography, bottom friction and capillary effects. *European Journal of Mechanic /B : Fluid*, 26 :49–63, 2007.

[111] O. K. Matar and P. D. M. Spelt. Dynamics of thin free films with reaction-driven density and viscosity variations. *Phys. Fluids*, 17(12) :122102, 15, 2005.

[112] B. Mauroy, C. Fausser, D. Pelca, J. Merckx, and P. Flaud. Toward the modeling of mucus draining from the human lung : role of the geometry of the airway tree. *Phys. Biol.*, 8(5) :056006, 12, 2011.

[113] B. Maury. Characteristics ALE method for the unsteady 3D Navier-Stokes equations with a free surface. *Comp. Fluid Dyn.*, 6 :175–188, 1996.

[114] B. Maury. A time-stepping scheme for inelastic collisions. Numerical handling of the nonoverlapping constraint. *Numer. Math.*, 102(4) :649–679, 2006.

[115] B. Maury. Numerical analysis of a finite element / volume penalty method. *SIAM J. Numer. Anal.*, 47 :1126–1148, 2009.

[116] B. Metzger and J. E. Butler. Irreversibility and chaos : Role of long-range hydrodynamic interactions in sheared suspensions. *Jason E.*, 82, 2010.

[117] S. Mitran. Continuum-kinetic-microscopic model of lung clearance due to core-annular fluid entrainment. *J Comput Phys.*, 244 :193–211, 2013.

[118] S. M. Mitran. Metachronal wave formation in a model of pulmonary cilia. *Computers and Structures*, 85(11) :763–774, 2007.

[119] Y. Payan and J. Ohayon. *Biomechanics of living organs : hyperelastic constitutive laws for finite element modeling.* Academic Press, 2017.

[120] T. J. Pedley. Collective behaviour of swimming micro-organisms. *Exp. Mech.*, 50(9) :1293–1301, 2010.

[121] T. J. Pedley and J. O. Kessler. Hydrodynamic phenomena in suspensions of swimming microorganisms. *Annu. Rev. Fluid Mech.*, 24 :313–358, 1992.

[122] C. S. Peskin. The immersed boundary method. *Acta numerica*, 11 :479–517, 2002.

[123] N. A. Phillips. A coordinate system having some special advantages for numerical forecasting. *J. Meteorol.*, 14 :184–185, 1957.

[124] D. J. Pine, J. P. Gollub, J.F. Brady, and A. M. Leshansky. Chaos and threshold for irreversibility in sheared suspensions. *Nature*, 438(7070) :997–1000, 2005.

[125] O. Pironneau. *Méthode des éléments finis pour les fluides.* RMA 7 ed. Masson, 2006.

[126] P. Quemar. *Modeling and numerical analysis for free surface flows.* Thèse de Doctorat de l'Université Paris 13, 2019.

[127] A. Rabani, G. Ariel, and A. Be'er. Collective motion of spherical bacteria. *PLoS ONE*, 8(12) :e83760, 12 2013.

[128] K. Rachid. *Estimation de la pression aortique à l'aide de l'imagerie par résonance magnétique : développement d'un modèle biomécanique d'écoulement.* Thèse de doctorat en Physique, Université Paris-Saclay, 2018.

[129] S. Rafaï, L. Jibuti, and P. Peyla. Effective viscosity of microswimmer suspensions. *Phys. Rev. Lett.*, 104 :098102, Mar 2010.

[130] P. Reymond, F. Merenda, F. Perren, D. Rufenacht, and N. Stergiopulos. Validation of a one-dimensional model of the systemic arterial tree. *Am. J. Physiol. - Heart Circ. Physiol.*, 297(1) :208–222, 2009.

[131] W. Rodi. *Turbulence models and their application in hydraulics : A state of the art review.* Book publication of IAHR, Delft, The Netherlands, 1980.

[132] J.M. Rodriguez and R. Taboada-Vazquez. A finite element method for 3D hydrostatic water flows. *Comput. Vis. Sci.*, 38(I. 6) :399–409, 2007.

[133] D. Saintillan and M. J. Shelley. Orientational order and instabilities in suspensions of self-locomoting rods. *Phys. Rev. Lett.*, 99 :058102, Jul 2007.

[134] D. Saintillan and M. J. Shelley. Instabilities and pattern formation in active particle suspensions : kinetic theory and continuum simulations. *Phys. Rev. Lett.*, 100 :178103, Apr 2008.

[135] M. J. Sanderson and E. R. Dirksen. A versatile and quantitative computer-assisted photoelectronic technique used for the analysis of ciliary beat cycles. *Cell Motil.*, 5 :267–292, 1985.

[136] M. J. Sanderson and M. A. Sleigh. Ciliary activity of cultured rabbit tracheal epithelium : beat pattern and metachrony. *J. Cell Sci.*, 47(1) :331–347, 1981.

[137] L. R. Scott. Finite element convergence for singular data. *Numer. Math.*, 21 :317–327, 1973/74.

[138] M Sefidgar, M. Soltani, K. Raahemia, M. Sadeghi, H. Bazmara, M. Bazargan, M. Mousavi, and M. Naeenian. Numerical modeling of drug delivery in a dynamic solid. *Microvas. Res.*, 99 :43–56, 2015.

[139] J. E. Segall, S.M. Block, and H. C. Berg. Temporal comparisons in bacterial chemotaxis. *Proc. Natl. Acad. Sci. USA Proc.*, 83(23) :8987–8991, 1986.

[140] B. Semin, A. Decoene, J.-P. Hulin, M. François, and H. Auradou. Flow-induced oscillation of a confined tethered cylinder below the vortex shedding threshold. *J. Fluid Mech.*, 690(690) :345–365, 2012.

[141] A.F. Shchepetkin and J.C. McWilliams. The regional ocean model system (roms) : A split-explicit, free-surface, topography-following coordinate ocean model. *Ocean Modelling*, 9 :347–404, 2005.

[142] M. A. Sleigh, J. R. Blake, and N. Liron. The propulsion of mucus by cilia. *Am. Rev. Respir. Dis.*, 137(3) :726–741, 1988.

[143] D. J. Smith, E. A. Gaffney, and J. R. Blake. A viscoelastic traction layer model of mucociliary transport. *Bull. Math. Biol.*, 69(1) :289–327, 2007.

[144] D. J. Smith, E. A. Gaffney, and J. R. Blake. Mathematical modelling of cilia-driven transport of biological fluids. *Proceedings of the Royal Society of London A : Mathematical, Physical and Engineering Sciences*, 465(2108) :2417–2439, 2009.

[145] D.J. Smith, E.A. Gaffney, and J.R. Blake. Modelling mucociliary clearance. *Physiol. Neurobiol.*, 163(1–3) :178–188, 2008.

[146] A. Sokolov and I. S. Aranson. Reduction of viscosity in suspension of swimming bacteria. *Phys. Rev. Lett.*, 103 :148101, Sep 2009.

[147] A. Sokolov, I. S. Aranson, J. O. Kessler, and R. E. Goldstein. Concentration dependence of the collective dynamics of swimming bacteria. *Phys. Rev. Lett.*, 98 :158102, 2007.

[148] C. A. Solari, J. O. Kessler, and R. E. Goldstein. Motility, mixing, and multicellularity. *Genet. Program Evol. M.*, 8(2) :115–129, 2007.

[149] A. Soulaimani and Y. Saad. An arbitrary lagrangian-eulerian finite element method for solving three-dimensional free surface flows. *Comput. Methods Appl. Mech. Engrg.*, 162 :79–106, 1998.

[150] I. Tuval, C. Cisneros, Dombrowski, C. W. Wolgemuth, R. E. Goldstein, and J. O. Kessler. Bacterial swimming and oxygen transport near contact lines. *Proc. Natl. Acad. Sci. USA*, 102(7) :2277–2282, 2005.

[151] F. Vergnet. *Structures actives dans un fluide visqueux : modélisation, analyse mathématique et simulations numériques.* Thèse de doctorat en mathématiques appliquées de l'Université Paris Saclay, 2018.

[152] E. Vidotto, T. Koch, T. Köppl, R. Helmig, and B. Wohlmuth. Hybrid models for simulating blood flow in microvascular networks. *arXiv preprint arXiv :1811.10373*, page https ://arxiv.org/pdf/1811.10373.pdf, 2018.

[153] S. Vincent, J.P. Caltagirone, P. Lubin, and T. N. Randrianarivelo. An adaptative augmented Lagrangian method for three-dimensional multimaterial flows. *Computers and. Fluids*, 33 :1273–1289, 2004.

[154] G.B. Whitham. *Linear and non-linear waves.* John Wiley and Sons Inc., New York, 1999.

[155] G. B. Witman. *Introduction to cilia and flagella.* in Ciliary and Flagellar Membranes, R.A. Blood-good, Ed 1(30), Plenum. New York, 1990.

[156] X. Yang, R. H. Dillon, and L. J. Fauci. An integrative computational model of multiciliary beating. *Bulletin of Mathematical Biology*, 70(4) :1192–1215, 2008.

[157] Z. Yu. A dlm/fd method for fluid/flexible-body interactions. *Journal of Computational Physics*, 207(1) :1–27, 2005.